OPTIMIZATION FOR FINITE ELEMENT MODELING OF ELECTRONIC

COMPONENTS UNDER DYNAMIC LOADING

by

Srujanbabu Sridharala

Bachelor of Technology in Mechanical Engineering
Nagarjuna University,
Andhra Pradesh, India
1999

Master of Science in Mechanical Engineering
Tennessee Technological University,
Cookeville, Tennessee, USA
2002

A dissertation submitted in partial fulfillment
of the requirements for the

Doctor of Philosophy in Mechanical Engineering
Department of Mechanical Engineering
Howard R. Hughes College of Engineering

Graduate College
University of Nevada, Las Vegas
December 2006

UNLV
UNIVERSITY OF NEVADA LAS VEGAS

Dissertation Approval

The Graduate College
University of Nevada, Las Vegas

<u>   November 30</u> , 20 <u>06</u>

The Dissertation prepared by

<u>Srujanbabu Sridharala   </u>

Entitled

<u>Optimization for Finite Element Modeling of Electronic Components</u>

<u>Under Dynamic Loading   </u>

is approved in partial fulfillment of the requirements for the degree of
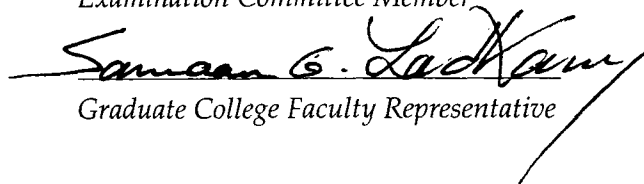
<u>Doctor of Philosophy in Mechanical Engineering   </u>
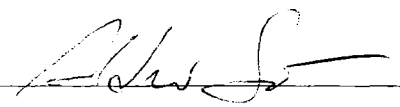
Examination Committee Chair

Examination Committee Member

Examination Committee Member

Examination Committee Member

Graduate College Faculty Representative

Dean of the Graduate College

1017-52

ii

ABSTRACT

Optimization for Finite Element Modeling of Electronic Components Under Dynamic Loading

By

Srujanbabu Sridhrala

Dr. Mohamed B. Trabia, Examination Committee Chair
Professor and Chairperson of Mechanical Engineering
University of Nevada, Las Vegas

And

Dr. Brendan J. O'Toole, Examination Committee Chair
Associate Professor of Mechanical Engineering
University of Nevada, Las Vegas

Usage of electronic components in the U.S. ARMY applications is becoming more challenging due to their usage in harsh environments. Experimental verification of these components is expensive and it can yield information about specific locations only. This research outlines the finite element modeling methodology for these electronic components that are subjected to high acceleration loads that occur over extremely short time such as impact, gun firing and blast events. Due to their miniature size these finite element models are computationally expensive. An optimization engine was presented to have an efficient analysis procedure that provides a combination of accuracy, computational speed and modeling simplicity. This research also involves experimental testing of the electronic components mounted on the circuit boards. Testing was

iii

conducted at different strain levels in order to study the behavior of boards. Finite

element models were developed for these tests and compared with experimental results.

TABLE OF CONTENTS

LIST OF FIGURES

LIST OF TABLES

ACKNOWLEDGEMENTS

I express my sincere gratitude to my thesis advisors Dr. Mohamed B. Trabia and Dr. Brendan J. O'Toole for their invaluable guidance and suggestions throughout the entire course of this research project.

I would like to thank Dr.Mostafiz Chowdhury, Dr. Ajit K Roy, Dr. Samaan G. Ladkany and Dr. Woosoon Yim for their time in reviewing the prospectus, participation of defense, and counseling of the thesis as the committee members.

The financial support provided by the Army Research laboratory (ARL), under project G2a is thankfully acknowledged.

I would also like to express my heartiest gratitude to my colleagues, friends and family for their unrelenting support and motivation throughout this research activity.

LIST OF ABBREVATIONS

ARL   Army Research Laboratory

ASTM   American Society for Testing and Materials

BGA   Ball Grid Array

CNC   Computer Numerically Controlled

CSP   Chip Scale Package

FE   Finite Element

FEA   Finite Element Analysis

FR-4   Fiberglass-epoxy Circuit Board Material

G   Acceleration of gravity

LSS   Large Space Structure

LSTC   Livermore Software Technology Corporation

PBGA   Plastic Ball Grid Array

PCB   Printed Circuit Board

PWA   Printed Wiring Assembly

PWB   Printed Wiring Board

SAE   Society of Automotive Engineers

SCSP   Stacked Chip Scale Package

SMT   Surface Mount Technology

TFBGA   Thin Profile Fine Pitch Ball Grid Array

VFBGA   Very Thin Profile Fine Pitch Ball Grid Array

CHAPTER 1

RESEARCH OBJECTIVES

The research outlined in this dissertation was used to develop algorithm that can optimize finite element models subjected to shock environments. It is anticipated that the results of this research will contribute in understanding the survivability of electronic components subjected to shock environment. To predict failures, a combination of experimental and finite element analysis (FEA) results can be used. However experimental results can yield information about specific locations only, so it will be more beneficial if the user can access the FEA results with higher degree of certainty and lesser computational time. As the accuracy and computational time are competing objectives; consequently, a trade-off between them is necessary. Significant part of this research is to develop an optimization scheme to tune the FEA modeling to increase the confidence in the predicted results.

The second objective of this research is to assess the behavior of circuit boards and components mounted on them under mechanical shock loading. Mechanical shock loading occurs in many commercial and military applications. For commercial applications, shock loads may be produced by transportation, operation in vehicles, operation in aircraft, dropping an electronic assembly and maintenance. In addition to the shock loading seen in commercial applications, military applications also have gunfire shock, missile acceleration, projectile launch shock, and spin-up accelerations. Electronic

1

components subjected to high acceleration loads that occur over extremely short period of time such as impact, gun firing, and blast events, can be on the order of tens of G's (acceleration of gravity) to hundreds of G's.

To achieve the research objectives, the effort was divided into following tasks:

1. Review and evaluate the existing optimization algorithms.

2. Identify solid modeling and FEA software packages that will be able to analyze this type of problem. This package should either have some programming capability or the ability to be used as a subroutine within a programming language so that it can be incorporated with the optimization programs.

3. Explore the nature of the problem to determine the most suitable optimization algorithm.

4. Implement an optimization engine to combine the finite element model with the optimization algorithm in order to produce a more reliable finite element model that can reduce dependence on experimental data.

5. Apply the proposed algorithm to FEA of electronic components inside the projectile where they are subjected to shock/impact during launch.

6. Create the experimental set-up for impact testing of printed circuit boards (PCB).

7. Conduct experiments to study the response of these boards under impact.

8. Study these boards using FEA and explore the possibility of tuning the models using optimization techniques.

9. Extend the proposed optimization engine to FEA created for impact testing of electronic boards.

CHAPTER 2

BACKGROUND AND LITERATURE REVIEW

2.1 Background

At the first Shock and Vibration Symposium in 1947, mechanical shock was defined as "a sudden and violent change in the state of motion of the component parts or particles of a body or medium resulting from the sudden application of a relatively large external force, such as a blow or impact" [1]. Since then the specific words used have changed somewhat but the meaning remains the same. Most analysts treat shock as a transient vibration. No matter how it is described or what source produced it, the effects of mechanical shock on structures and equipment create major design problems for a wide variety of systems.

Impact and shock to electronic components can cause significant functional and physical damage in the form of internal component failure, damage on the external housing, or solder-joint breakage. The components can be subjected to very large forces and accelerations during impact and are dependent on factors such as mass, impact orientation and the surface of impact. Resulting stresses and strains induced can cause failure of the components. To avoid the cost and inconvenience associated with repair or replacement, such components must be able to accommodate occasional severe impacts and yet sustain minimal damage. Therefore one has to consider both the physical

Reproduced with permission of the copyright owner. Further reproduction prohibited without permission.

ruggedness of the electronic components along with the reliability to impact and shock [2].

Since experimental testing of smart munitions is fairly expensive, one of the objectives of this proposed research is to develop an FEA methodology which allows a high degree of confidence in predicted results. A smart FEA system can allow the designer to analyze several design alternatives and various testing scenarios before creating a prototype. The proposed system can allow the user to guide and control the direction of the modeling process.

2.2 Literature Review

Literature related to electronic components subjected to shock loading and their modeling using FEA is discussed in detail, but literature directly relevant to optimization of FEA is not available as this is a unique method developed by combination of available software packages and optimization algorithms. However, a detailed literature search relative to optimization algorithms, assistance for finite element modeling and structural optimization techniques has been conducted.

2.2.1 FEA Modeling Assistance

While FEA programs and their pre-processors and post-processors have reached high levels of maturity and sophistication in their analytical capabilities, systems that can assist engineers in the critical tasks of modeling and model interpretation are not fully developed yet. Current FEA programs cannot easily evaluate the reasonableness of the assumptions that are used to create a model. They cannot readily suggest strategies for model modifications, beyond adaptive meshing. If tools for such needs are developed,

4

they can improve the overall efficiency and reliability of analysis. Few researchers approached the issue of creating an expert system that can be used within FEA for such purpose. For example, Turkiyyah and Fenves [3], presented a knowledge-based framework to assist users in reaching necessary modeling decisions regarding element types, element properties, loading conditions, mesh size, boundary conditions, and solution procedures. At the back end, modeling-assistance tools can abstract and evaluate the massive output typically produced by finite-element programs, to produce high-level descriptions of the model behavior and to modify modeling assumptions as appropriate. Such modeling assistants can reduce the number of tasks related to the user, thus allowing a faster turn around time for analysis.

Fonseca, et al. [4], presented the integrated structural/control optimization approach to optimize the structure and the control of a large space structure (LSS) based on the study of the CPU time. According to them the solution of the integrated optimization problem requires sensitivity analysis implying computing the derivatives of the constraints imposed on the optimization problem with respect to the design variables. These derivatives can be obtained from the finite difference approach but, this procedure may result in a significant consumption of computer time. So they developed a process in which the structural objective function and the control index are taken simultaneously into account in only one software package. They developed a FORTRAN software package integrating two major computer programs, the NEWSUMT-A and the ORACLS to solve the optimization problem. The NEWSUMT_A is a set of subroutines used for the structural optimization, including routines for the sensitivity calculation. The ORACLS is the acronym for Optimal Regulator Algorithms for the Control of Linear Systems. It

5

includes all subroutines necessary for matrix algebra including also routines to solve eigenvalue problems. Their MAIN PROGRAM initializes the process with all initial data and dimensions, and the initial structure. Then the NEWSUMT-A starts the process by sending the initial structure to the ANALYSIS routine where the structure is sent to ORACLS for the optimization control problem solution. ORACLS returns to the ANALYSIS routine the closed-loop eigenvalues from which the control damping was evaluated. Then the structural eigenvalue problem was solved. Next, the constraints regarding control damping and structural fundamental frequency were checked. Finally, the ANALYSIS routine calculates the first and second derivatives of the objective function and constraints. The results of this analysis are sent back to NEWSUMT-A. If the structural/control convergence criteria and the constraints are satisfied, the NEWSUMT-A sends the final structure to the MAIN PROGRAM and stops. If not, NEWSUMT-A generates a new structure and the loop continues until the optimized structure satisfies the convergence criteria and constraints imposed on the integrated structural/control problem.

In the current research similar idea is applied by combining an Optimization Algorithm with LS-DYNA using Matlab. It is discussed in detail in Optimization chapter.

Holzhauer and Grosse [5] proposed a knowledge-based control of finite element thermal analysis. They implemented an architecture in which database structures interact with knowledge sources. They performed finite element analysis by decomposing the system into different levels of components and allowing the use of different time steps when solving each component's matrix equation based on feedback from knowledge source. Their study indicated that while decomposition causes some levels of inaccuracy

6

in the final solution, it may be an acceptable trade-off for many situations, such as the stage of early product design. In [6], Pinfold and Chapman used knowledge-based engineering techniques to generate finite element mesh for automotive applications. They developed the knowledge-based engineering for common automotive parts. When geometry of the automotive body is imported for meshing, knowledge-based engineering simplifies the geometry for meshing according to specific rules. The authors concluded that this automated system could reduce pre-processing time significantly. Pinfold and Chapman [7] described the use of a knowledge-based engineering environment to automate the post-processing phase of the analysis. They described the stages of automating the feedback of finite element analysis results into the original design model. They selected adaptive modeling language (AML) knowledge-based engineering environment as a tool that is compatible with PATRAN and NASTRAN. The knowledge-based environment was developed to fit a family of mechanical components. Lee and Kim [8] developed a design system that can process knowledge and numerical computation by integrating multi-objective optimization method and the knowledge-based system. Their system was applied to the optimal design of a ship. Preprocessor phase information was extracted by analyzing the database of an existing ship in knowledge base. For the postprocessor phase, information was obtained from the trade-off relations in the knowledge base. The authors concluded that their system can efficiently control optimization procedures and it can be also used to assist designers with decisions that require heuristic knowledge of the design processes.

7

2.2.2 Optimization Algorithms

The simplex method for minimization of a function of n variables was first introduced by Spendley, et al. [9]. These simplex algorithms determine the search direction based on the function evaluations only, which is useful when the function is highly nonlinear and has discontinuities. For a problem with n number of independent variables, search for extremum starts by generating a simplex with n+1 vertices. The algorithm evaluates the function values at these points, and replaces the point of the highest function value with its reflection along a vector passing through the center of the remaining points. Despite the simplicity of this algorithm, it can have problems such as slow rate of convergence or cycling.

Further enhancement of the simplex algorithm was done by Nelder and Mead [10], who proposed expanding or contracting the simplex based on evaluating the function values of the simplex vertices and the reflection point. The amount of contraction or expansion of the new point that will replace the point of highest function value does not include the relative weights of the function values at the simplex vertices. For example, it can be argued that if the function value at the point of the lowest function value in the simplex is much larger than the function value at the reflection point, a significant expansion of the simplex is recommended. On the other hand, if the function value at the point of the lowest function value in the simplex is little bit larger than function value at the reflection point, a moderate expansion of the simplex should be recommended. These two statements are linguistic, which is the medium of fuzzy logic. Trabia and Lu [11], used fuzzy logic to produce a more efficient simplex (a search that requires lesser number of function evaluations) by making simplex movements adaptive. Their fuzzy simplex

8

algorithm determines the movement of the simplex based on fuzzy evaluation of the function values at the simplex points. More specifically, fuzzy logic controllers determine the direction of simplex reflection and control the expansion and contraction of the simplex to achieve faster convergence. This fuzzy simplex algorithm is used in the current research.

2.2.3 Test Methodology for Shock Survivability of Electronic Components

Portable electronic devices are often subjected to shock and vibration loading due to mechanical handling, accidental misuse, drop or shipping. Military electronic devices are often subjected to repetitive shocks (artillery fire), sudden high G loading during launching or maneuvering projectiles or ballistic impact. Dynamic loading plays a crucial role in the performance and reliability of electronic devices used in a wide range of applications. At present manufacturers of hand-held electronic devices use the JEDEC JESD22-B104-B standard for mechanical drop testing [12]. According to this standard the drop-durability of portable electronic products is quantified and ranked by the number of drops to failure. The product is held in the desired orientation on a drop carriage that is allowed to fall onto a fixed target. Goyal and Buratynski [13] showed that even a single drop event of an electronic product can produce a complex multi-modal transient response history. Lim and Low [14] showed that the structural response of the printed wiring assembly (PWA) is strongly dependent on the mass distribution of the internal electronics, the mounting of the PWA, and the orientation of drop.

Drop tests conducted by Lim, et al. [14], [15] and Seah, et al. [16] showed that the PWA strains and accelerations vary with the electronic device for the same orientation of drop. Also for the same electronic device, the PWA strains and accelerations vary with

9

drop orientation. Tests conducted by Yu, et al. [17] and Juso, et al. [18] indicated that the number of cycles to failure decreases as the PWA strain and strain rate increases. In both of the above cases, the failure was in the bulk solder. Varghese and Dasgupta [19] ran impact tests on PWAs in the in-plane and out-of-plane orientations and showed that the number of impacts to failure decreased with increasing PWA strain. The failure site for both impact orientations was the interfacial intermetallic layer.

Varghese and Dasgupta [20] subjected PWAs to flexural strain rate ranging from 10-3/sec to 101/sec, and observed a failure site transition from the solder to the copper trace beyond a critical PWA strain rate. They used commercially available servo-hydraulic bend testing machine (Figure 2.1) and a drop tower (Figure 2.2) for their study. Their LVDT has 0mm to 100mm displacement range and 0mm/sec to 12.5mm/sec. Their drop tower is equipped with steel spheres which were dropped on the fixture holding the specimen to conduct high speed bending tests. Their sphere mass can be varied from 65 grams to 450 grams and can achieve 0 to 6m/sec by changing the sphere drop height.
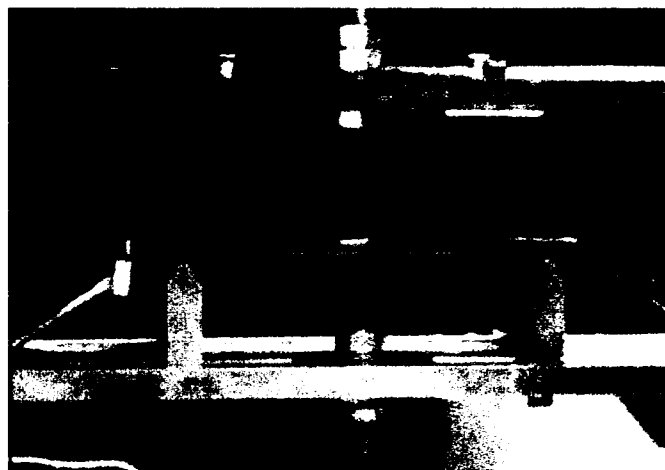
Figure 2.1 Four Point Bend Test Fixture on Servo-Hydraulic Mechanical Tester [20]

10
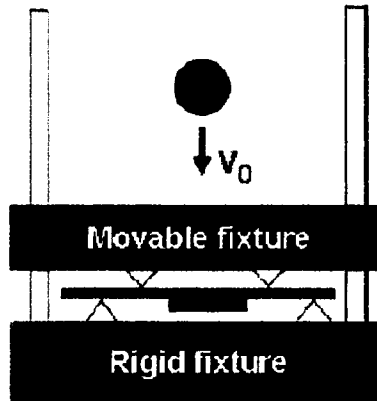
Figure 2.2 Schematic Diagram of the Ball Drop Test Setup [20]

Heaslip, et al. [21] compared the drop durability of Sn-Pb and Pb-free solders and showed that the failure sites and failure mechanisms change with drop height and solder type.

2.2.4 Board Level Reliability Tests

Due to market-driven demand of miniaturization and more functionality of portable microelectronic products, the development of IC (Integrated Circuit) packages has been pushed toward to a smaller, thinner, lighter and higher density package configuration. As a result, the second level reliability became a major concern for the chip scale packages (CSPs). Most of the reliability studies have been focusing on the thermal cyclic fatigue life of CSPs [22-27]. Ho [28] proposed and addressed certain test methods and the preliminary fatigue data of a PBGA (Plastic Ball Grid Array) package. The effects of maximum deflection and excitation frequency of a cyclic loading on a joint fatigue life were reported. He concluded that deflection affects joint's integrity more severely and directly than vibration frequency does.

11

Wu, et al., [29] conducted a second level reliability of a stacked chip scale package (SCSP) under cyclic bending to evaluate the structural integrity of solder interconnects. Their test vehicle (on-board SCSP) was simply supported at both ends and subjected to repetitive deflection in the middle (three-point bend) as shown in Figure 2.3. They examined cyclic deformation histories such as sinusoidal, triangular, and square waveforms. They observed tremendous joint damage as square-wave loading history was applied. They concluded that difference in relative bending rigidity between the component and PCB will affect the deformation and fracture of solder joints.
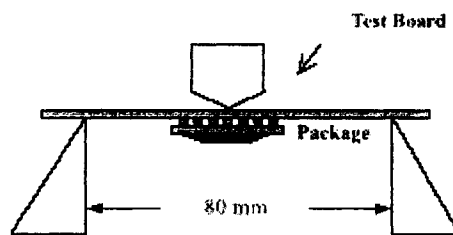
Figure 2.3 The Configuration of Three-Point Bend Test [29]

Hung, et al. [30] studied the effects of die size, board surface finish, substrate gold plating thickness, epoxy thickness, polyimide thickness and underfill material utilization on the fatigue life of solder interconnect of BGA (Ball Grid Array) using flex substrate under thermal cycle test. Their study showed that Chip size, polymide thickness and the utilization of underfill material has significant impacts on the joint fatigue life. Especially the effect of applying underfill material to the joint is tremendous according to their observation. Their study also showed that there is very little effect on the joint fatigue life with epoxy thickness.

2.2.5 Failure Mechanisms in Electronic Products

12

There is considerable reported evidence that a large percentage of portable electronics product failure is due to impact or shock during use. Failures of the external housing, internal electronic components, package-to-board interconnects, and liquid crystal display panels may occur as the result of dropping. Goyal, et al. [31] reported that the drop testing of an electronic product touches down first and there will be clattering as other corners strike repeatedly due to rebounds. Those cause velocity shocks at each impact, which will be several times higher than those experienced in standardized testing at a drop-table. He also addressed that clattering of the product can lead to alternating shocks that would cause resonance in suspended fragile components. Varghese and Dasgupta [32] addressed that when a product is dropped, the PWB (Printed Wiring Board) undergoes flexural deformation and the components accelerate due to inertial effects. According to them both these factors contribute to damage of interconnects. Accelerometer history of impact force alone won't provide all of the parameters required to describe impact damage. It was proposed that local flexural strain, flexural strain rate and inertial acceleration be used to describe the impact damage in interconnects. According to them damage is quantified in terms of structural response of the specimen, and is independent of geometry, loading and boundary conditions. Their observations indicate that for the same acceleration, as the strain increases, the damage per impact increases and hence the number of impacts to failure decreases. Similarly, damage due to impact loading will depend on the rate dependent material properties of the solder ball.

13
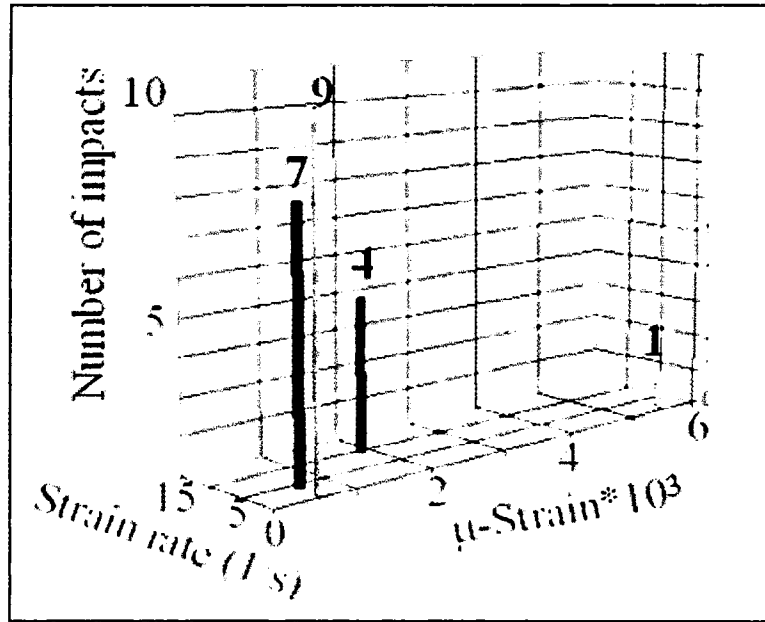
Figure 2.4 Damage as a Function of PWB Strain and Strain Rate [32]

Their conclusion states that the number of impacts is low for high strain rate impacts. For low strain rate impacts, the damage per impact is low, hence number of impacts to failure increases; this is represented in Figure 2.4.

Frank [33] explored the criteria that should be used to determine the electrical failure during accelerated testing of underfill flip chip joints as a function of both thermal cycling conditions and different sampling methods. His criterion was based on resistance measurements of daisy-chained solder joints monitored in situ and by end pointing. He also proposed a tunneling model to explain the resistance behavior of cracked joints.

Shetty, et al. [34] conducted monotonic bend tests to determine the overstress curvature limits for CSP interconnects. His overstress bend test setup is as shown in Figure 2.5. They found the average moment limit and curvature limit on the CSPs. They

14

are considering failure as either cracking of the board or interconnect delaminating from the board which ever happens first.

Figure 2.5 Overstress Bend Test [34]

Michael, et al. [35,36], discussed various failures and failure analysis of electronic assemblies and devices. Blattau and Hillman [37] studied the failure mechanisms in electronic products of laptop computers, in a non-commercial environment for military purposes. Their environment is that of an unpressurized aircraft cockpit operating at 35,000 feet. Their work showed that failure mechanisms of greatest concern are liquid crystal display (LCD) seal, battery leakage, and lack of sufficient air cushion for the hard drive. They also suggested that battery leakage issue should be seriously considered as a design limitation due to the potential for fire and explosion.

Wong, et al. [38, 39, 40] addressed that differential flexing between the PCB and the packaging as the main failure driver for the package to board interconnection; where as inertia due to acceleration as a secondary failure driver.

15

2.2.6 Reliability of Electronic Components

Evaluating the reliability of modern electronic components is an involved and costly problem, exacerbated by continual improvements in failure rates and by continual changes in technology. In order to improve reliability we must first of all be able to measure it; having measured it we must be in a position to understand the failure mechanisms and to diminish their effects through changes in design or technology.

Mackintosh [41] addressed the reliability of the integrated circuit; he described the problems and techniques in terms of simpler and discrete components. Zhang, et al. [42], presented a quantitative assessment of the state of semiconductor component reliability. Then he employed the findings to evaluate the effect of reliability improvements on present and future reliability modeling and predictions, and accelerated life testing. He used activation-energy-based reliability models to statistically correlate time to failure.

Michael, et al. [43] established the minimum criteria needed to assess the value of a reliability model. His criterion emphasizes the influence of environmental and operational stresses; variability in failure mechanisms, modes, and sites; design parameters; manufacturing processes and defects; and the statistical distribution of failures. According to him if a model satisfies the above criteria, it is certified as robust enough to provide competent assessments.

Margaret, et al. [44] presented a process to assess the reliability of electronic parts. According to them reliability assessment is by definition an application-specific process, the assessment results are applicable only to the given application. If the part's application-specific reliability meets the requirements, it is accepted for the given application; if the application-reliability requirements are not met, the part is rejected for

the given application from the reliability perspective. The application-specific reliability assessment may be conducted using one or all of three tools; integrity tests, virtual qualification and accelerated testing, which is depicted in Figure 2.6.
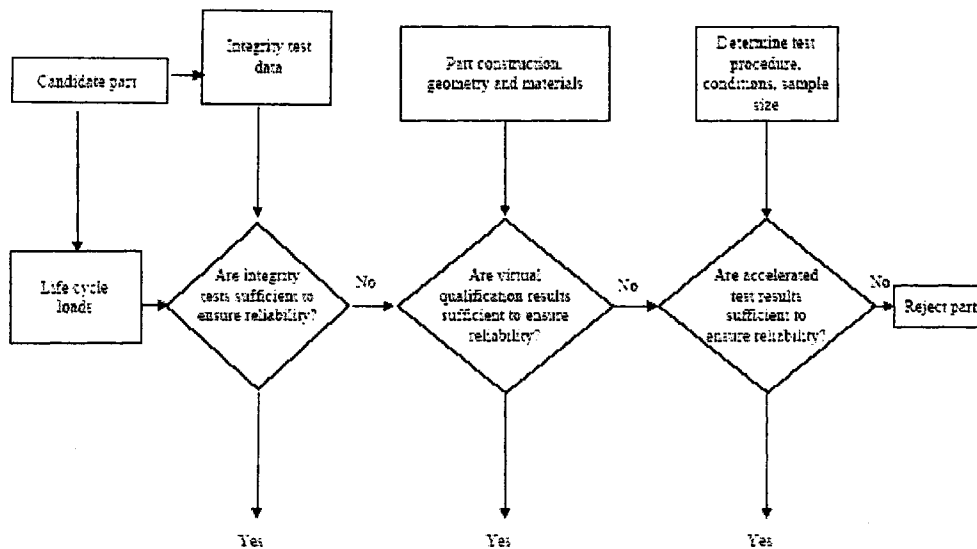
Figure 2.6 Reliability Assessment Process. [44]

Michael [45] presented the reliability assessment predictions of electronic products and systems. Figure 2.7 depicts the interactions between reliability prediction and various design, development, and support tasks.

17

reliability
allocation

logistics

system and
part
architecture

RELIABILITY
PREDICTION

maintainability

derating

FMECA

cooling system
definition

stress
screening

reliability
growth
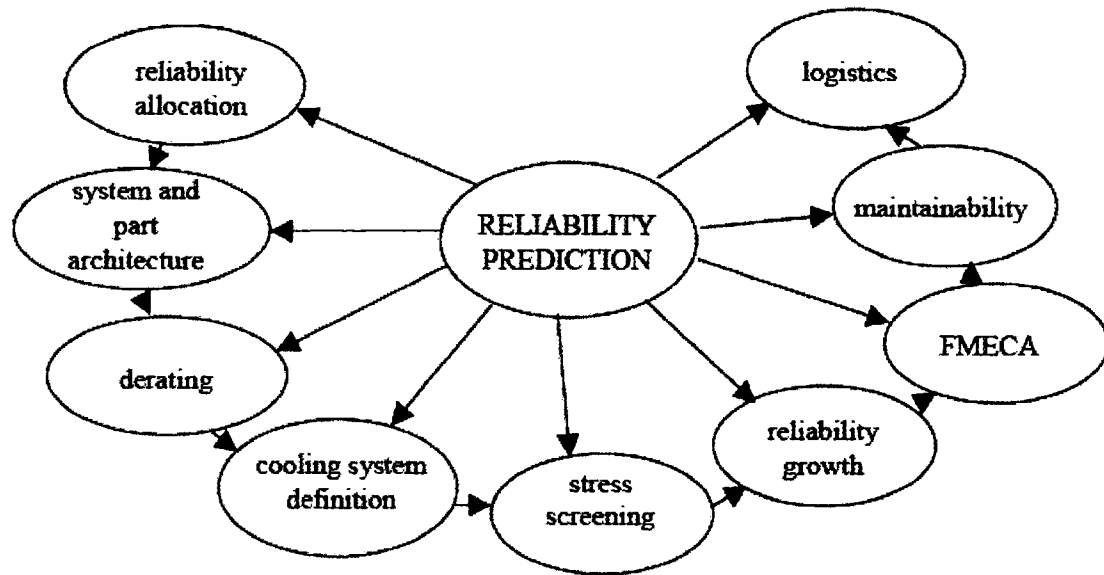
Figure 2.7 Impact of Reliability Tasks on Electronics [45]

Alander, et al. [46] studied the impact of component placement on solder joint reliability. They presented the relation between placement and the solder joint reliability of BGA components. They studied with computational methods in 3-D and verified with experimental tests. They utilized FEA to calculate the accumulation of plastic work in solder joints. Based on the failure criteria obtained in the process, simple design rules were extracted and presented.

2.2.7 Modeling of Electronic Components Subjected to Shock/Impact

Most shock test standards [47, 48] including the JEDEC board-level drop impact standard [49] prescribed a half sine acceleration pulse measured on the base. They suggest that when the fundamental frequency of the test structures, namely, the base and the connectors, are significantly higher than that of the input pulse and the board, the same half sine acceleration input pulse will be transmitted to the supports of the PCB without distortion. In another word, the test structure behaves as a rigid body. In such

18

cases the dynamics of the board-level drop impact can be analyzed simply through application of acceleration input directly on the PCB at the supports, where it is connected to the test structure.

Wong [50] modeled the dynamic response of the PCB in a standard board-level drop impact test as a spring-mass system, a beam, and a plate. He developed analytical solutions for the time-response and amplification of the deflection, bending moment and acceleration at any point on the PCB and validated with FEA. His analysis showed that the response of PCB was dominated by the fundamental mode and also it depends heavily on the ratio between the frequency of the PCB and the input acceleration pulse. It also showed that the bending moment on the PCB is responsible for the interconnection stress, and the maximum moment and it can be most effectively reduced through reducing the PCB thickness.

Tong, et al. [51] created a detailed drop test simulations on TFBGA (thin-profile fine-pitch BGA) and VFBGA (very-thin-profile fine-pitch BGA) packages. Figure 2.8 depicts the FEA of TFBGA46. Their observations indicate critical solder ball occurs at the outermost corner solder joint and fails (Figure 2.9) along the solder and PCB pad interface. Various testing parameters are studied to understand the effects of drop height, drop orientation, number of PCB mounting screws to fixture, position of component on board, PCB bending and solder materials. They used drop height, felt thickness, and contact definitions to fine-tune the shape and level of shock pulse required. They performed dynamic simulation to compare with the experimental results and their established model has close values of peak acceleration and impact duration as measured

19

in actual drop test. Their failure mode and critical solder ball location predicted by modeling correlate well with testing.
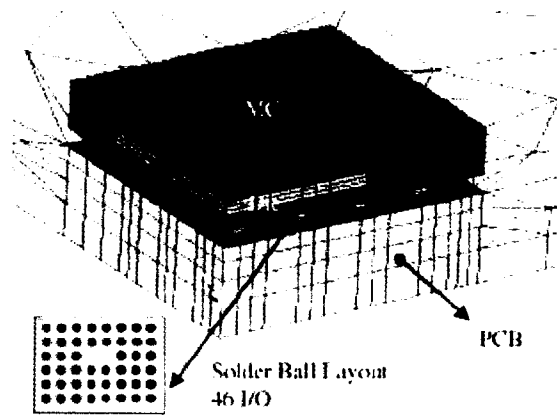
Figure 2.8 Board Level Drop Test Model for TFBGA46 [51]
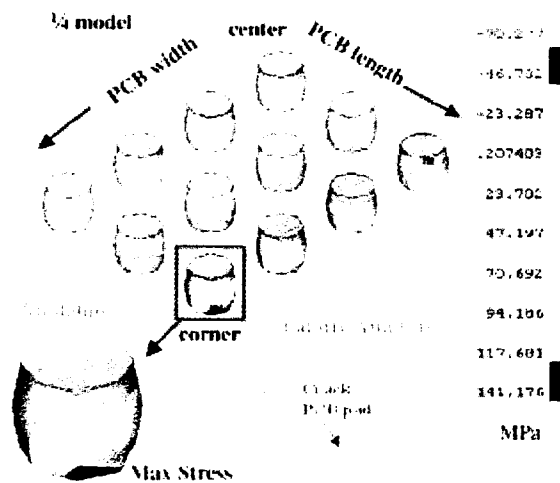
Figure 2.9 Critical Solder Ball and Failure Interface [51]

To investigate the long term reliability of PBGA packages in aerospace application, accelerated tests were conducted on non-underfilled and underfilled packages under

20

multiple environmental loadings at board level by Haiyu, et al. [52]. Three dimensional FEA models for non-underfilled and underfilled packages were developed and used to predict the time to failure.

According to the study carried by Heaslip and Punch [53], for many orientations of drop, the PWB will flex significantly during the impact event and subsequent clattering. Reducing the curvature and acceleration of the PWB during impact is an integral part of the design strategy for such products. They represented a PWB as a clamped-clamped prismatic beam in a drop test scenario which predicts deflection, bending moments and strain at any point along the beam length. Their strains calculated from this model showed high levels of strain at clamped edges. The values were higher than those measured experimentally and less than simulated. Their explicit finite element simulation showed high levels of strain than those predicted by the theory.

In a research carried by Deiters, et al. [54], the requirement for many products is survival of a mechanical shock test which might be described by an acceleration time-history or a specific test description such as a drop from a given height. They simulated the controlled drop of a personal computer assembled from parts, from a number of different suppliers. Their objective was to configure the computer so that it could withstand a drop without mechanical failures, and in addition, the internal components such as the disk drive and the CD drive needed to have peak accelerations within the manufacturer rated values. They developed a simple model of a generic computer box with floppy drive, CD drive and support bracket. They used spring elements which were used to modify the stiffness of the mounting. Their analysis was used in determining the peak acceleration values along with the natural frequencies. They suggested that by

21

providing this information to suppliers, they will be able to optimize their designs better for the true operating environment, resulting in less overdesign and lower cost per product. They also addressed that for many products, one of the main design limitation is disassembly which is highly nonlinear response. Representing this and the dynamic response due to drop in just one event would require a very computationally intensive simulation. They suggested an alternative, to use the initial linear simulation to understand the peak acceleration values to which a product is subjected. Then these accelerations can be used in parallel with a static contact analysis where the acceleration is varied until the onset of separation of components.

Jung, et al. [55] carried a study on failures of electronic equipment during the process of launching the satellite. The impulse between the launch vehicle and the atmosphere can generate a lot of noise and vibration. In this situation, random vibrations can cause the malfunction of the electronic equipment of the device. According to them the safety of the electronic equipment is related to the natural frequency, shapes of mode and dynamic deflection of the PCB. They modeled the PCB using a simple 1DOF system and calculated the margin of safety for the electronic components using the natural frequency and the dynamic deflection in order to evaluate the safety. In addition, through comparison of the results of the FEA and the natural frequency test, their study proved that it is reasonable to include the electronic component and lead wire in the FE model to find the exact 1st natural frequency of the PCB with FEA.

Drop test performance for the Computer, Communication, and Consumer (3C) products has become one of the most crucial evaluations. Wang, et al. [56] developed a drop test platform with impact angle control repeatability and analysis capability.

22

According to them, good control on impact angle provides product engineers a better understanding on the failure pattern of specific drop orientation and the damage mechanism of structures. Their numerical simulation provided stress wave propagating directions within internal components, where it is unlike to mount any mechanical sensors in a compact space. They suggested using a low pass filter to remove unrelated high frequency noises during impact test. They also cited that by using a low pass filter following SAE (Society of Automotive Engineer) specification for both experimental data and simulation outputs present an easier understanding of those signals.

To numerically study the failure associated with the small components embedded in electronic devices, the required output at the small components needs very fine local mesh, which causes unbearable CPU cost and makes the simulation impossible. A global-and-local coupling approach is presented by Jason Wu [57]. His idea is based on the fact that the global dynamic response affects the local behavior, but the local behavior has little contribution to change the global performance. The loading condition to local analysis was provided by global analysis. The local analysis at fine meshing will not loose its accuracy using the loads obtained from the global simulation at coarsely meshed model. He created two models of a component in a device, one with very fine mesh locally and the other with coarse mesh along with the device. For the fine mesh local model the loading conditions were given from the output of coarse mesh global model. His studies demonstrated excellent agreement of displacements in the two models.

Carroll, et al. [58] modeled the bending simulation of BGA SMT (Surface Mount Technology) for drop test. They modeled both in static and dynamic environments with four point bend fixtures. For static model a known deflection was given as input for the

23

top fixture, while the bottom rollers were fixed. In the dynamic case an initial velocity was given to the top fixture and a zero velocity boundary condition was applied to the bottom rollers. They observed higher equivalent plastic strains in dynamic bending than in static bending for the same amount of strain. They also demonstrated that single, linear, beam elements with distributed coupling can be used to capture the joint displacements more accurately.

CHAPTER 3

OPTIMIZATION

3.1 Definition and Background

Optimization can be defined as finding one or more feasible solutions which correspond to extreme values of one or more objectives. The purpose of optimization comes from the extreme need of either designing a solution for minimum possible cost, or for maximum possible reliability or others. Optimal solutions and optimization methods are of great importance particularly in engineering design, scientific experiments and business decision making.

When optimization problem involves finding an optimum solution with only one objective function it is called single-objective optimization. When optimization search involves more than one objective function, it is called multi-objective function.

According to Diwekar [59] general optimization problem can be stated as the following:

Find the extremum of $Z = z(x)$ (3.1)

subjected to

$h(x) = 0$ (3.2)

$g(x) \leq 0$ (3.3)

The goal of an optimization problem is to determine the decision variables x that optimize the objective function Z, while ensuring that the model operates within

25

established limits enforced by the equality constraints h and inequality constraints g. Figure 3.1 illustrates schematically the iterative procedure employed in a numerical optimization technique. As seen in the figure, the optimizer invokes the model with a set of values of decision variables x. The model simulates the phenomena and calculates the objective function and constraints. This information is utilized by the optimizer to calculate new set of decision variables. This iterative sequence is continued until the optimization criteria pertaining to the optimization algorithm are satisfied.
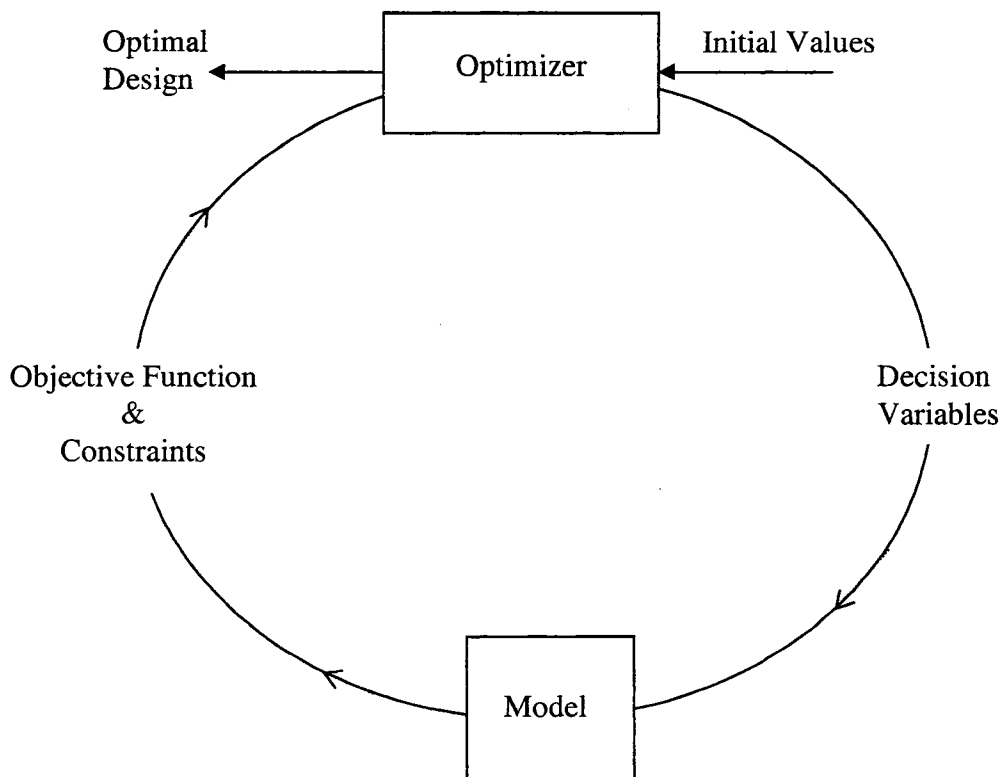
Figure 3.1 Pictorial Representation of Numerical Optimization Framework [59]

3.2 Optimization Engine

Current research involves optimization of various parameters involved in the finite element models of the structures subjected to high G loads. This can be categorized as the numerical optimization. Most of the current work involves optimization of a single objective function subjected to several equality and inequality constraints. A thorough search has been conducted to identify the modeling and FEA software packages that will be able to analyze and also be able to allow programming capabilities, to be incorporated with the optimization programs. We couldn't find the readily available software package which has the required capabilities.

In order to achieve the objective of the current research, the following areas were explored:

1. FEA packages which outputs the model in editable text format.

2. Optimization algorithms.

3. Programming languages which can link the FEA package with optimization algorithms.

3.2.1 FEA Package

LS-DYNA [60, 61] developed by Livermore Software Technology Corp. (LSTC) was found to serve our purpose for the FEA package. It is a general purpose, explicit and implicit finite element program used for the nonlinear dynamic response of the three dimensional structures. The simulation process can be initiated from the DOS command which is advantageous as most of the programming languages has the capability to communicate with DOS commands. It has the capability of writing the created structural model for analysis in text format. Parametric study of the model can be performed by

27

varying the parameters in the text file. Variation of these parameters should be done using a suitable optimization algorithm, which can yield the optimum result at a faster rate.

3.2.2 Optimization Algorithm

A fuzzy adaptive simplex search optimization algorithm presented by M. Trabia and X.Lu [11] was used for the current research. This algorithm chooses the adaptive parameters as part of the search strategy to make the search more responsive to changes in the problem by incorporating fuzzy logic in optimization algorithms. It has the capability of minimizing a function of n variables, the search starts by generating a simplex with n+1 vertices and the algorithm then repeatedly replaces the point with the highest function value by a new point. The initial simplex was created according to Spindley et al. [9] by generating n+1 equally spaced points according to the equation,

$$X_i = X_0 + \delta_1 U_i + \sum_{j=1, j \neq i}^{n} \delta_2 U_j \qquad (3.4)$$

where,

$$\delta_1 = \frac{\sqrt{n+1} + n - 1}{n\sqrt{2}} \alpha \qquad (3.5)$$

$$\delta_2 = \frac{\sqrt{n+1} - 1}{n\sqrt{2}} \alpha \qquad (3.6)$$

α is the simplex size factor

U_i – Unit Vector in the ith coordinate axis.

After the algorithm generates the first simplex, it tries to move the simplex toward the minimum. The first step in their process [11] is to identify the simplex points with the

28

highest and lowest function values. Then the simplex moves towards the minimum using three operations: reflection, expansion, and contraction.

3.2.2.1 Fuzzy Reflection

Reflecting the simplex starts by calculating the coordinates of point X_c, which is the centroid of all the simplex points except X_h (Simplex point with highest function value). A new point X_{new} will be created as a reflection of X_h along X_h-X_{cf} vector, Figure 3.2. The coordinates of the reflected point, X_{new}, will be generated using the equation 3.7.

where,

X_{cf} – shifted centroid of all the simplex points except X_h towards the lowest function

value X_l

$$X_{new} = 2X_{cf} - X_h \qquad (3.7)$$

$$X_{cf} = (1 - \theta_c)X_c + \theta_c X_i \qquad (3.8)$$

θ_c, is the output of the fuzzy logic controller or simplex reflection scaling factor, which determines the magnitude of the shift toward X_l.
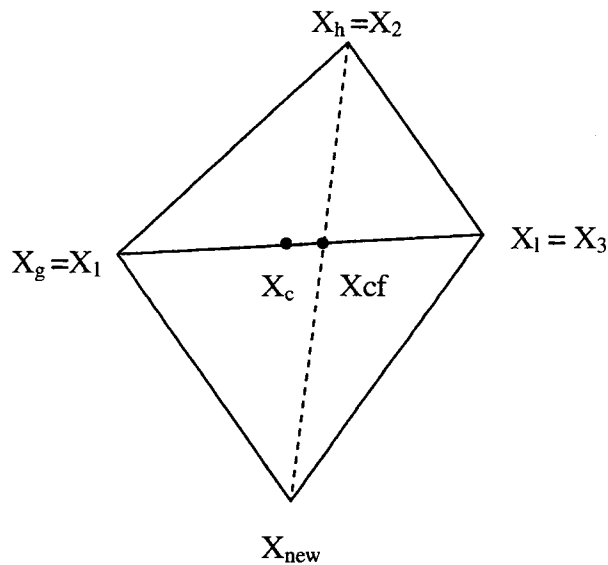
Figure 3.2 Reflection of Highest Function in Fuzzy Simplex Algorithm

29

3.2.2.2 Decision for the Simplex Movement

The function values at the simplex points along with that of the new point X_{new} will be calculated and one of these decisions is taken,

$$\begin{array}{lll} if & f(X_{new}) \leq f(X_l), & \text{\textit{Explore} exp\textit{ansion by generating }} X_{new1} \\ if & f(X_l) < f(X_{new}) \leq f(X_h), & \text{Re\textit{ place }} X_h \text{ \textit{by}} X_{new} \\ if & f(X_{new}) > f(X_h), & \text{\textit{Explore contraction by generating }} X_{new2} \end{array} \qquad (3.9)$$

The two new points described in the above equation are generated as follows,

$$X_{new1} = X_{cf} + (\theta_{ex} + 1)(X_{cf} - X_h) \qquad (3.10)$$

$$X_{new2} = X_{cf} + \theta_{co}(X_{cf} - X_h) \qquad (3.11)$$

where θ_{ex} and θ_{co} are simplex expansion and contraction scaling factors. Detailed examples of this optimization algorithm were described by Trabia & Lu in [11]. This optimization algorithm was used in the current study by defining the variables as parameters defining the FEA.

3.2.3 FEA and Programming Language

In order to establish a communication between the optimization algorithm and LS-DYNA, an interface engine in Matlab [62] was developed. This engine has the capability of accessing and editing the text file generated by LS-DYNA, as wells as sending variables back and forth from the optimization algorithm to LS-DYNA text file.

The FEA code written in text format was divided into two portions, fixed portion and variable portion.

- Fixed Code: This portion of the code contains all the information related to the given FEA model except the information related to variables of optimization. For example, if we want to optimize the contact parameters, then our fixed code will

30

have all the information related to the model except the parameters related to contact definitions. This portion of the code remains constant through out the optimization study.

- Variable Code: This portion of the code contains only the variables of optimization. For the same above mentioned example, we will have only the parameters related to contact definitions. This portion of the code will be created for each set of variables obtained from optimization algorithm.

The objective function along with the optimization variables are defined in Matlab optimization engine. With the initial values of the variables, the optimization engine creates the input text file for LS-DYNA and it runs the model, extracts the user requested data out of the run and compares it with the criteria described by user, and it creates new variable values according to the optimization algorithm and creates a new model. This iterative sequence goes repeatedly until the termination criteria set by the user in the optimization engine is satisfied. This optimization scheme was shown in Figure 3.3. Application of this optimization engine to FEA models was discussed in detail in the following chapter. Quick steps to apply optimization engine were described in Appendix M with an example.

31
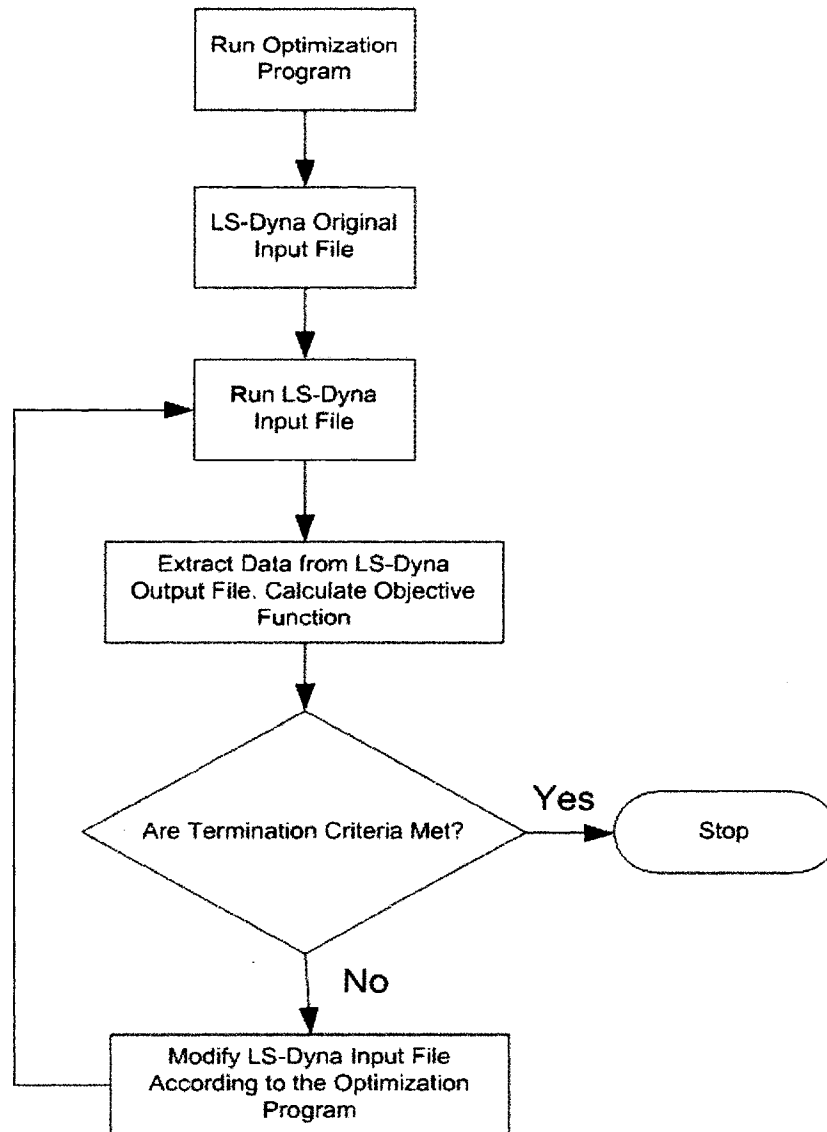
Figure 3.3 Flow Chart Showing the Optimization Scheme

CHAPTER 4

OPTIMIZATION OF COMPUTATIONAL TIME IN PROJECTILE LAUNCH EVENT

4.1 Background

Projectiles are subjected to extremely harsh environments during the launching process. Berman et al. [63] stated that projectiles are subjected to a quasi-static axial load in excess of 15,000 g's augmented by a transient load of up to 5000 g's. Use of electronic components inside projectiles (smart munitions) has been increasing recently as they have the potential of improving the precision and range of projectiles. Heaslip and Punch [53] concluded that there is a considerable evidence that a large percentage of portable electronic products fail due to impact or shock during use. Since experimental testing of smart munitions is fairly expensive and can yield information about specific locations only, developing FEA models that can accurately predict projectile launch offers an attractive alternative. However, an extremely dense FEA of a projectile and gun may consist of millions of degrees of freedom. A complete transient simulation of the launch event for such a model may take long time to execute, even with the use of parallel processing techniques. Cordes et al. [64] suggested creating a simplified model that uses shell elements for the projectile and do not include the gun. Hollis [65] developed a two dimensional quasi-static model of a training projectile. The projectile was redesigned to reduce stresses.

33

The proposed optimization approach in this research can allow the user to guide and control the direction of the modeling process. Trabia et al. [66] created FEA of a projectile and gun. The projectile was modified to include an electronic payload using brick elements. Effects of gun flexibility and friction between the gun and the projectile were included. This model was selected as the basis of this work.

The objective of this research is to apply optimization engine described earlier in "Optimization" chapter for modeling projectile launch process through the following steps:

- Developing equivalent projectile for the one presented in [66]. The equivalent projectile has a simpler geometry than the original projectile. It is used to accelerate mesh density optimization studies.

- Use optimization techniques to reduce computational time for modeling launch event of the equivalent projectile subject to acceleration accuracy constraints with respect to the corresponding results on a densely meshed model.

- Suggest appropriate mesh densities for various components based on the previous steps.

4.2 Description of the Projectile

The projectile described in [66] consists of six parts: Windshield, Nacelle, M795 Ogive, M795 Body, Plate, Electronic Payload and Band as shown in Figure 4.1. The projectile is placed within a gun barrel that is composed of three cylindrical sections with gradually reduced thickness (same inner diameter), Figure 4.2. The outer diameters of the three sections of the gun, starting from its base, are 12, 10.248, and 8 inches respectively. The

34

heights of these sections are 90.63, 84.5, and 51.49 inches respectively. The first two sections are connected using a gradually tapered section that is 5.72 inches long. Similarly, the second and third sections are connected using a gradually tapered section that is 7.66 inches long.

The projectile and the gun barrel are in contact at the surface of the band. Based on data provided by ARL (Army Research Laboratory), a 0.1 coefficient of friction between the band and the gun barrel was used. The properties for all parts were listed in Table 4.1 and Table 4.2.

The projectile and gun model is analyzed using LS-DYNA [60,61]. All presented analyses were run on double precision. Bonded contact was used between all neighboring components within the projectile. Surface to surface contact is used to simulate contact between the projectile and gun barrel.

Table 4.1 Material Properties of Projectile Parts and Gun Barrel

Part Name	Material	Specific Weight (lbf/in^3)	Young's Modulus (psi)
Windshield	Ultem 2300 (30% glass)	0.055	8.00E+05
Nacelle	Aluminum 7075-T6511	0.103	1.04E+07
Ogive, M795, Plate, Payload, Band, Gun Barrel	4030 Steel	0.283	2.90E+07

35

Table 4.2 Mechanical Characteristics of Projectile Parts and Gun Barrel

Part Name	Young's Modulus (psi)	Poisson's Ratio	Yield Stress (psi)	Tangent Modulus (psi)
Windshield	8.00E+05	0.40	24.5E+03	-
Nacelle	1.04E+07	0.33	68.0E+03	1.85E+04
Ogive, M795, Plate, Payload, Band, Gun Barrel	2.90E+07	0.32	120E+03	5.21E+04

The projectile launch event was modeled in two phases. In the first phase, the gun barrel was allowed to deflect due to gravity only. This analysis is conducted for 0.5 seconds. In the second phase of the analysis, a typical pressure-time curve, [66] was applied to the bottom part of the projectile (below the band) in presence of the initial conditions obtained from the first phase of the analysis. The pressure pushes the projectile through the deformed gun barrel for 0.0125 seconds. The projectile is out of the gun barrel by the time pressure is zero. Gravity load continues to be active in this phase. The duration of the simulation for the second phase is 0.02 seconds. Acceleration results are recorded for nodes on the projectile body and the payload.

Originally, a model with an extremely dense mesh of 51,680 elements on the gun-barrel and 9,470 elements on the projectile were created, Figure 4.2. All components have forty divisions in the tangential direction. Two divisions were created along the radial direction of the gun barrel throughout this study. PC XEON (TM CPU), 3 GHz, 2 GB RAM was used in all simulations. Simulating the motion of the projectile using the dense model takes 69,887 seconds (19.4 hours). Accelerations at selected locations were recorded at a frequency of 0.001 milliseconds. Acceleration results are filtered at 6,000

36

Hz to eliminate higher-order numerical noise as suggested in [67] using a Butterworth filter. Figure 4.5 and Figure 4.6 show acceleration results for these two nodes. These results are denoted 'Original Projectile.' The payload acceleration results show that the model was able to simulate the 'ringing' phenomenon that is observed experimentally.
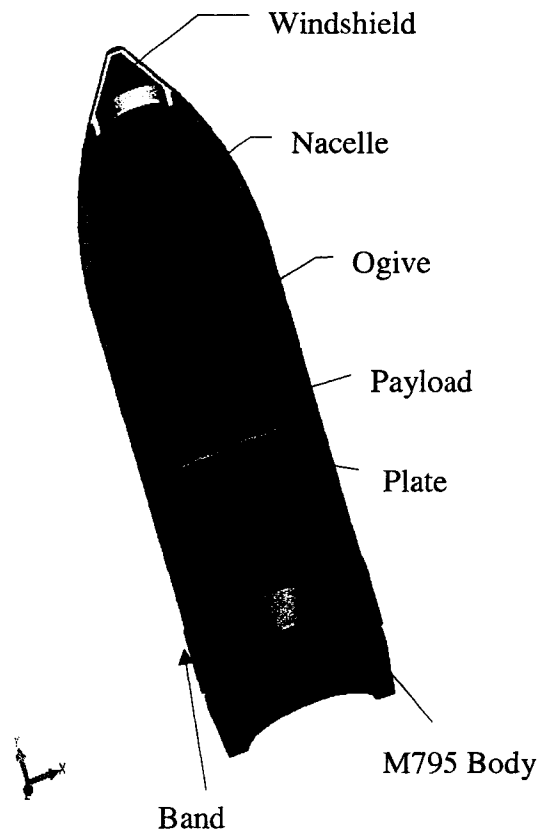
Figure 4.1 Sectional View of a Projectile

37
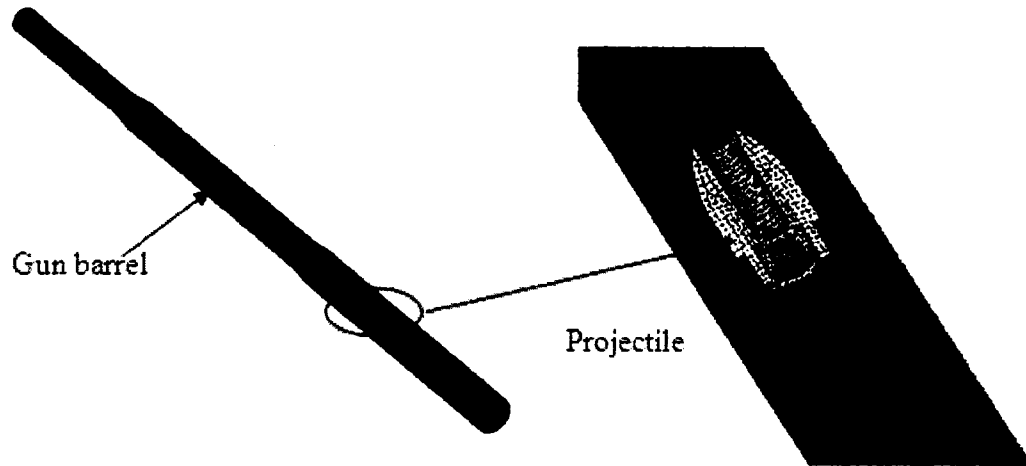
Figure 4.2 A Densely Meshed Finite Element Model of a Projectile and Gun Barrel

4.3 Optimization of FEA Computational Time for a Projectile Launch Event

To reduce the computational time, this work proposes a method for identifying proper aspect ratios for elements of various parts of the projectile-gun system while maintaining accuracy of the model. As the geometry of the projectile is complex, the search for optimal aspect ratios for its various components may be a daunting task. Instead, an equivalent projectile with simpler geometry was created to reduce the complexity of the model. Variables controlling the mesh density of this model were used within an optimization scheme to reduce computational time. During optimization search, acceleration results of equivalent projectile models were compared to the corresponding results of the densely meshed model of Section 4.2 to ensure accuracy of the model.

4.3.1 Equivalent Projectile

The projectile, Figure 4.1, was replaced with an equivalent one with simpler geometry. The equivalent projectile consisted of three cylinders, a solid one at the bottom, and two hollow cylinders in the central and top portion respectively, Figure 4.3.

38

Equivalent projectile should have the same following characteristics as the original projectile to ensure close behavior:

1. Mass (M)

2. Center of mass (C)

3. Mass moment of inertia in the axial direction (J_{yy})

4. Mass moment of inertia in a direction normal to the axis of the projectile (J_{xx})

Equations for mass, center of mass along axial direction, mass moment of inertia along axial and normal directions were written as shown in the following equations:

$$M = \frac{\rho\pi}{4}\left(t_1 d_1^2 + h\left(d_1^2 - d_2^2\right) + t_2\left(d_3^2 - d_4^2\right)\right) \tag{4.1}$$

$$C = \frac{\left(\left(d_1 t_1\right)^2 + h\left(d_1^2 - d_2^2\right)\left(2t_1 + h\right) + t_2\left(2t_1 + 2ht_2\right)\left(d_3^2 - d_4^2\right)\right)}{2\left(t_1 d_1^2 + h\left(d_1^2 - d_2^2\right) + t_2\left(d_3^2 - d_4^2\right)\right)} \tag{4.2}$$

$$J_{yy} = \frac{\rho\pi}{32}\left(t_1 d_1^4 + h\left(d_1^4 - d_2^4\right) + t_2\left(d_3^2 - d_4^2\right)\right) \tag{4.3}$$

$$J_{xx} = \frac{\rho\pi}{64}\left(\begin{matrix} t_1 d_1^4 + \frac{1}{3}h\left(d_1^2 - d_2^2\right)\left(3d_1^2 + 3d_2^2 + 4h^2\right) + \\[2mm] \frac{1}{3}t_2\left(d_3^2 - d_4^2\right)\left(3d_3^2 + 3d_4^2 + 4t_2^2\right) + \\[2mm] 16t_1 d_1^2\left(C - \frac{t_1}{2}\right)^2 + 16h\left(d_1^2 - d_2^2\right)\left(C - t_1 - \frac{h}{2}\right)^2 + \\[2mm] 16t_2\left(d_3^2 - d_4^2\right)\left(C - t_1 - h - \frac{t_2}{2}\right)^2 \end{matrix}\right) \tag{4.4}$$

where

ρ – Density of steel

t_1, t_2, h, d_1, d_2, d_3, d_4 are the lengths and diameters for the three cylinders as shown in Figure 4.3.

39

Table 4.1 and Table 4.2 show that most of the parts in the original projectile were made of steel. Therefore, all three cylinders of the equivalent projectile were assumed to be made of steel. The above four equations have seven variables. For a realistic equivalent projectile model, it is specified that this model should have the same outer diameter as the original projectile, d_1 (6.1 inches). Additionally, t_1 and d_2, Figure 4.3, are assigned values of 1.5 inch and 3.5 inch respectively. The remaining four equations were solved simultaneously to obtain the values of t_2, d_3, d_4, and h. Table 4.3 lists the values of these four variables.

Table 4.3 Variables of the Equivalent Projectile Geometry

t_2 (in.)	d_3 (in.)	d_4 (in.)	h (in.)
3.92	5.02	1.02	10.66

The band on the projectile was not accounted for in the equivalent projectile model. A band similar to that in Figure 4.1 was added to the equivalent projectile. Distance between the center of mass and the band was maintained as in the original model.

40
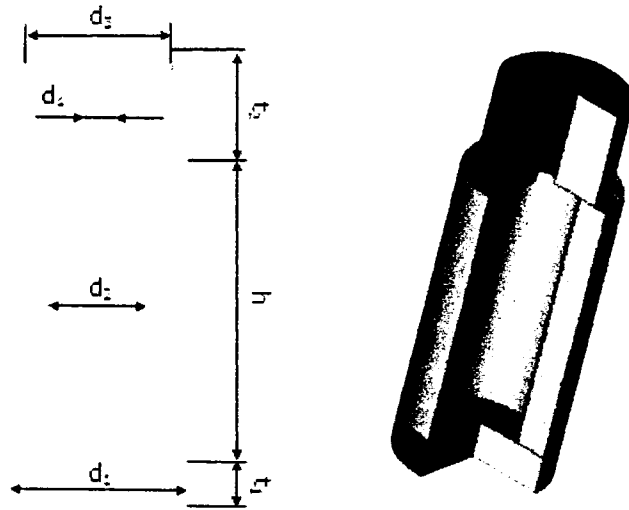
Figure 4.3 Front and Sectional Isometric Views of the Equivalent Projectile

The equivalent projectile model was meshed using elements of relatively the same size, Figure 4.4. Forty divisions were maintained in the tangential direction as discussed in Section 4.2. The mesh of the gun barrel was maintained as shown in Figure 4.2. The band has one element in the radial direction. Elements of the band in the axial direction match the neighboring ones on the projectile.

41
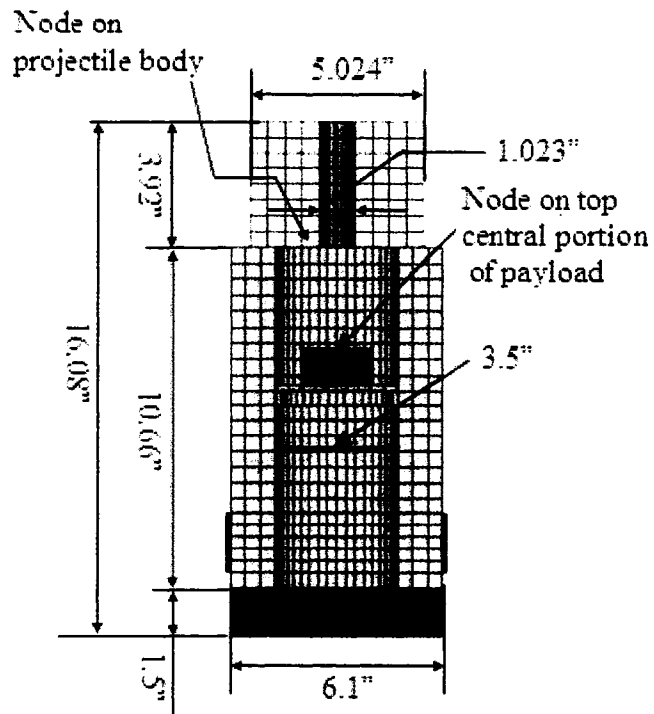
Figure 4.4 Sectional View of the Finite Element Model of the Equivalent Projectile

The equivalent geometry has 51,680 elements on gun-barrel and 6,000 elements on projectile. Computational time is of the same order as the original model. Resultant accelerations, measured at two locations on the projectile body and payload as indicated in Figure 4.4, were shown in Figure 4.5 and Figure 4.6 respectively. While the overall accelerations were matched, peak accelerations at both locations are less for the equivalent model by about 15%. The equivalent model also failed to capture acceleration 'ringing' that payload experiences after the projectile leaves the gun barrel.

42
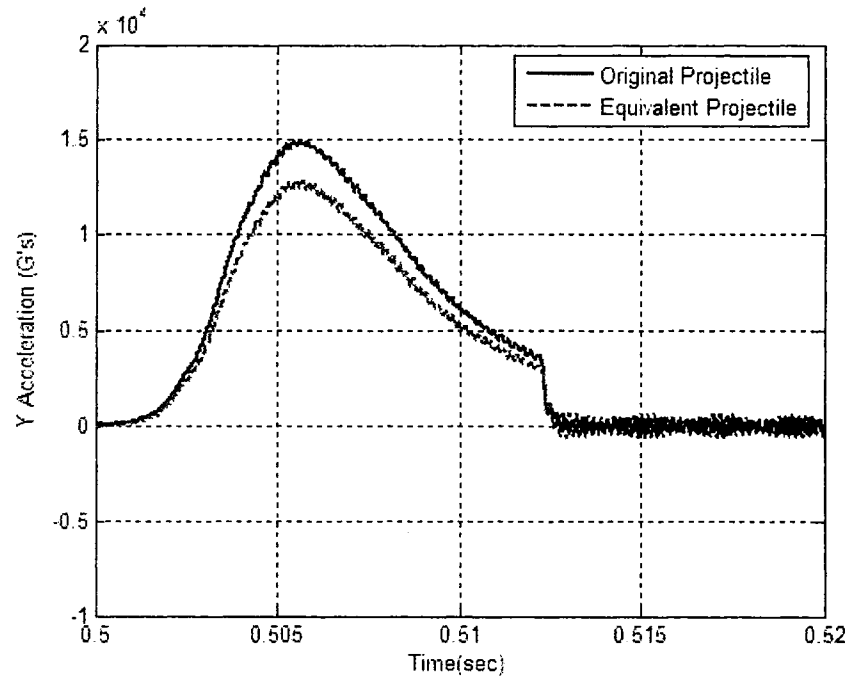
Figure 4.5 Axial Acceleration for a Node Located on the Projectile Body (Filtered at 6000Hz)
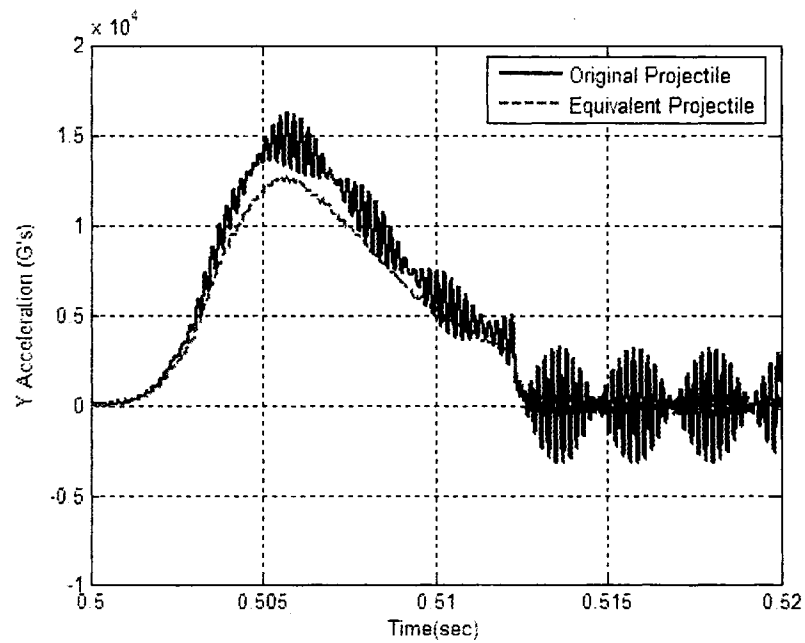
Figure 4.6 Axial Acceleration for a node located on the payload (Filtered at 6000Hz)

43

The following measure was proposed to compare accelerations produced by two different models for the same location:

$$A = \frac{\sum_{i=1}^{n}\left(A_{E_i} - A_{P_i}\right)^2}{\sum_{i=1}^{n}\left(A_{P_i}\right)^2} \qquad (4.5)$$

where

A - Acceleration relative difference measure

A_P – Acceleration of a node on the initial projectile model

A_E – Acceleration of the corresponding node on the equivalent projectile model

n – Number of data points

Comparison of values of A for a node on the projectile body and a corresponding node on the payload for the original projectile and the equivalent one were listed in Table 4.4. This tells the results of the equivalent projectile are with in 2.4 and 4.8% of actual projectile results for nodes on projectile body and payload respectively.

Table 4.4 Acceleration Relative Difference Measure for the Original Projectile and the Equivalent Projectile Models

Node Location	Acceleration Relative Difference Measure
Projectile Body	0.024
Payload	0.048

4.3.2 Optimization of the Equivalent Projectile Mesh Density

The geometry of the equivalent projectile of the previous section and the gun barrel are divided into several cylinders. For the equivalent projectile, these cylinders (starting from the bottom of the projectile) are:

- Bottom Cylinder (solid)

- Below-Band Cylinder

- Adjacent-To-Band Cylinder

- Above-Band Cylinder

- Below-Supporting-Plate Cylinder

- Ogive Cylinder

- Nacelle Cylinder

All these cylinders were hollow except for the first one. The variables of the optimization problem were the number of elements assigned to the variables of each of these cylinders as shown in Figure 4.7. These variables describe the number of elements on the axial, tangential, and radial direction of each primitive.

The number of elements on the radial direction of the gun is fixed to two for all cylinders of the gun. The number of elements in the radial and axial directions on the Bottom Cylinder of the equivalent projectile is fixed to five and two elements respectively as preliminary study showed that the problem is not sensitive to variations of these two variables. Number of elements in the axial direction of the Below-Band Cylinder and Below-Supporting-Plate Cylinder is fixed to one element because of their limited height. The mesh of the band is generated according to the discussion of the previous section.

45
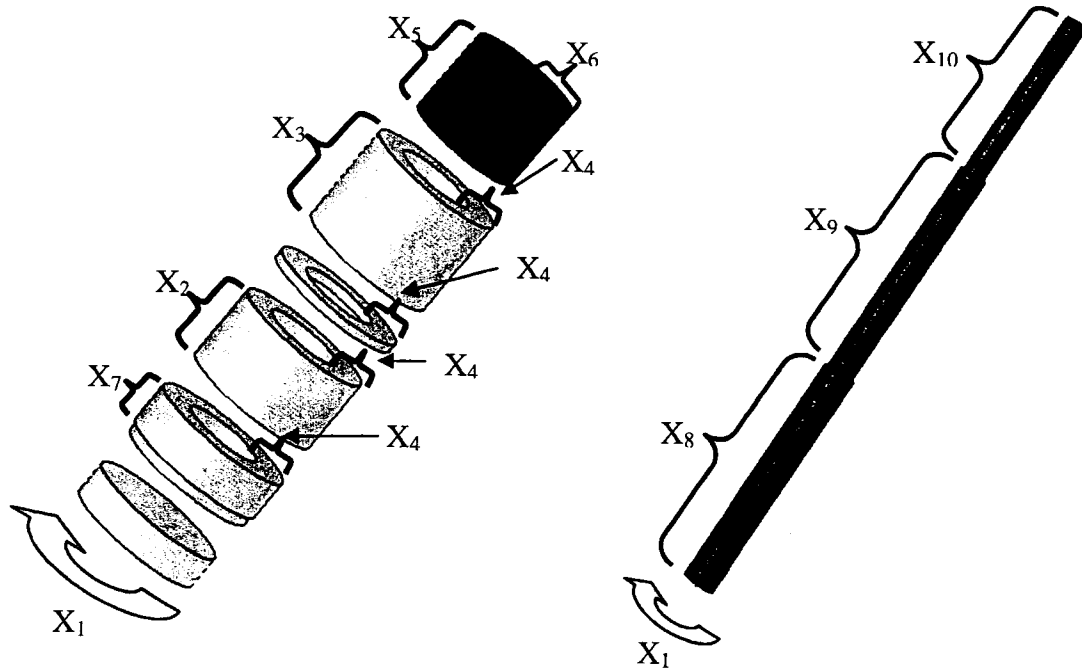
Figure 4.7 Optimization Variables

The objective of the optimization problem is to minimize computational time (T) by varying the mesh densities on the above-mentioned cylinders. The problem is subject to the following constraints:

$$A \leq 0.05 \qquad (4.6)$$

$$15 \leq x_i \leq 30 \qquad (4.7)$$

$$2 \leq x_i \leq 6 \qquad i = 2,3,\ldots..6 \qquad (4.8)$$

$$2 \leq x_i \leq 4 \qquad (4.9)$$

$$3 \leq x_i \leq 6 \qquad (4.10)$$

$$80 \leq x_i \leq 160 \qquad (4.11)$$

$$70 \leq x_i \leq 140 \qquad (4.12)$$

46

$$40 \leq x_i \leq 80 \tag{4.13}$$

For the sake of uniformity, these constraints were formulated as,

$$g_i \geq 0 \qquad i = 1,2,\ldots\ldots\ldots 21 \tag{4.14}$$

The constraints were incorporated in the objective function using penalty terms. The modified objective function was,

$$\text{minimize,} \qquad F = T + \sum_{i=1}^{m} \Omega_i \tag{4.15}$$

if $g_i \leq 0 \quad \Omega_i = R g_i^2$
if $g_i > 0 \quad \Omega_i = 0$

R is a penalty parameter, whose value was 10^{10}.

The FEA text file format is divided into two portions:

- Fixed portion: This portion of the code contains information such as, material characteristics, output control cards, and load history.

- Variable portion: This portion of the code contains the nodal and element information for the gun barrel and equivalent projectile components. This portion creates a parametric mesh that is function of the problem variables. This program correlates the element information on neighboring components to define the proper contact between them as well as boundary conditions.

The optimization process starts by generating the variable portion of the code for the initial guess within MATLAB. This portion of the code was combined with the fixed portion of the code to create the LS-DYNA input file. This input file was run within MATLAB environment. A MATLAB program then extracts relevant results from the output file of LS-DYNA. Similar optimization scheme as discussed in optimization chapter was followed.

47

The initial simplex was created according to Spendley et al. [9] by generating n equally-spaced points with respect to an initial guess, x_0, according to the following equation,

$$x_i = x_0 + \delta_1 U_i + \sum_{j=1, j \neq i}^{n} \delta_2 U_j \qquad (4.16)$$

where,

$$\delta_1 = \frac{\sqrt{n+1} + n - 1}{n\sqrt{2}}$$

$$\delta_2 = \frac{\sqrt{n+1} - 1}{n\sqrt{2}} \qquad (4.17)$$

In this research, U_1 through U_7 were equal to 2 while U_8 through U_{10} were equal to 15 due to the variation of the ranges of the variables.

A total of 248 function evaluations were evaluated during the process of optimization. Computational time was reduced from 27,084s to 5,428s. Correspondingly, the total number of elements was reduced from 28,950 to 11,145. Acceleration relative difference measure was changed from 0.006 to 0.0067 by the end of the search. The strongest contributing factor to this improvement is reduction of the number of elements in the tangential direction from 30 to 15. The only variable that remains unaffected by the optimization search is x_7 (number of elements in the axial direction of the Adjacent-To-Band Cylinder). Otherwise, all components on the projectile have coarser mesh as shown in Figure 4.8 and Figure 4.9. The Ogive Cylinder and the tip section of the gun experience the most significant reduction in the number of elements.

48
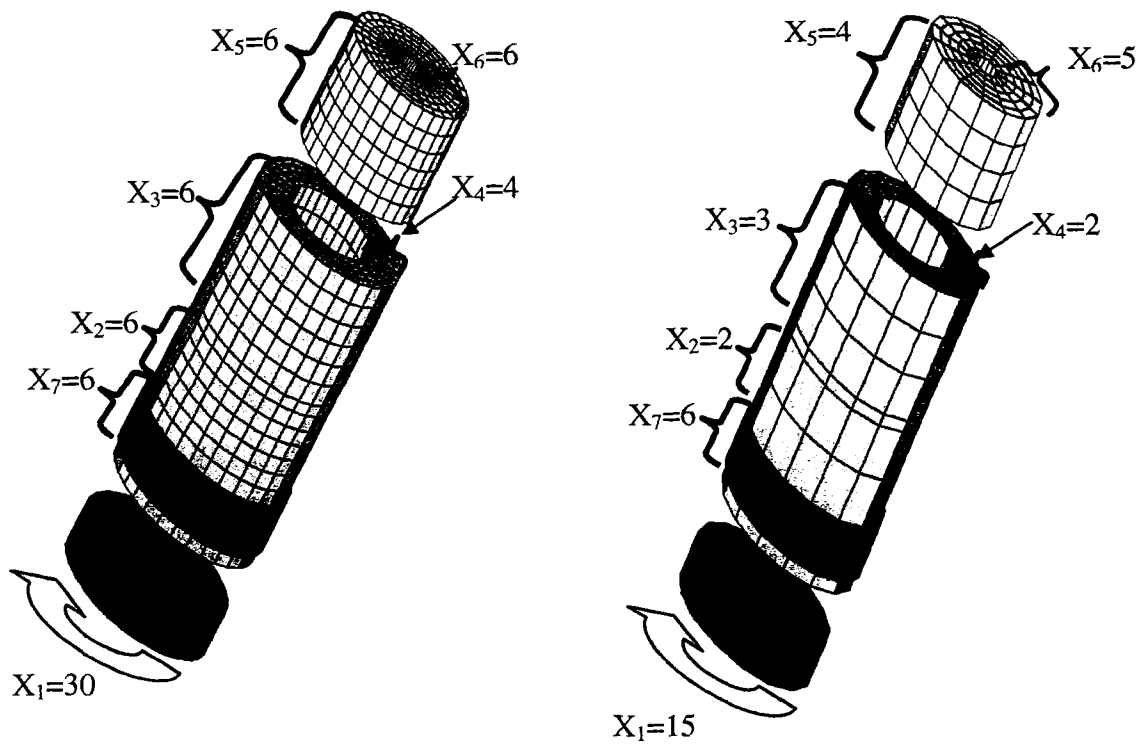
Figure 4.8 Equivalent Projectile Before and After Optimization
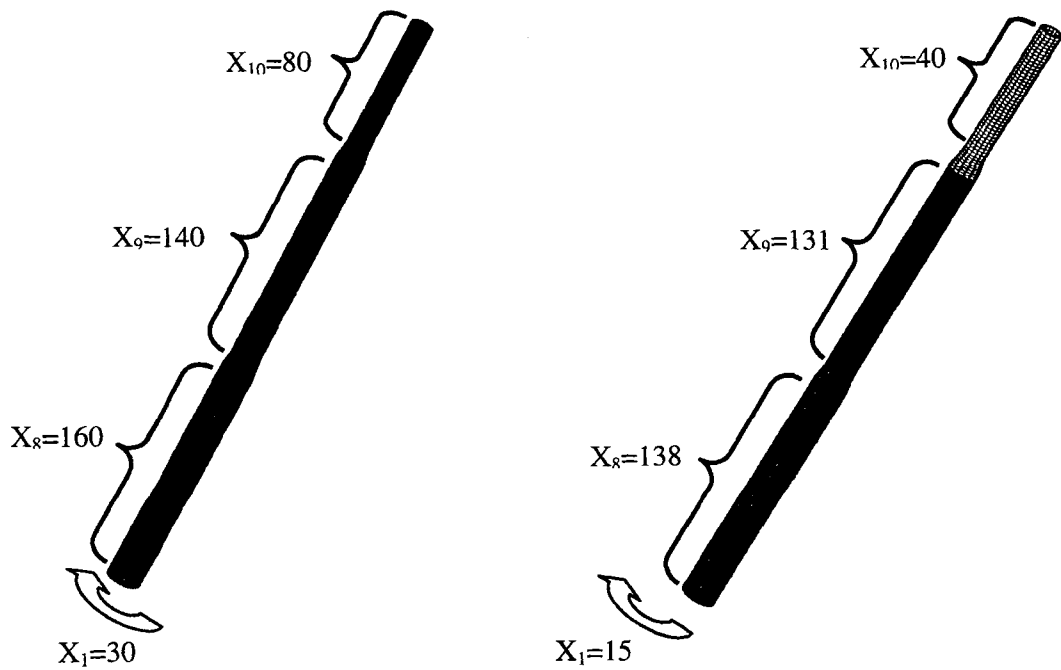
Figure 4.9 Gun-Barrel Before and After Optimization

49

4.4 Application of Optimization Results to the Original Projectile Model

The optimization search results were used to reach recommendations for the aspect ratio of solid elements on hollow cylindrical objects that are subjected to shock environments. Aspect ratio of the solid elements describing a cylinder can be obtained by comparing the ratio between the length of each of the three parameters describing the cylinder (axial length, radial thickness, and inner circumference) with respect to the number of elements in each direction, Figure 4.10. The ratio between them can be described as follows,

$$\frac{L_1}{N_1} : \frac{L_2}{N_2} : \frac{L_3}{N_3} \qquad\qquad (4.18)$$
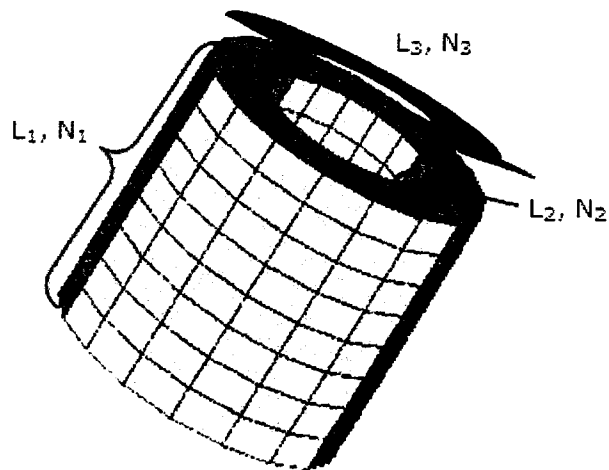
Figure 4.10 Aspect Ratio Parameters for a Hollow Cylinder

Where,

L_1 – Length along axial direction

N_1 – Number of divisions along axial direction

L_2 – Length along radial direction

50

N_2 – Number of divisions along radial direction

L_3 – Length along circumferential direction

N_3 – Number of divisions along the circumferential direction

Current FE model has two types of components, stationary (gun barrel) and moving components (projectile). The aspect ratio was considered separately for each category of cylinders. Projectile consists of three hollow cylinders (with x_2, x_3, and x_5 divisions axially as shown in Figure 4.8) while gun barrel also consists of three hollow cylinders (with x_8, x_9, and x_{10} divisions axially as shown in Figure 4.9).

By fixing the number of elements in the tangential direction to 15, the above equation reduces to,

$$\frac{L_1}{N_1} : \frac{L_2}{N_2} \quad\quad\quad (4.19)$$

Equation (4.19) was modulated by including the volume effect when calculating the recommended aspect ratio for meshing moving and stationary components. Therefore, the average aspect ratio can be expressed as,

$$AR = \frac{\sum_{i=1}^{k}\left(\frac{L_{1_i}}{N_{1_i}} \frac{N_{2_i}}{L_{2_i}}\right)v_i}{\sum_{i=1}^{k}v_i} \quad\quad\quad (4.20)$$

where,

AR – Average axial to radial aspect ratio modulated by volume

v_i – Volume of the ith component

k - Total number of components

Using Equation (4.20), the average aspect ratio for cylinders of the projectile is found to be equal to 2.44. Applying a similar approach to the gun barrel, results in an average aspect ratio of 0.71. This value increases the total number of elements as it has the

51

highest length to thickness ratio of the three cylinders. Therefore, an average value of 0.52 is calculated for the two base sections of the gun barrel. The number of elements in the axial section of the tip section of the gun is left as 40.

The original geometry of projectile and gun barrel was meshed using these values. A model with these aspect ratios was labeled 'Optimized Mesh Model' in the remainder of this work. These average aspect ratios were applied to the components of the projectile and gun barrel while maintaining the number of elements in the tangential direction. The number of elements of the plate and payload in the axial and radial directions was maintained as in the original model.

The number of elements was reduced from 51,680 to 8,310 in the gun barrel and from 9,470 to 1,440 in the projectile. Computational time was reduced from 69,887 seconds (19.4 hours) for the original densely meshed model to 3,496 seconds (0.97 hours) for the Optimized Mesh Model. The original dense mesh and the Optimized Mesh Model were shown in Figures 4.11 and 4.12 respectively. The new model was simulated to study the effects of the new mesh density.

52

Dense Mesh model   Optimized Mesh Model
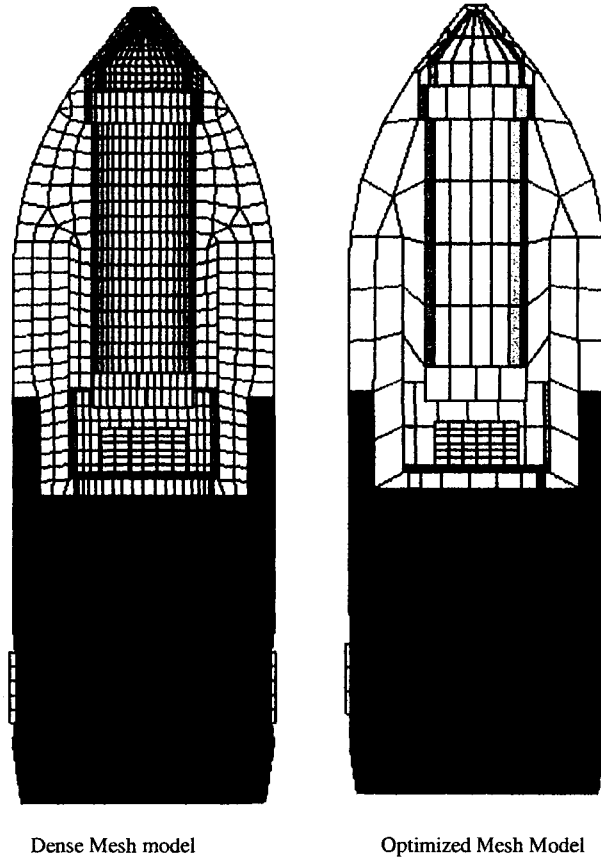
Figure 4.11 Original and Optimized Mesh of the Original Projectile

Dense Mesh model   Optimized Mesh Model
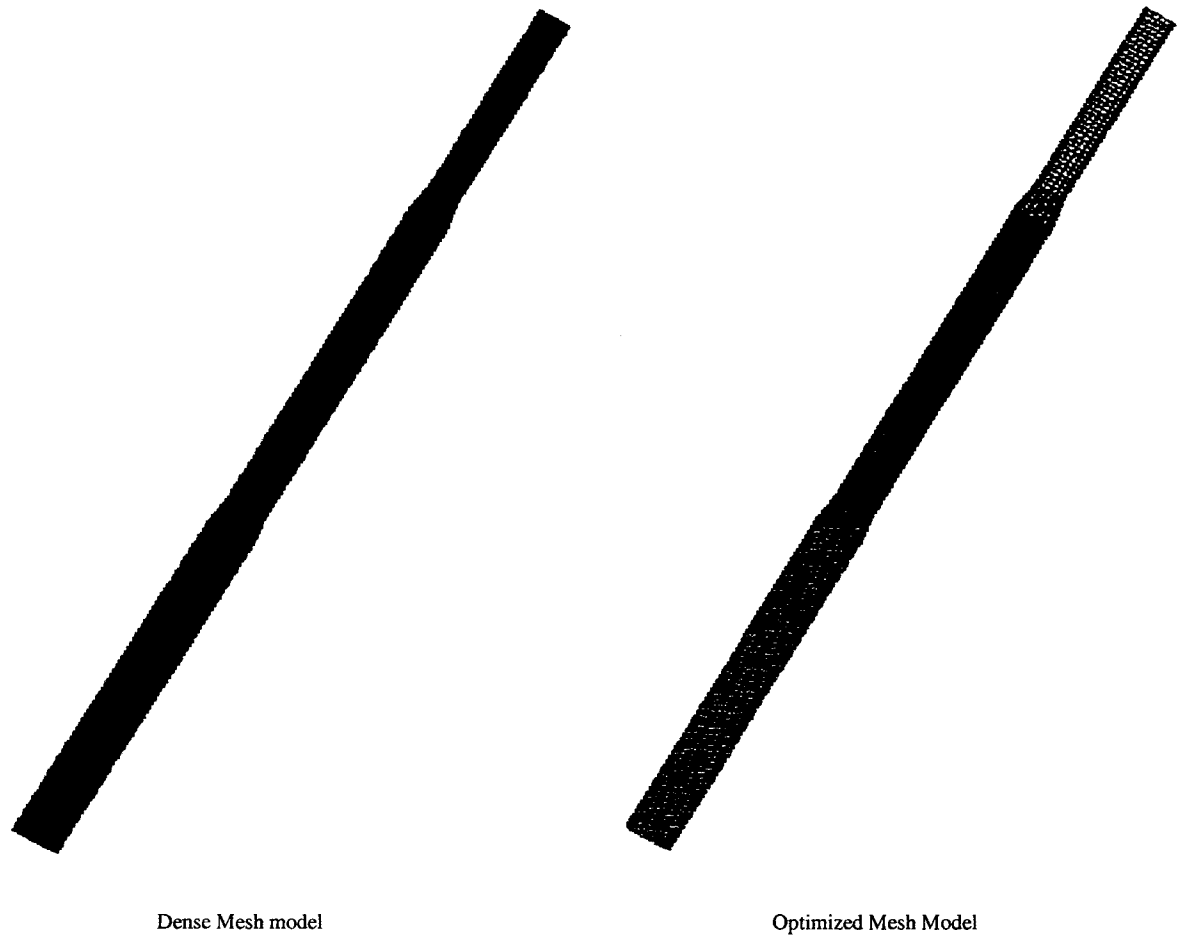
Figure 4.12 Original and Optimized Mesh on Gun Barrel

Axial acceleration (filtered at 6,000 Hz) for nodes on projectile body and payload using the original dense mesh and final results of optimization search were plotted in Figure 4.13 and Figure 4.14 respectively. The model that uses the recommended aspect ratio has the same peak acceleration as the original densely meshed model. Figure 4.14 also shows that the final model can capture the acceleration 'ringing' phenomenon that was observed experimentally. The relative difference measures between these curves were listed in Table 4.5.

54
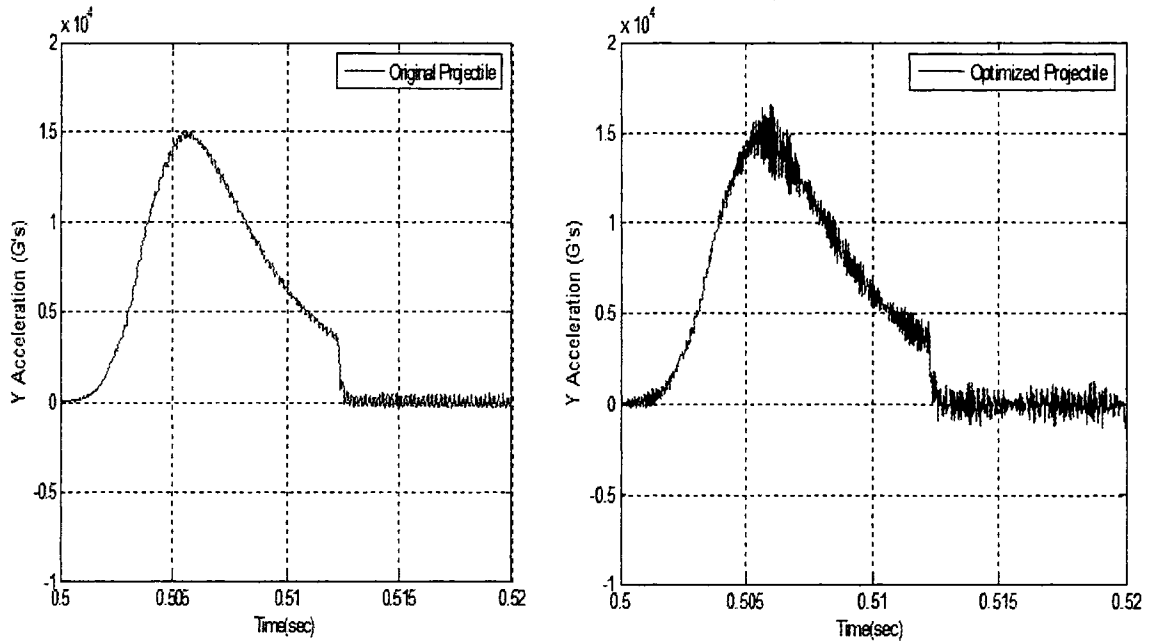
Figure 4.13 Axial Acceleration of a node Located on Projectile Body (Filtered at 6000 Hz)
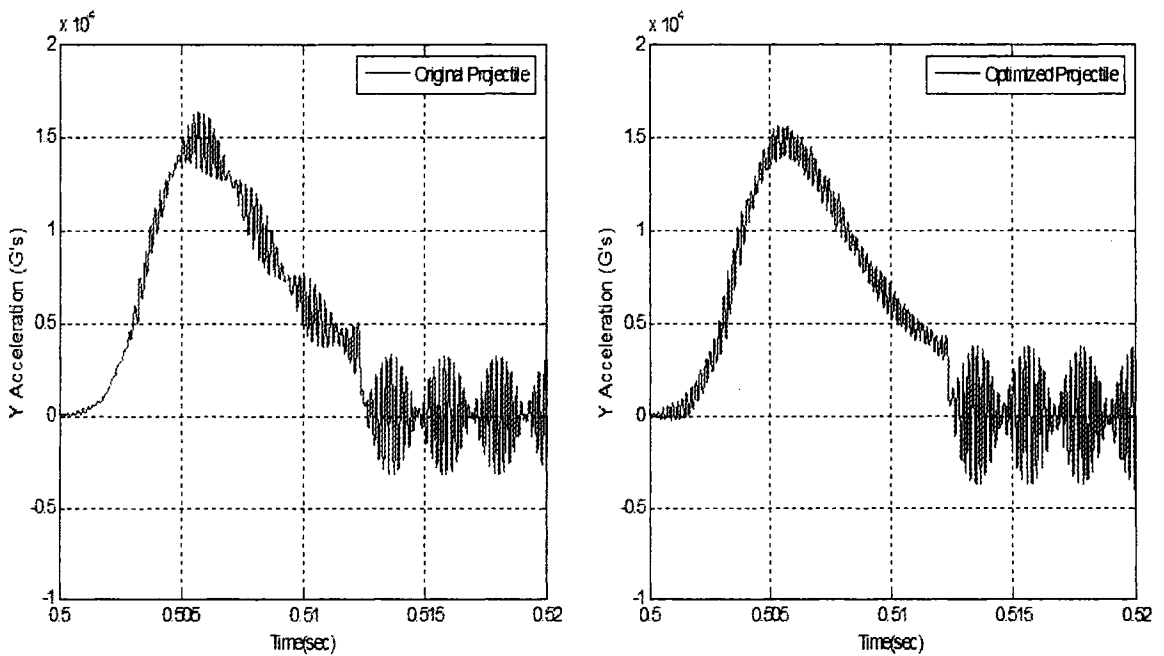
Figure 4.14 Axial Acceleration of a Node Located on Payload (Filtered at 6000 Hz)

55

Table 4.5 Acceleration Relative Difference Measure for the Original Projectile Model and the Optimized Projectile Model

Node Location	Acceleration Relative Difference Measure
Projectile Body	0.005
Payload	0.054

4.5 Conclusions and Observations

Finite element modeling of the projectile launch event is complex and computationally expensive. This research presents an approach to model this problem at a significantly faster rate through optimizing mesh density of a simplified equivalent projectile. A finite element model for a projectile behavior under shock load that includes the gun flexibility and friction between the gun and the projectile was used. A densely meshed version of this model requires 19.4 hours of computational time.

The process of reducing computational time while maintaining accuracy of the results starts by creating an equivalent projectile. This projectile shares the same mass, center of mass, mass moment of inertia in the axial direction, and mass moment of inertia in the radial direction as the original projectile. The equivalent projectile and the gun-barrel were divided into several cylinders. Optimization search was used to vary the mesh on the gun cylinders and most of the equivalent projectile cylinders with the objective of minimizing computational time. The search was subject to accuracy of resulting accelerations and dimensional constraints.

Optimization results were used to propose recommendation for meshing the projectile and gun-barrel. It was recommended to use fifteen divisions in the tangential direction for

56

both gun and projectile components. Average aspect ratios for solid brick elements in the axial and radial directions were also proposed. These ratios were 2.44 for projectile components and 0.52 for the two base sections of the gun barrel respectively. Results indicate that one can predict the shock transmitted to the components in a projectile that was meshed according to these values while reducing simulation time by a factor of almost twenty-five when compared to an extremely densely meshed model.

57

CHAPTER 5

EXPERIMENTAL PROCEDURE FOR SHOCK TESTING OF ELECTRONIC COMPONENTS

5.1 Background and Fixture Design

Impact testing is a means of imparting force and acceleration onto an item. For impact testing, an object at some velocity comes in contact to the stationary item under test. As the drop object comes into contact with the stationary object it decelerates, which imparts a force on the stationary object. Mechanical shock loading occurs in many commercial and military applications. For commercial applications, shock loads may be produced by transportation, operation in vehicles, operation in aircraft, dropping an electronic assembly and maintenance. In addition to the shock loading seen in commercial applications, military applications also have gunfire shock, missile acceleration, projectile launch shock, and spin-up accelerations.

The objective of the current research is to characterize the behavior of the circuit-board and components mounted on them, under shock/impact loading. The research outlined in this dissertation was used to develop practical assessment methodologies for circuit boards and components mounted on them under mechanical shock loading. Ground work to study the electronic components mounted on circuit-boards subjected to high acceleration loads that occur over extremely short period of time such as impact,

58

gun firing, and blast events has been laid out in this study. These shocks can be on the order of tens of G's (acceleration of gravity) to hundreds of G's. To predict failures, an experimental scheme has been developed. In order to subject portion of the board to constant moment, a four-point bending approach was used. ASTM (American Society for Testing and Materials) standard D6272 [68], was followed in performing these tests.

A configuration of one-third span described in [68] was as shown in Figure 5.1. Where 'L' is the support span and 'P' is the applied load. Test fixture was designed in solid works according to the above mentioned standards. It consists of three basic components: base plate (Figure 5.2), support (Figure 5.3), and impactor (Figure 5.4). The assembled view of these components in solid works was as shown in Figure 5.5. According to the dimensions shown in figures all the components of the fixture were machined using Haas VF5 CNC (computer numerically controlled) machine. 4140 alloy steel was used as a material for fixture components.
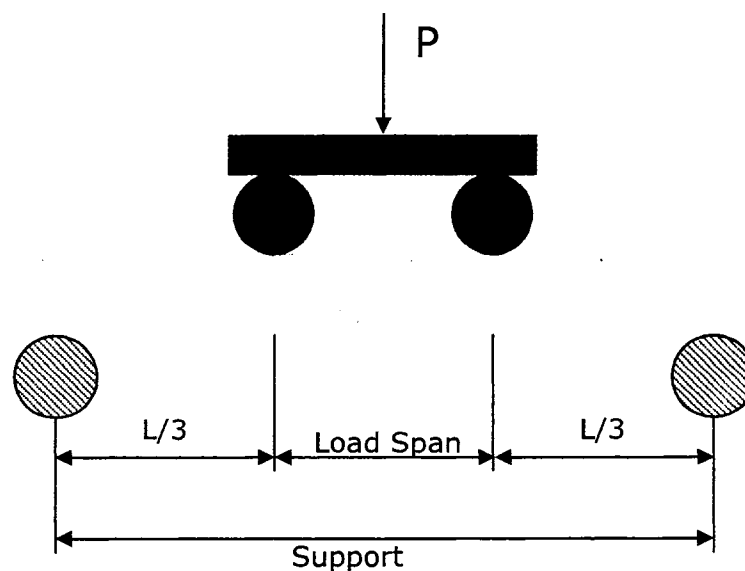
Figure 5.1 Typical Four Point Bending Set-up

59
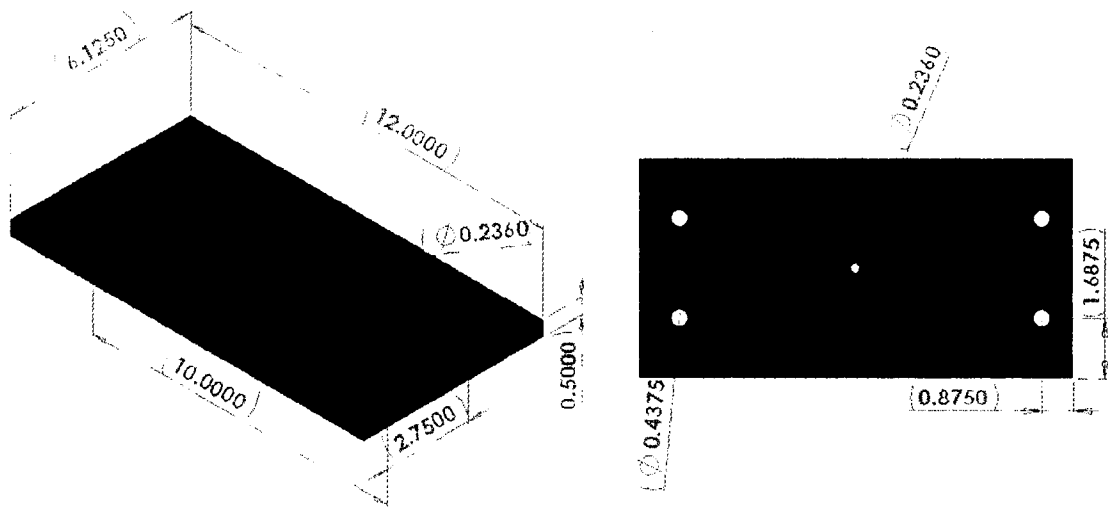
Figure 5.2 Base Plate with Dimensions (in)
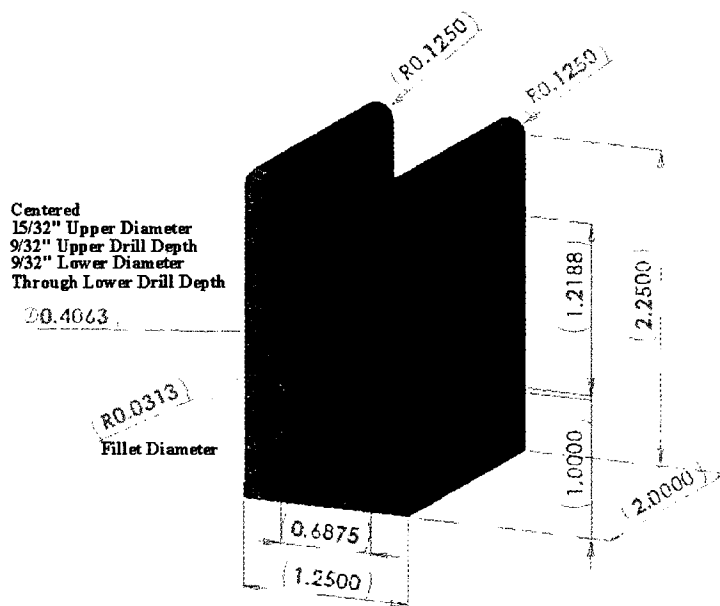
Figure 5.3 Support with Dimensions (in)

60
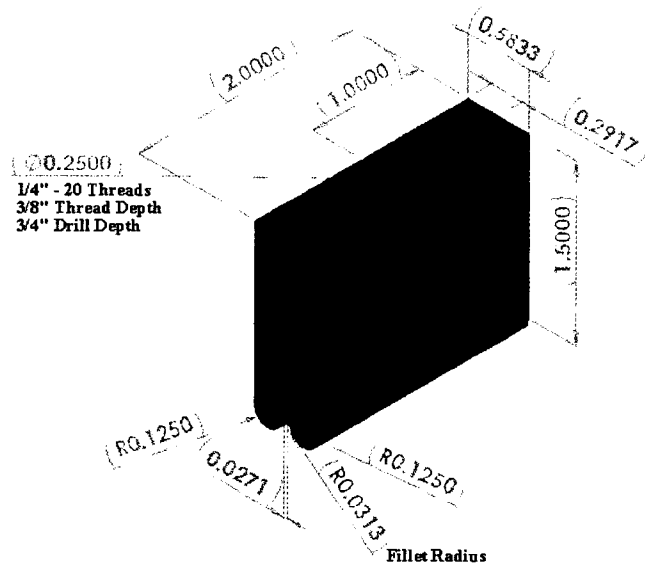
Figure 5.4 Impactor with Dimensions (in)
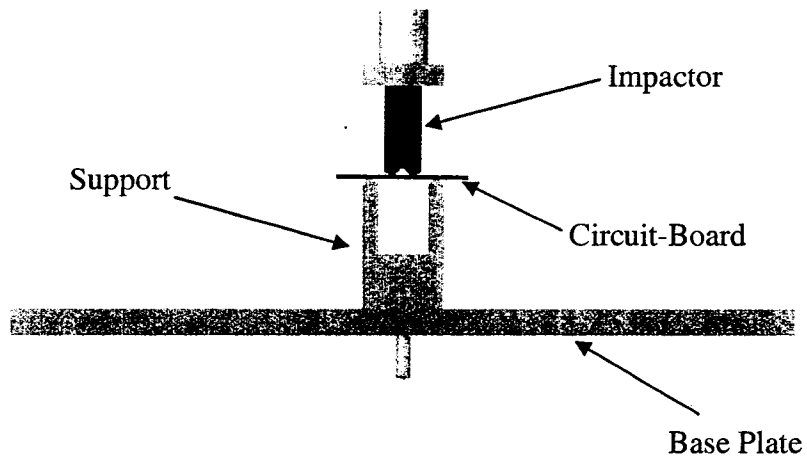
Figure 5.5 Assembled View of Fixture

To determine the strain rate dependency on the performance of the boards, it was

decided to test the boards at various levels of strain rate. In order to achieve very low

strain rates quasi-static testing was considered, and to achieve higher strain rates dynamic

61

testing was considered. To study the effect of components mounted on the boards, 1206 surface mount 0.15Ω resistors were mounted on the boards.

5.2 Dynamic Testing

To have the repeatable and controlled impact, Dynatup Instron 8250 drop weight impact tower was used as test equipment for performing the impact tests. Assembled fixture components inside the test equipment were shown in Figure 5.6.
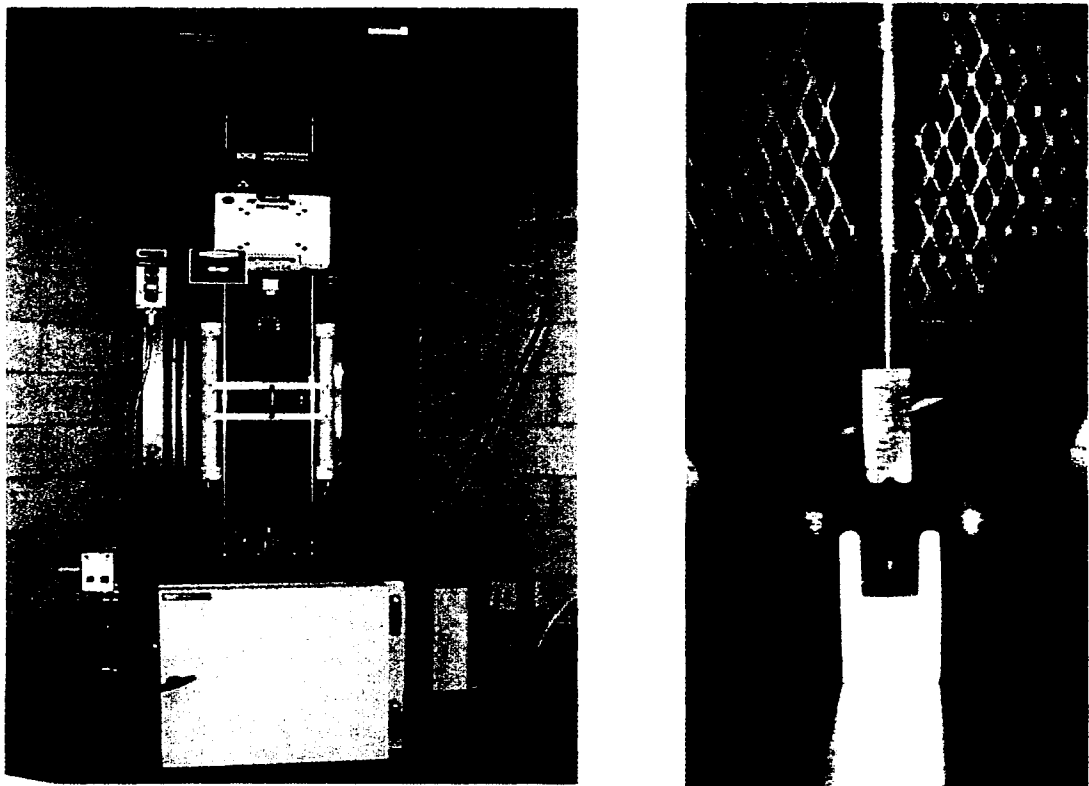
Figure 5.6 Dynatup Instron 8250 Drop Weight Impact Tower and Assembled Fixture

FR-4 circuit boards blank as well as boards with components (Figure 5.7) with six inches by two inches in dimension were used as the test specimens. A 350Ω resistance strain gage was mounted on the central lower portion of the specimens in order to acquire the

62

strain data. A PCB Piezotronics force transducer (Model: 200M70) (Figure 5.8) was placed below the support portion of the fixture from which the force input was acquired by dropping the weight. This force transducer was connected to the PCB signal Conditioner (Model: 482A21) as shown in Figure 5.9. The output of the conditioner was captured using the DL 750 scope corder oscilloscope (Figure 5.10). Strain gage data was acquired using a 2310A signal conditioning Amplifier (Figure 5.11). The calibration procedure for this signal conditioner was discussed in detail in Appendix A. The output from this conditioner was also captured using the DL 750 scope corder oscilloscope.
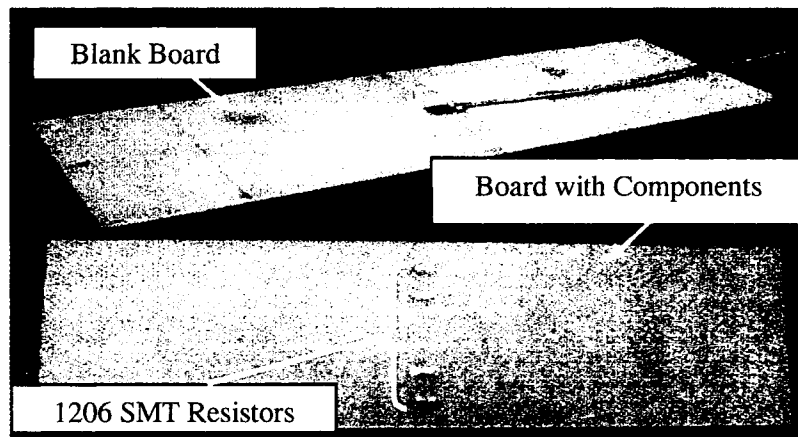
Figure 5.7 FR-4 Circuit-Board (Test Specimen)

Figure 5.8 PCB Piezotronics (Model: 200M70) Force Transducer
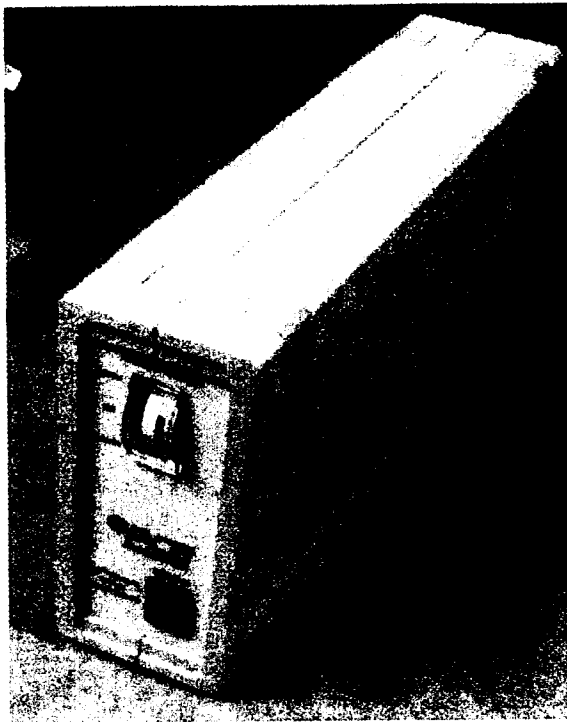
Figure 5.9 PCB Signal Conditioner Model: 482A21
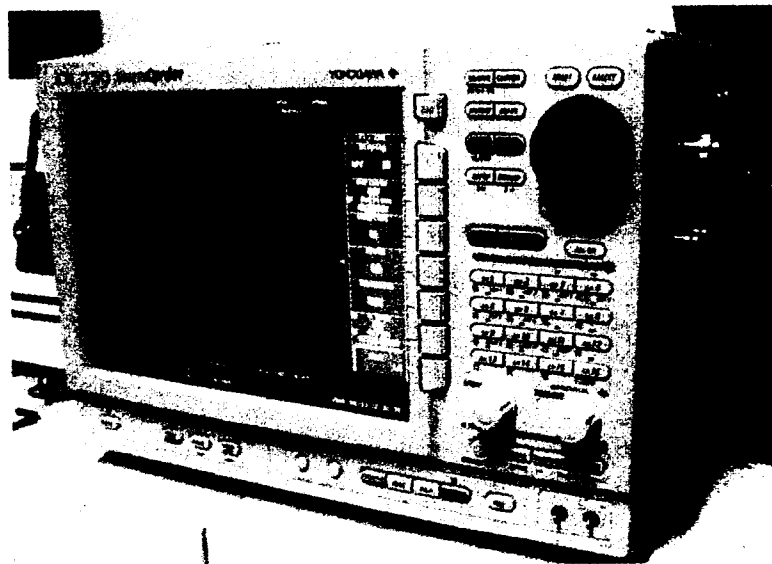
Figure 5.10 DL 750 Scope Corder Oscilloscope

64
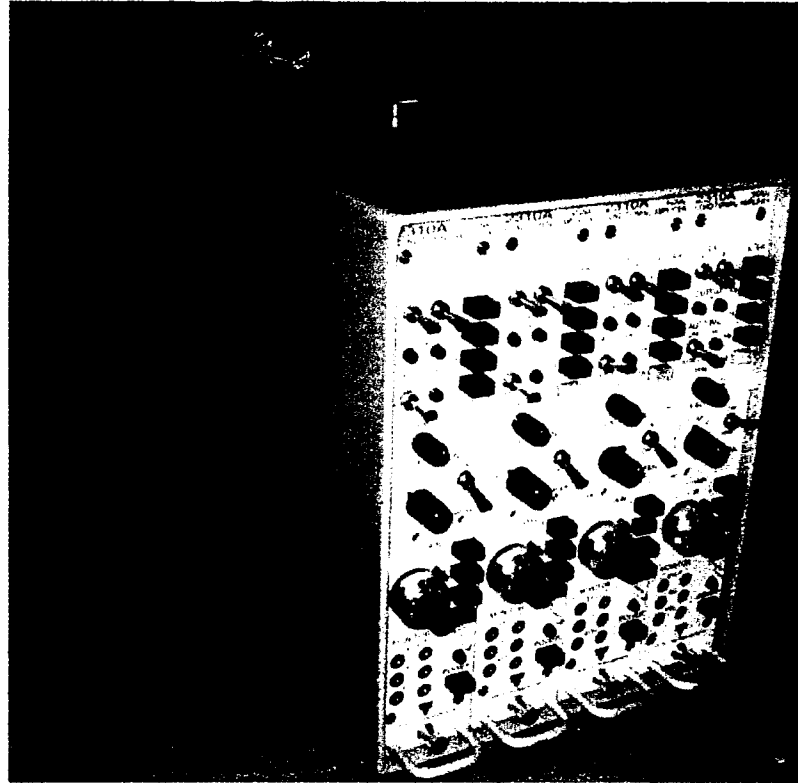
Figure 5.11 2310 A Signal Conditioning Amplifier

Experimental set-up for this dynamic testing was as shown in Figure 5.12. Zoomed view of the fixture and specimen along with force transducer was shown in Figure 5.13. For this study smallest weight of 5.27lbs was used at different heights to achieve different strain rates. Sampling rate of 500Ks/s was used in all the test cases for data acquisition. Testing was conducted at various heights as described in Table 5.1. Three samples were tested for each drop height in order to check for the repeatability of the test. The force and strain plots obtained from three samples of each drop height were shown from Figures 5.14 through 5.19.

65
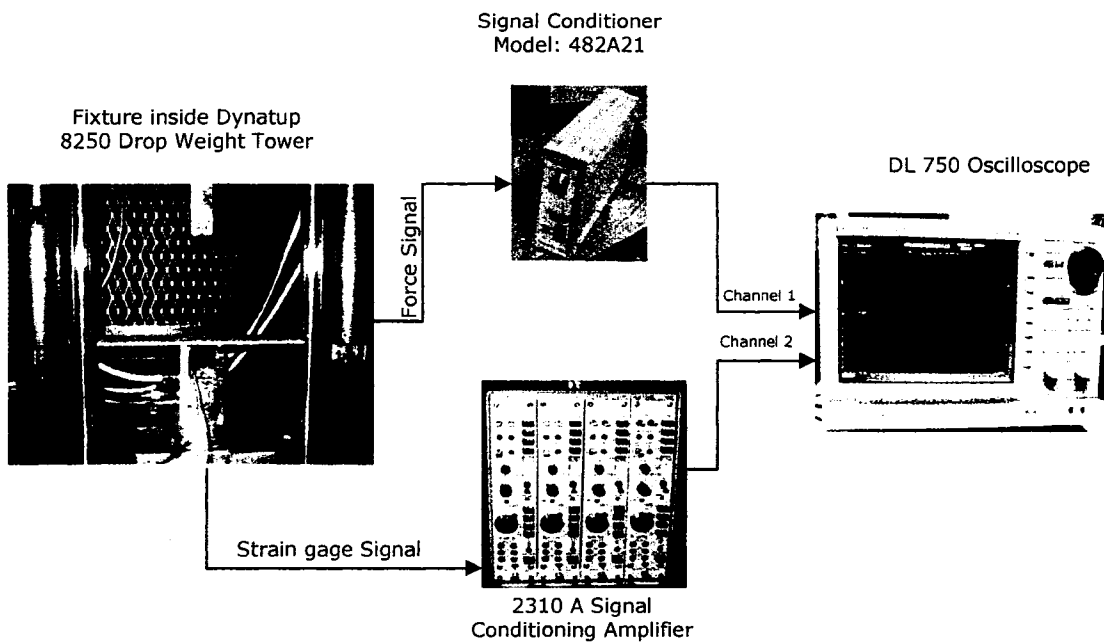
Figure 5.12 Experimental Set-up for Dynamic Testing
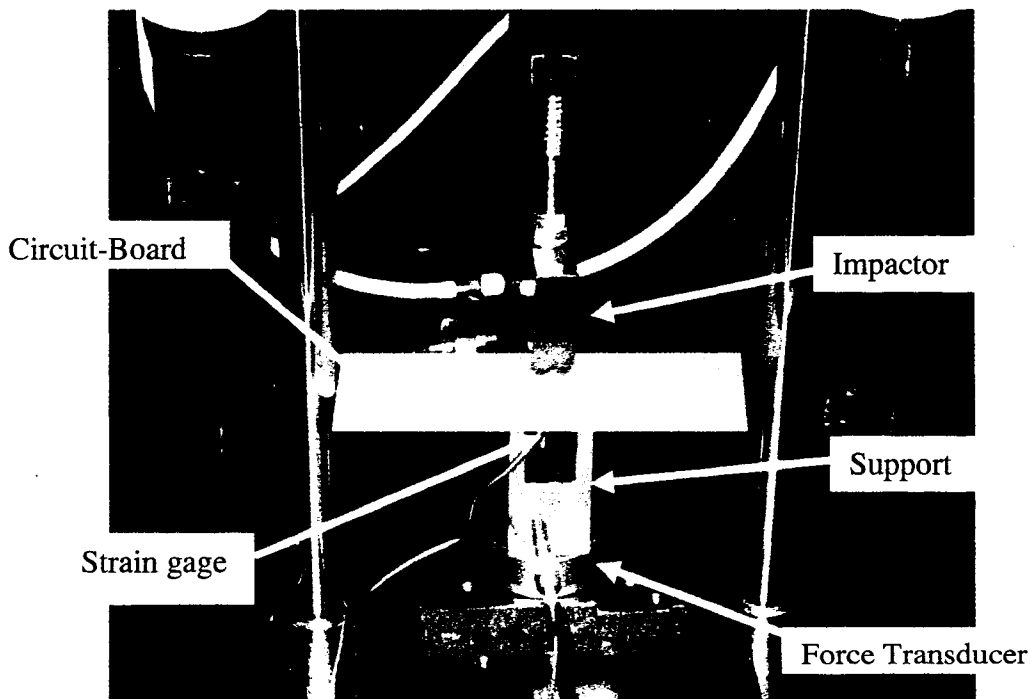
Figure 5.13 Zoomed View of the Specimen, Fixture, and Force Transducer

66

Table 5.1 Test Matrix for 6"x2" Specimens

Description	Dynamic Testing		
Drop Height (inches)	1.06	3	5
Number of Blank Boards	3	3	3
Number of Boards with Components	3	3	3
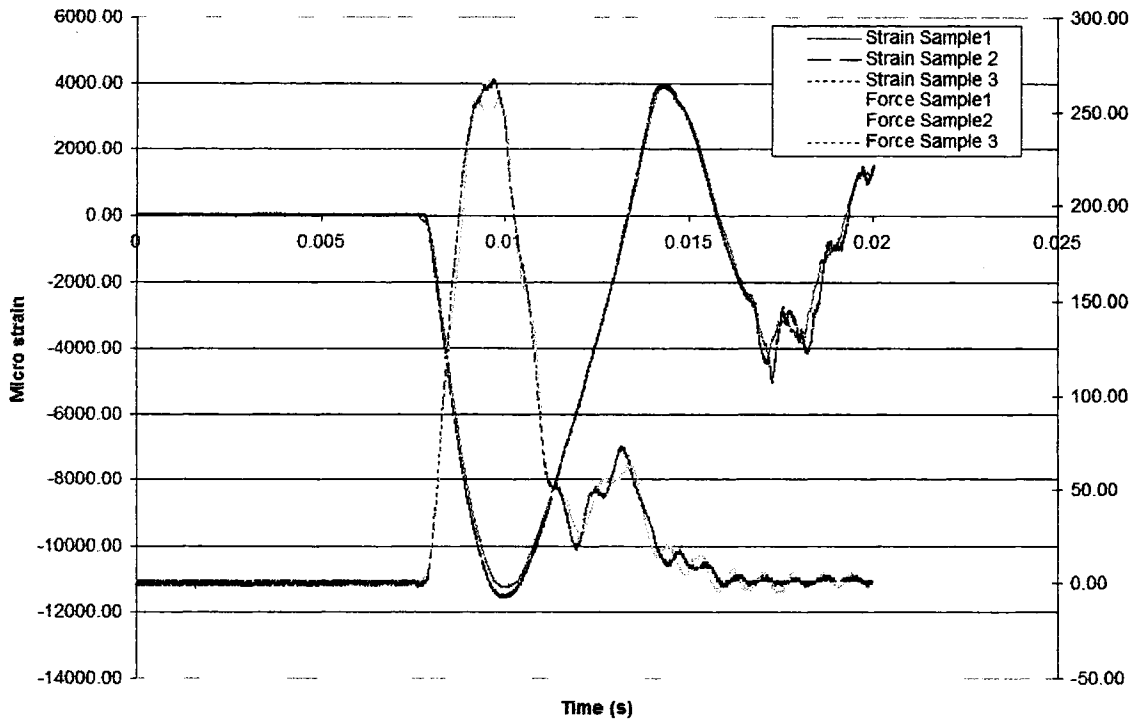
Figure 5.14 Test Data for 6"x2" Blank Boards at Drop Height of 1.06"

67
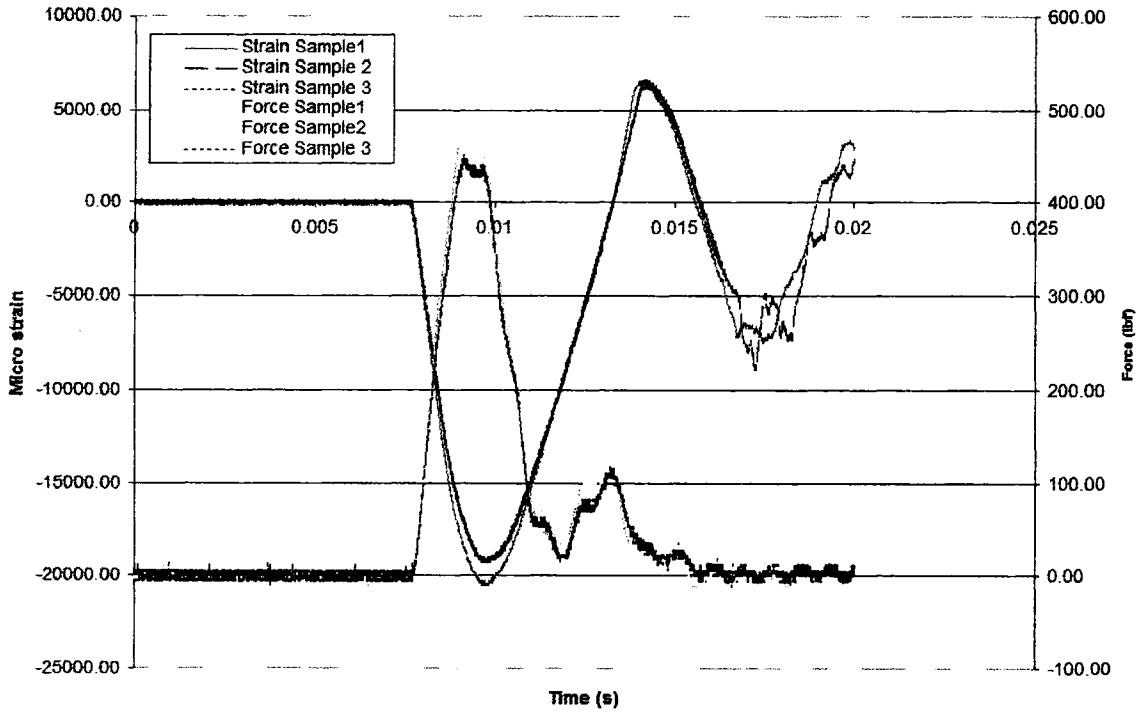
Figure 5.15 Test Data for 6"x2" Blank Boards at Drop Height of 3"
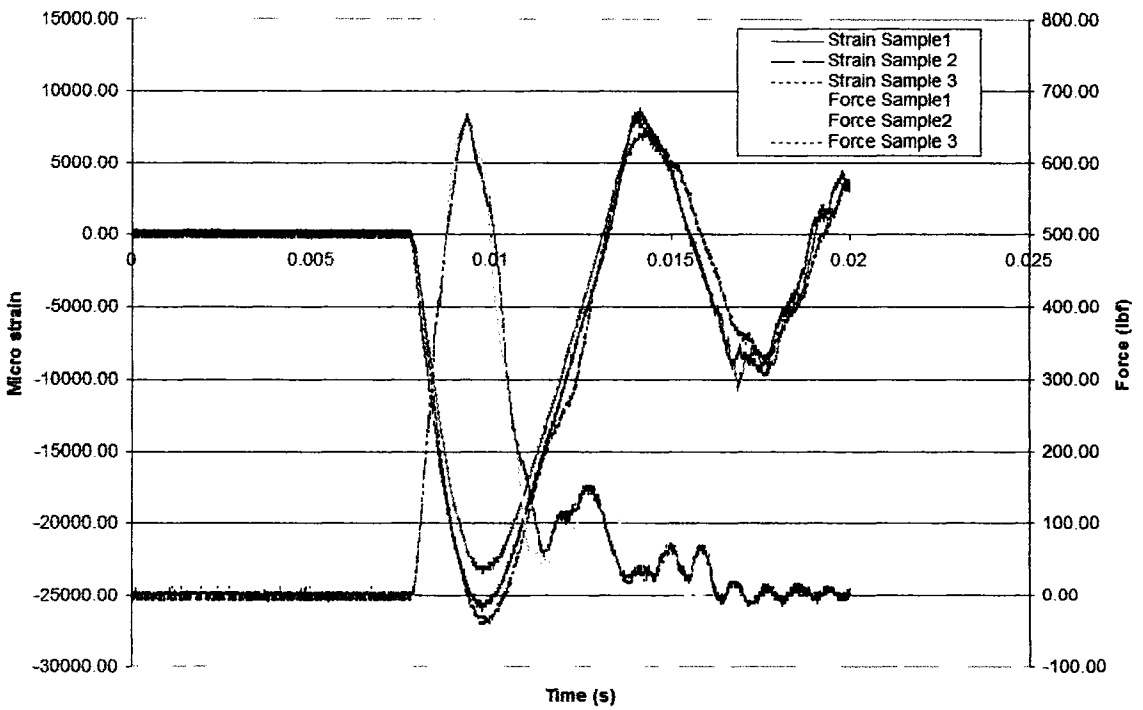
Figure 5.16 Test Data for 6"x2" Blank Boards at Drop Height of 5"

68
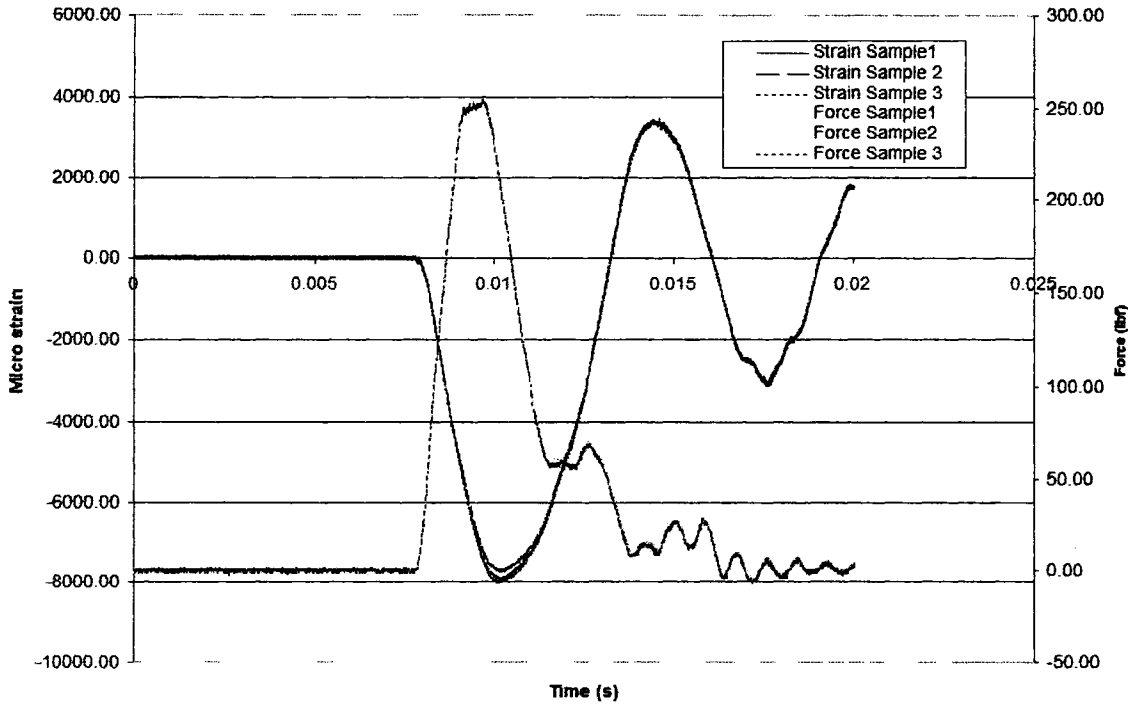
Figure 5.17 Test Data for 6"x2" Boards With Components at Drop Height of 1.06"
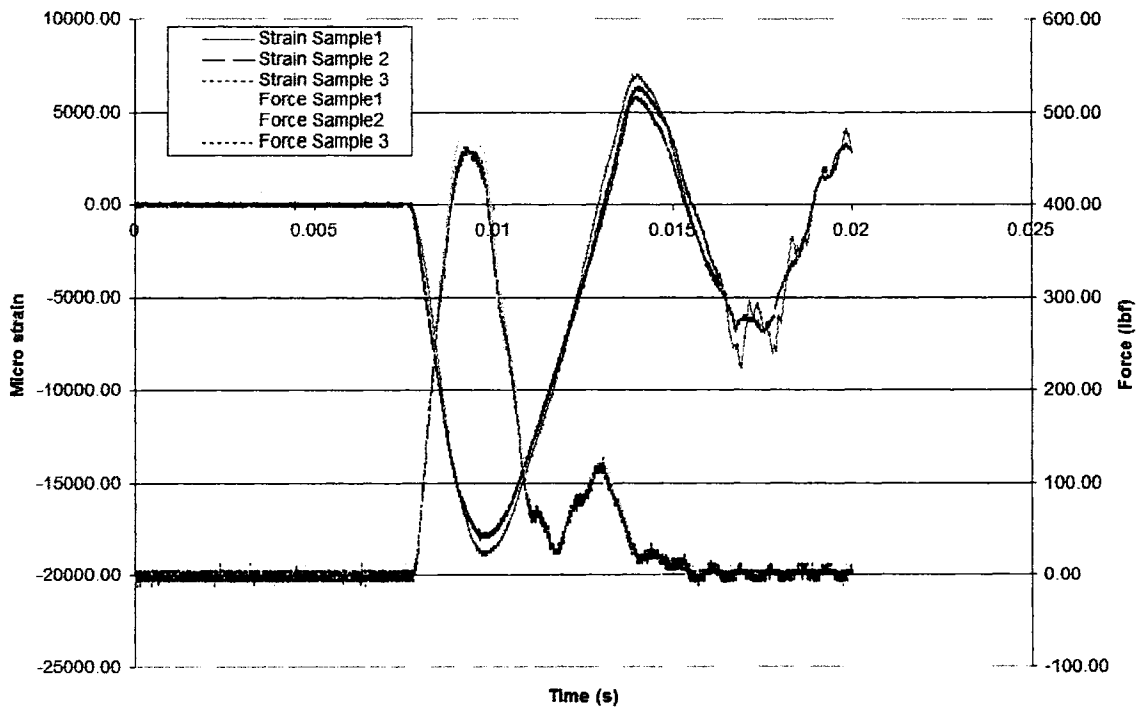
Figure 5.18 Test Data for 6"x2" Boards With Components at Drop Height of 3"

69
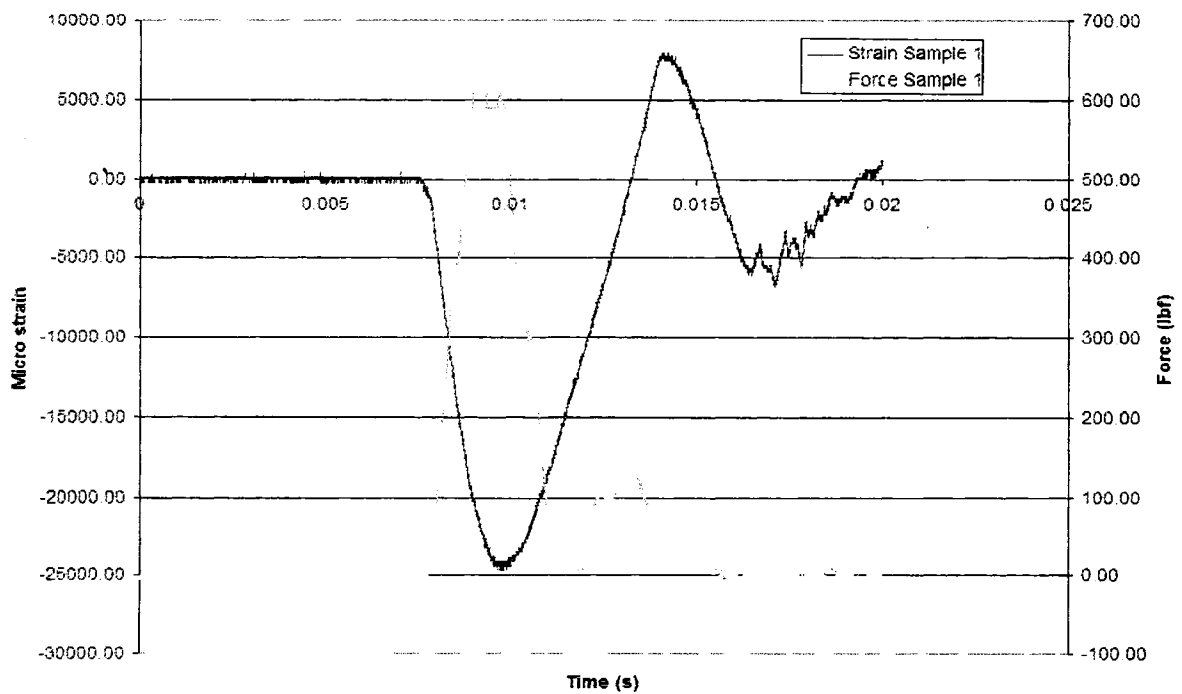
Figure 5.19 Test Data for 6"x2" Boards With Components at Drop Height of 5"

The summary of the above testing was shown in Table 5.2. It was observed that in all the tests with 6"x2" specimens force signals have shorter duration than strain signals. At 5" drop height, capturing data was difficult due to the limitation of the range of strain gage (0.035), due to this; only one data set was captured for board with components at this drop height. Lift-off of the component was observed at 5" drop height due to breakage of solder joint (Figure 5.20).

70

Table 5.2 Summary of Results for Dynamic Testing on 6"x2" Specimens

Drop Height (in)	6"x2"Blank Boards			6"x2"Boards with Components		
	Peak Force (Lbf)	Peak μStrain	Peak Strain Rate (/s)	Peak Force (Lbf)	Peak μStrain	Peak Strain Rate (/s)
1.06	262.22	11450	8.6	253.33	8016	5
3	460.00	19700	15	467.72	18933	14
5	643.39	25377	20.1	650.79	24666	19.64
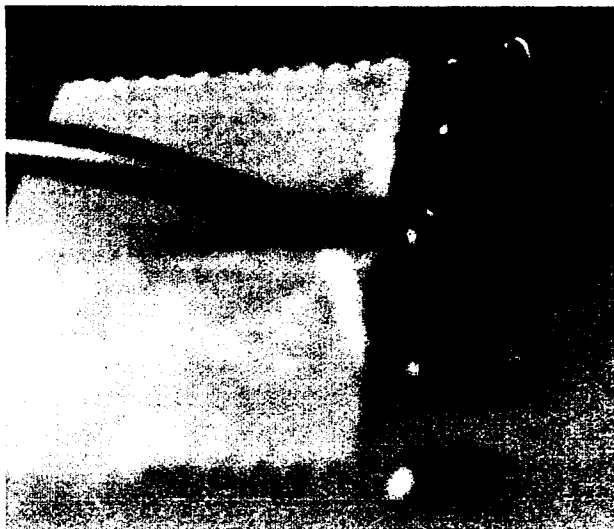
Figure 5.20 Lift off of the Components due to Breakage of Solder Joint

Previous results consistently exhibited a second force signal of smaller magnitude; it was suspected that this force signal and associated strain wave are the result of fluttering of the board. In order to study the effect of overhang length of the board beyond the support fixture, another set of tests were performed on 2"x2" specimens. As capturing of data was limited by the range of strain gage at 5" drop height, it was decided to conduct tests for 0.5", 1.06", and 3" (Table 5.3). Results for these tests were shown in Figures 5.21 through 5.26.

71

Table 5.3 Test Matrix for 2"x2" Specimens

Description	Dynamic Testing		
Drop Height (inches)	0.5	1.06	3
Number of Blank Boards	3	3	3
Number of Boards with Components	3	3	3
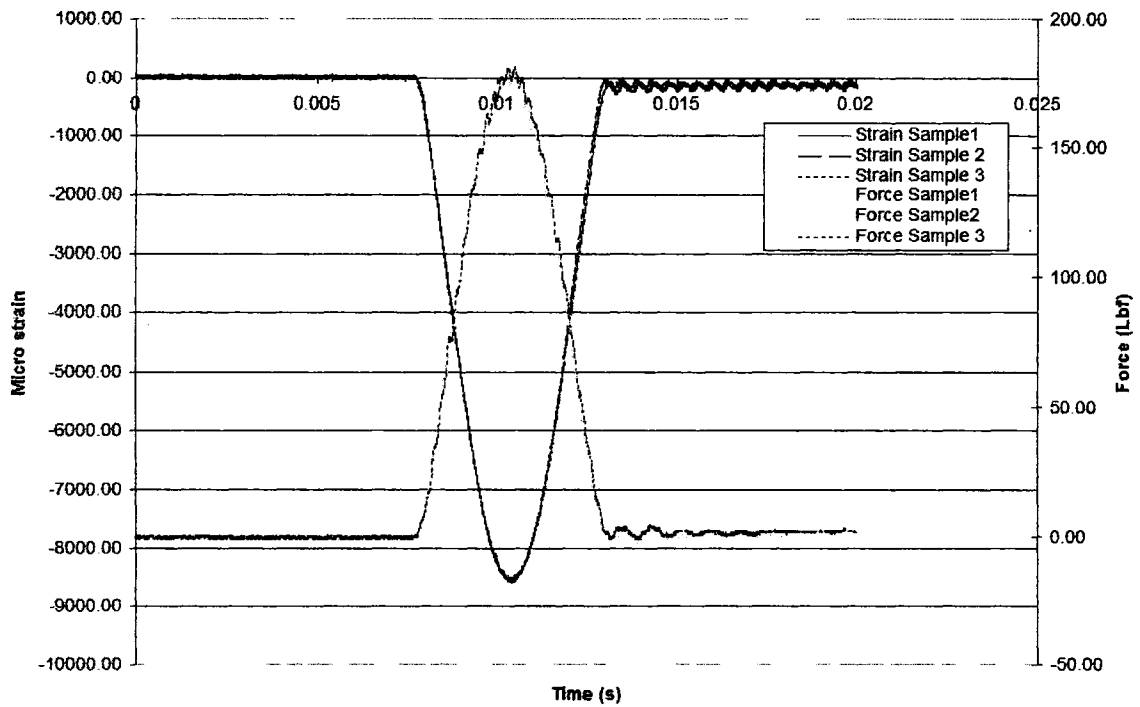
Figure 5.21 Test Data for 2"x2" Blank Boards at Drop Height of 0.5"

72
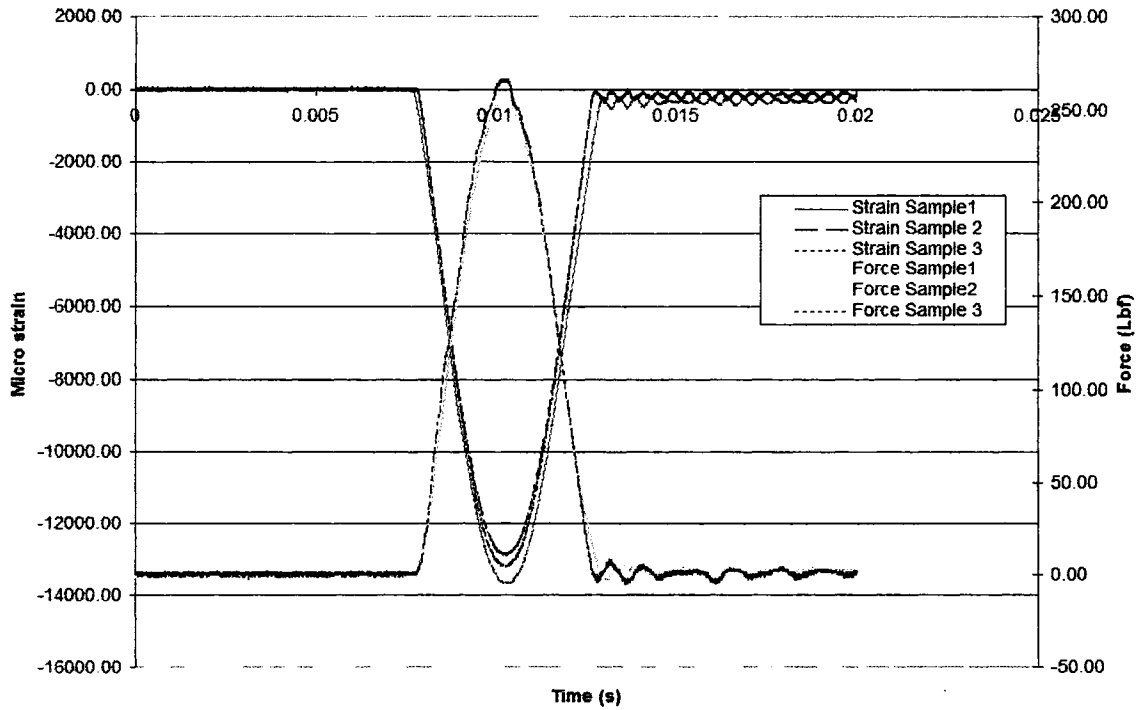
Figure 5.22 Test Data for 2"x2" Blank Boards at Drop Height of 1.06"
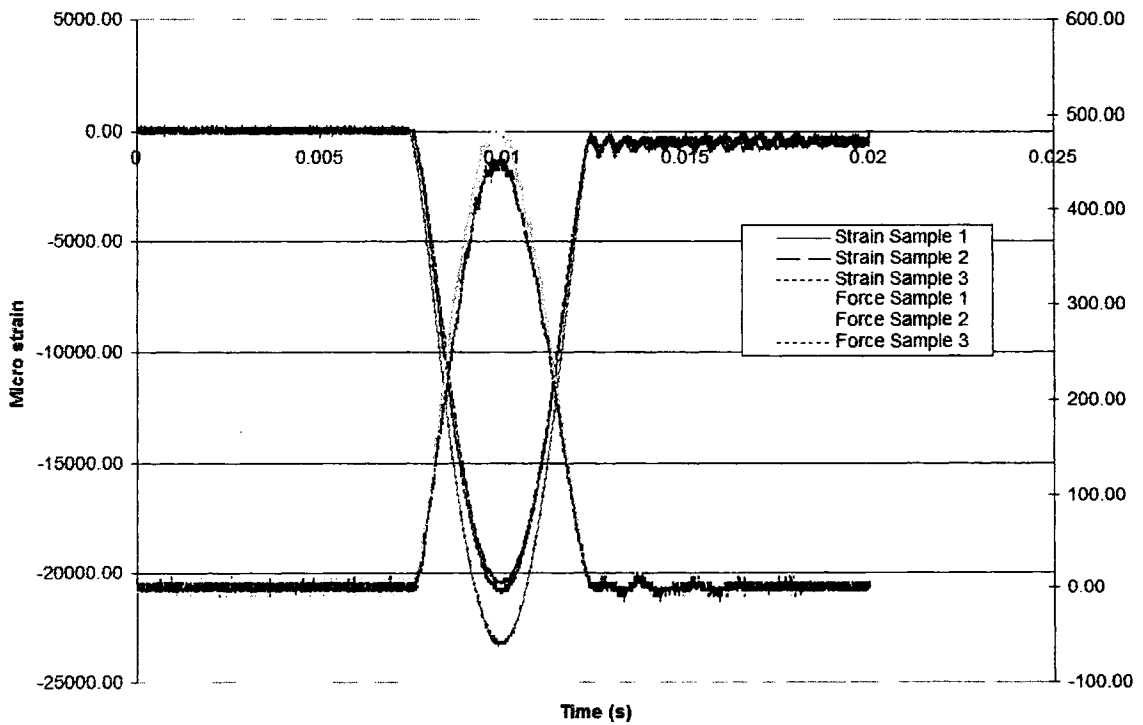
Figure 5.23 Test Data for 2"x2" Blank Boards at Drop Height of 3"

73
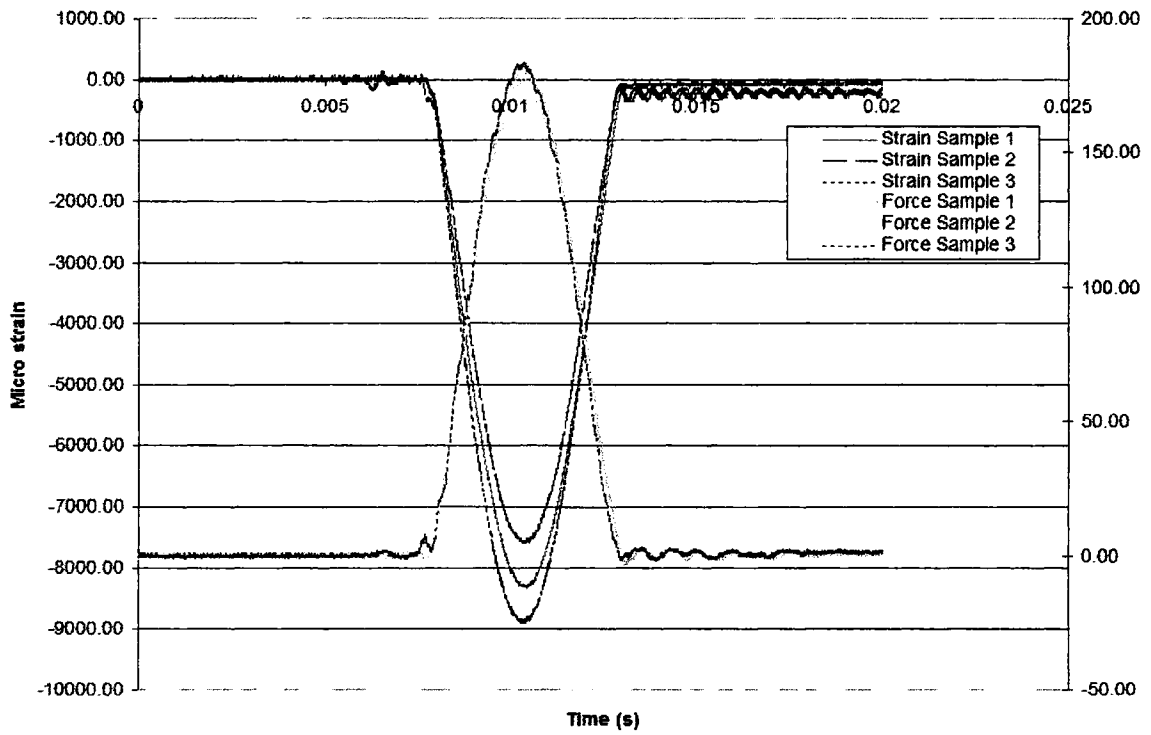
Figure 5.24 Test Data for 2"x2" Boards With Components at Drop Height of 0.5"
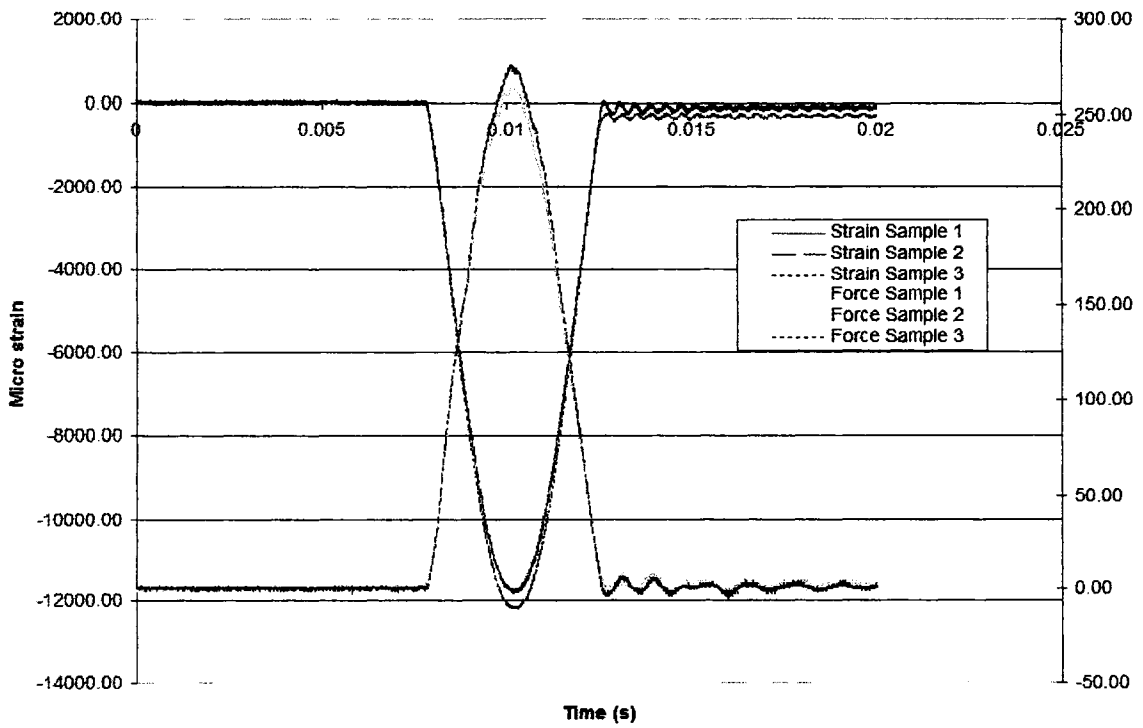
Figure 5.25 Test Data for 2"x2" Boards With Components at Drop Height of 1.06"

74
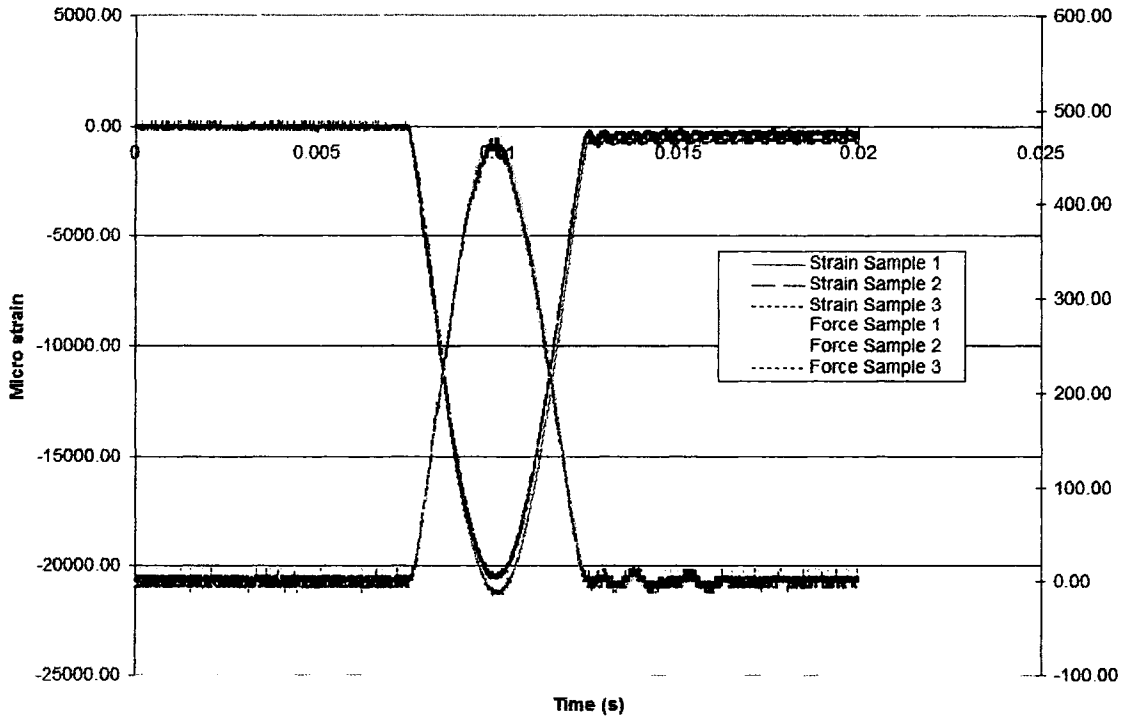
Figure 5.26 Test Data for 2"x2" Boards With Components at Drop Height of 3"

Test results of 2"x2" specimens show that the duration of force and strain signals were equal, based on this it was decided to use specimens of 2"x2" for the reminder of the study. Table 5.4 shows the summary of results for 2"x2" specimens.

Table 5.4 Summary of Results for Dynamic Testing on 2"x2" Specimens

Drop Height (in)	2"x2"Blank Boards				2"x2"Boards with Components			
	Peak Force (Lbf)	Peak μStrain	Peak Strain Rate (/s)	Average Strain Rate (/s)	Peak Force (Lbf)	Peak μStrain	Peak Strain Rate (/s)	Average Strain Rate (/s)
0.5	180.10	8566	4.8	3.1	181.26	8266	4.7	2.8
1.06	2661.58	13239	7.8	4.7	271.95	11933	7.5	4.6
3	468.78	21577	13.8	8.3	469.84	20800	13	8.0

75

5.3 Quasi-Static Testing

In order to study the boards at lower strain rates United Testing machine was used. Figure 5.27 shows the experimental set-up for the quasi-static testing. Force signal was acquired through the united machine's load cell, which was directly attached to the computer. Strain signal was acquired using 2310A signal conditioning amplifier, which in turn was connected to the oscilloscope. 2"x2" specimens as suggested by section 5.2 were considered for testing. The objective was to achieve three different strain rate levels in the specimens. According to standard D6272 [68], relation between the rate of cross head motion of the machine to strain rate is given by Equation 5.1 (Appendix B).

$$Z = \frac{Rd}{0.185L^2} \qquad (5.1)$$

where,

Z – Rate of straining the outer fibers (in./in.)

L – Support span (in.)

d – Depth of beam (in.)

R – Rate of crosshead motion (in./min)

In order to achieve three different strain rates, three different crosshead rates were used each differing by one tenth of other. Table 5.5 shows the test matrix for different crosshead motions. Figure 5.28 through Figure 5.33 show the experimental results obtained from these tests.

76
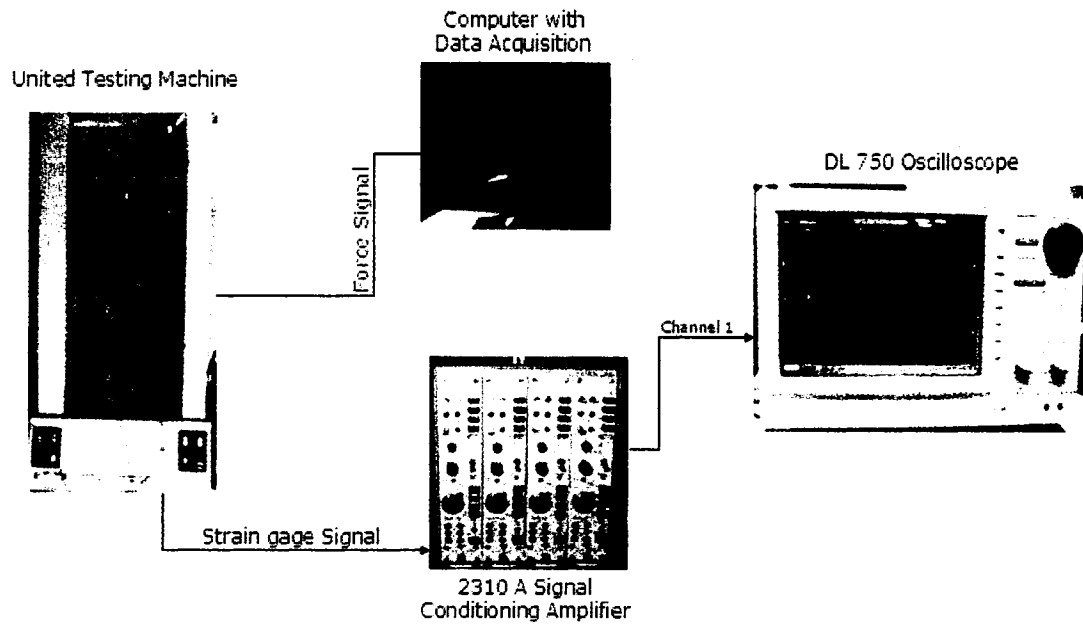
Figure 5.27 Quasi-Static Testing Experimental Set-up

Table 5.5 Test Matrix for 2"x2" Specimens for United Machine

Description	Static Testing		
Rate of Crosshead Motion (inches/min)	0.033	0.33	3.3
Number of Blank Boards	3	3	3
Number of Boards with Components	3	3	3

77
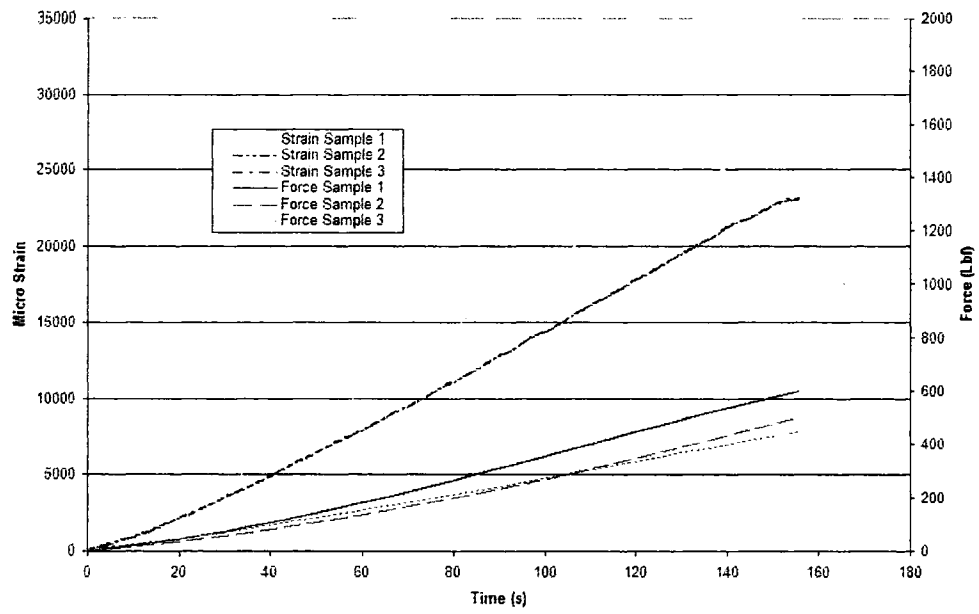
Figure 5.28 Test Data for 2"x2" Blank Boards at Crosshead Rate of 0.033in./min
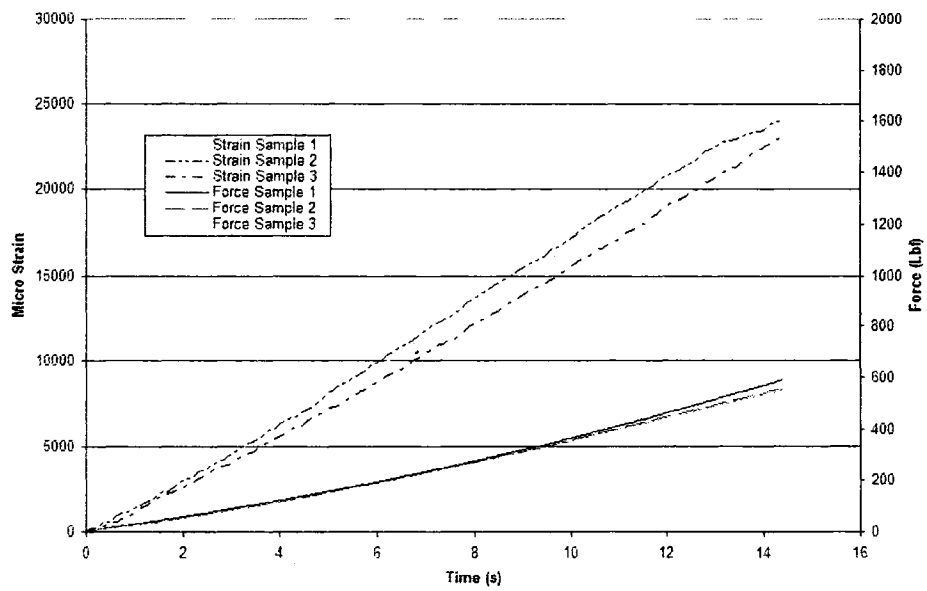
Figure 5.29 Test Data for 2"x2" Blank Boards at Crosshead Rate of 0.33in./min

78
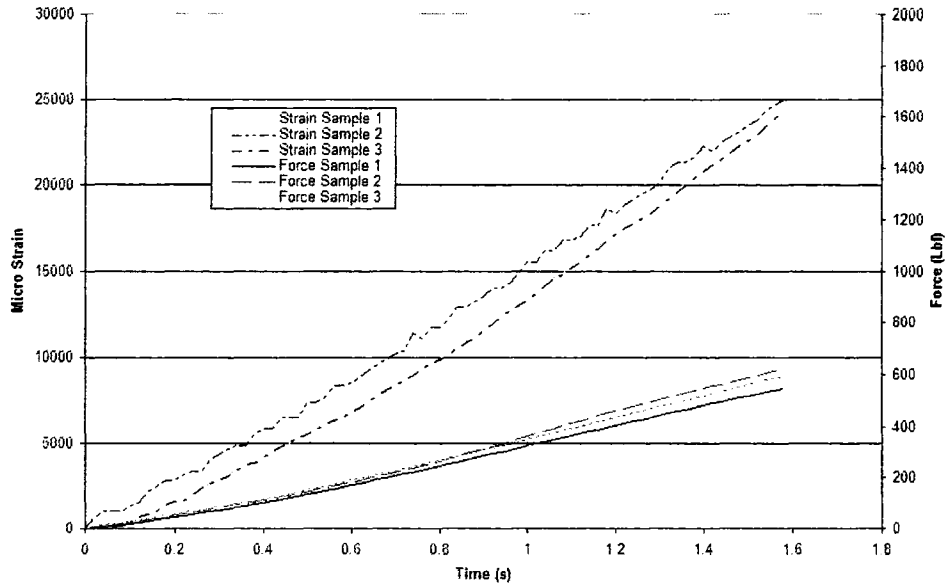
Figure 5.30 Test Data for 2"x2" Blank Boards at Crosshead Rate of 3.3in./min
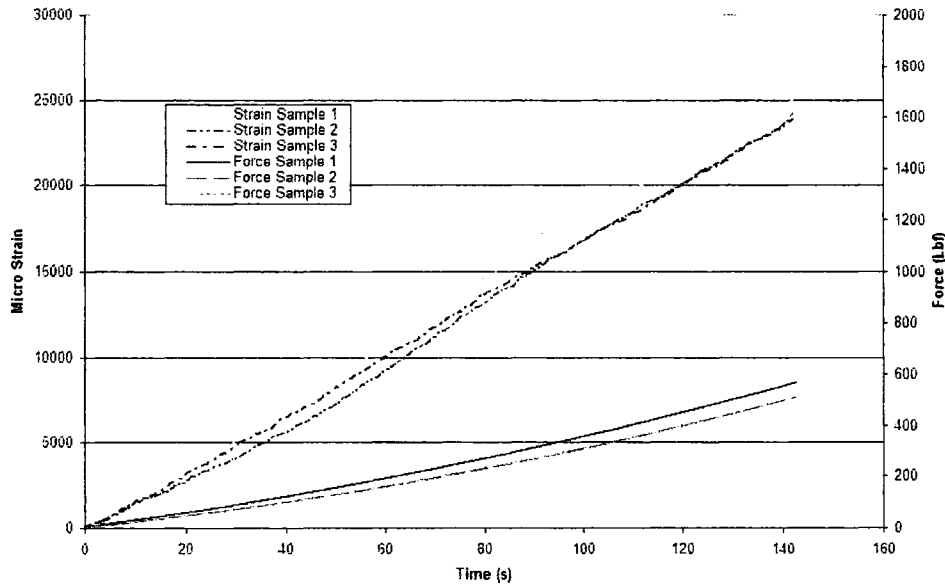
Figure 5.31 Test Data for 2"x2" Boards With Components at Crosshead Rate of 0.033in./min

79
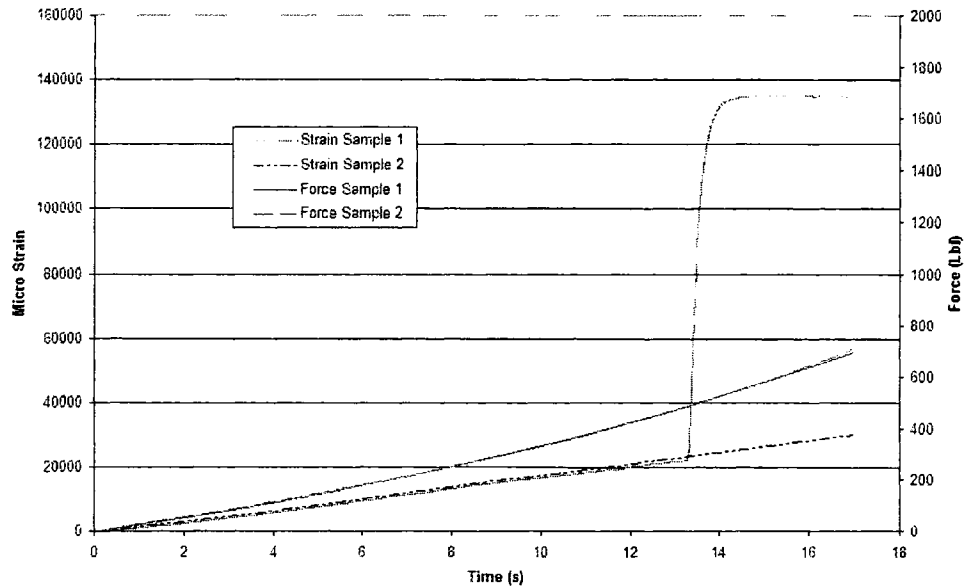
Figure 5.32 Test Data for 2"x2" Boards With Components at Crosshead Rate of 0.33in./min
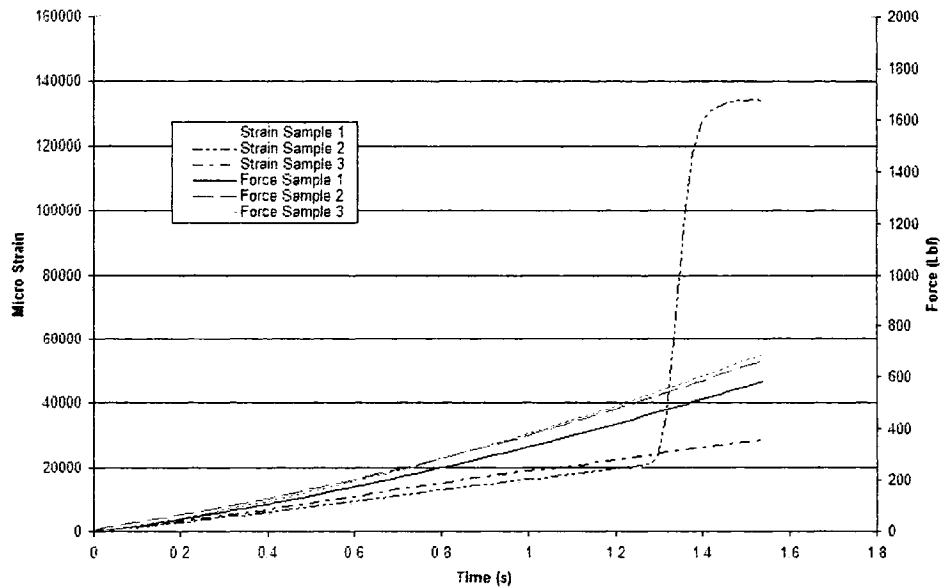
Figure 5.33 Test Data for 2"x2" Boards With Components at Crosshead Rate of 3.3in./min

All these tests were conducted until the specimen breaks (Figure 5.34). For each crosshead rate motion the data from all samples was averaged and peak force, peak strain rate and average strain rate were calculated for each case and listed in Table 5.6.

80

Table 5.6 Summary of Results for Static Testing on 2"x2" Specimens

Rate of Crosshead Motion (in./min)	2"x2"Blank Boards			2"x2"Boards with Components		
	Peak Force (Lbf)	Peak Strain Rate (/s)	Average Strain Rate (/s)	Peak Force (Lbf)	Peak Strain Rate (/s)	Average Strain Rate (/s)
0.033	516.97	2.037e-4	1.585e-4	529.55	2.102e-4	1.691e-4
0.33	565.46	0.0021	0.0016	707.02	0.0025	0.0017
3.3	585.79	0.0216	0.0151	645.45	0.0208	0.0166
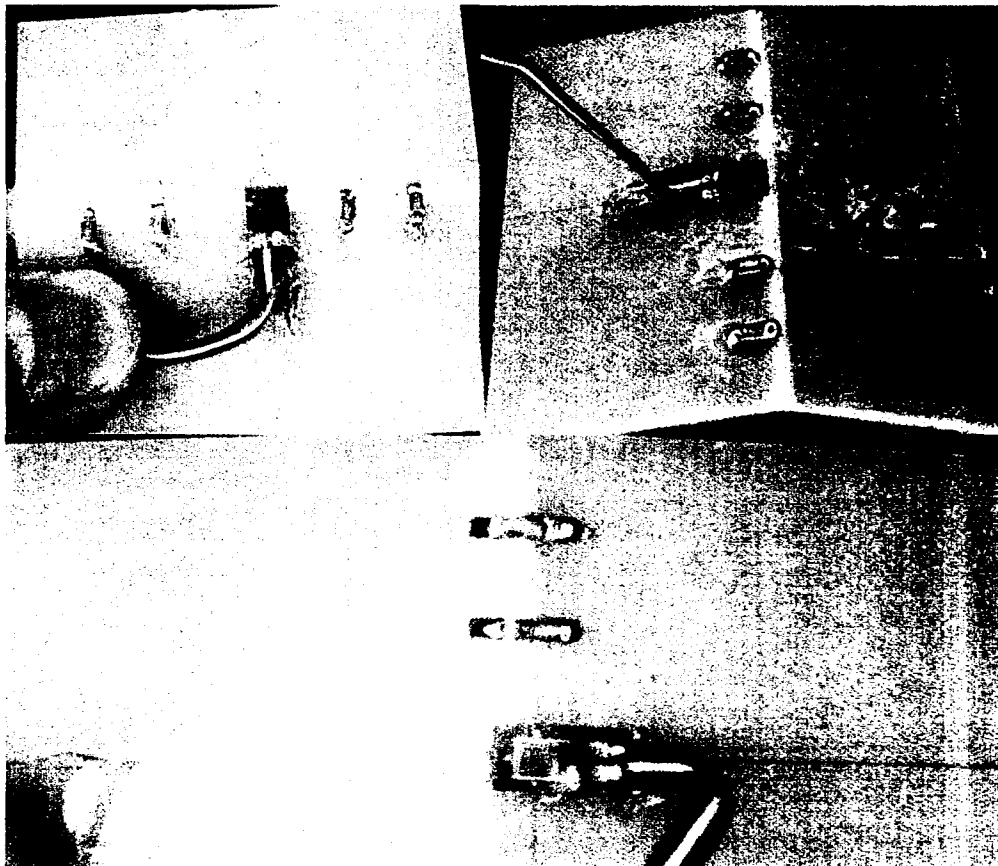
Figure 5.34 Test Specimens after Static Testing

The computational models for the dynamic testing cases were developed using ANSYS-LSDYNA software. Detailed description of the models, input functions and output were given in the following chapter.

81

5.4 Conclusions

Experimental procedure for shock testing of electronic components was developed. The boards were studied for both dynamic and static conditions. In dynamic testing the experimental procedure developed showed a repeatable impact for each height. The overhang length for the board has the effect on duration for the force and strain signal. We were able to achieve same time duration for boards with 2"x2" dimensions. Lift-off of the components was observed at a drop height of 5". It was also observed that the strain gages reach their limitation at drop height of 5". Three different strain rates were considered for static cases by applying three different cross head rate motions. In future to get the complete characteristics for the board, tensile testing in axial direction may be useful. Once we have the complete characteristics for the board, they can be utilized in modeling FEA for these impact tests.

82

CHAPTER 6

FEA AND OPTIMIZATION STUDIES OF IMPACT TESTING

6.1 Finite Element Analysis

FEA for the test cases were modeled in order to compare them with the experimental

results. In order to study the strain rate dependency of optimization algorithm, all the

three cases of FEA were modeled and optimization engine was applied on them. FEA of

the setup has three basic components similar to experimental fixture as shown in Figure

5.5. Impactor was modeled using solid elements, circuit-board was modeled using shell

elements, and support was modeled using rigid body elements.

6.1.1 Meshing

HYPERMESH 7.0 was used for meshing all three components. Two dimensional

surface as shown in Figure 6.1 was meshed for the impactor and then it was dragged

normal to the surface to form the three dimensional surface (Figure 6.2).
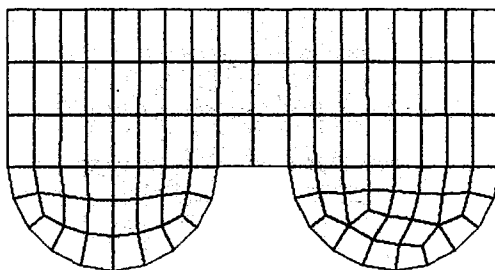
Figure 6.1 Two Dimensional Mesh of the Impactor

83
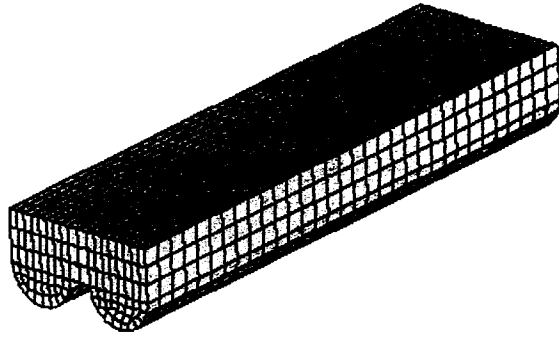
Figure 6.2 Three Dimensional Meshed Impactor

Circuit board was meshed with equal number of divisions (96x96) along the width

and length in order to achieve an aspect ratio of 1. Meshed model of the circuit board was

shown in Figure 6.3.
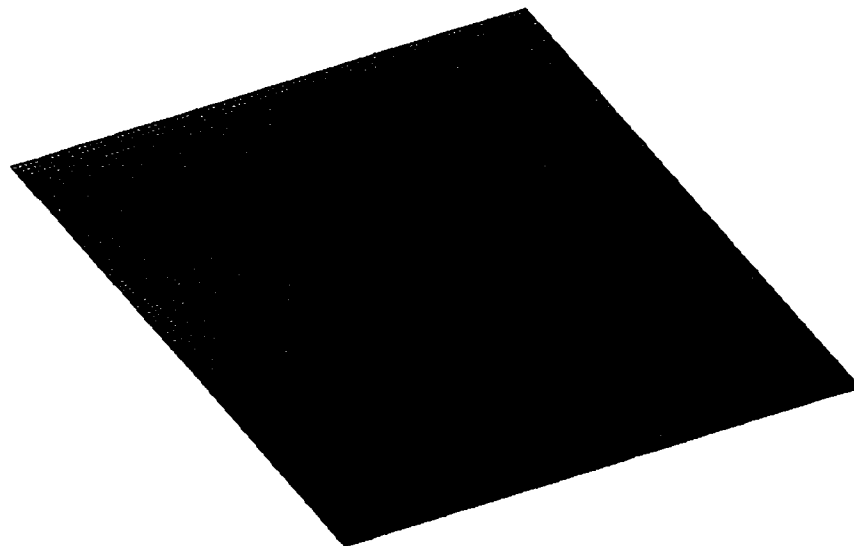
Figure 6.3 Meshed Model of the Circuit Board

Support was modeled as two rigid cylinders using rigid bodies (Figure 6.4) option in

LS-DYNA. The advantage of using rigid bodies was they do not require meshing which

84

contributes to the reduction of elements. This will be helpful in improving the overall computational time of the model. Figure 6.4 shows the complete meshed model of the impact testing setup.
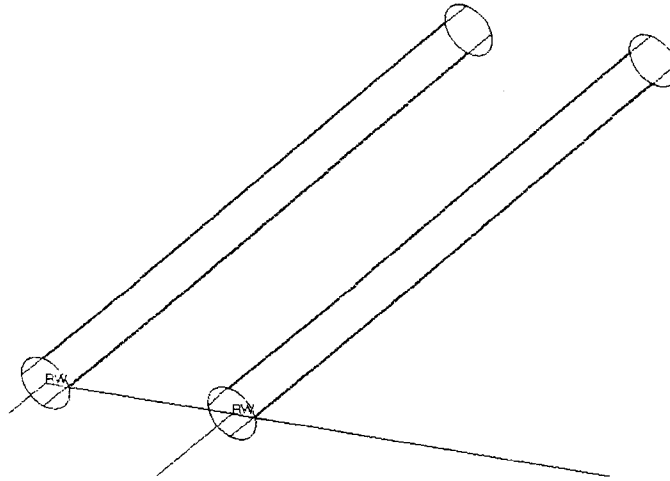
Figure 6.4 Rigid Cylinders Acting as Support
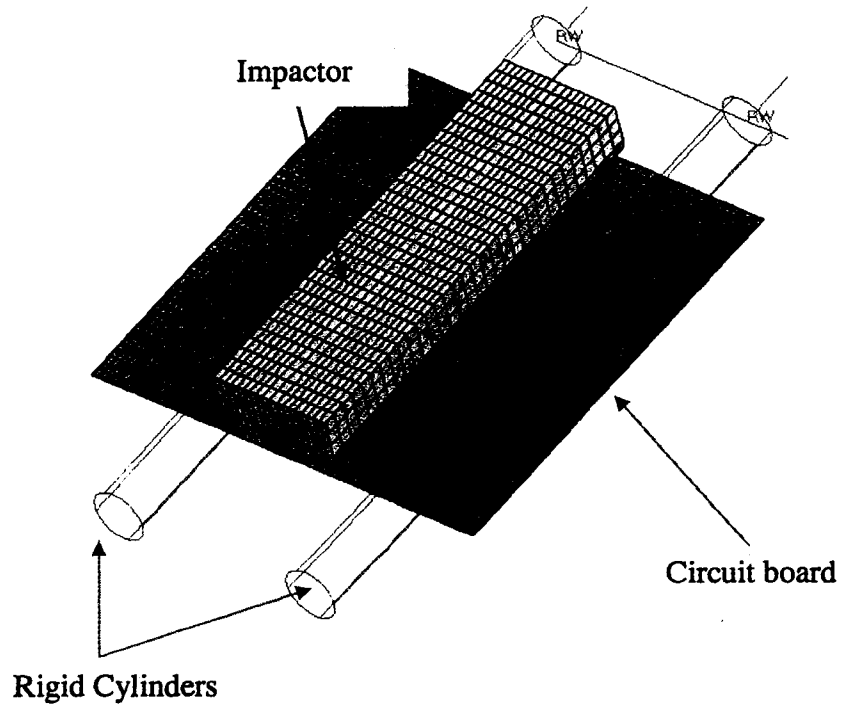
Figure 6.5 Meshed Model of Impact Testing Setup

85

6.1.2 LS-DYNA Input Cards

An input file was created in LS-DYNA after modeling the whole setup. In LS-DYNA all the information about the model was written in the form of cards in the input file. Cards are the commands, which contain information about various aspects of the model such as node and element definitions, materials, loads, boundary conditions etc. The following cards were used in the current model.

1. Control cards

2. Database cards

3. Material cards

4. Cards defining the parts and sections

5. Cards defining the nodes, elements

6. Contact cards

7. Cards defining the boundary conditions

8. Cards defining the loads

9. Cards defining box

10. Cards defining output

Detailed description of these cards was given in Appendix C through L respectively.

6.1.3 Material Characteristics

Orthotropic material model was used for the circuit board and elastic isotropic material model was used for the impactor. Material properties used for the components were listed in Table 6.1 and Table 6.2. For impactor modified density as listed in Table 6.1 was used. This low density made the impactor not to absorb any amount of energy during its motion.

86

Table 6.1 Material Properties of the Circuit Board (ARL)
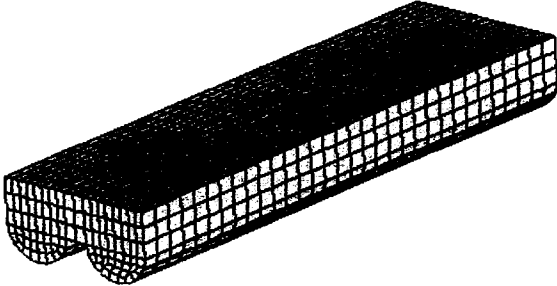
	Density (lb-s^2/in.)	Young's Modulus (psi)	Poisson's Ratio	Modulus of Rigidity (psi)
		Ex = 2.86E6	NUXY = 0.14	Gxy = 5.37E5
	1.98E-4	Ey = 2.86E6	NUXY = 0.18	Gyz = 5.37E5
		Ez = 1.32E6	NUXY = 0.18	Gxz = 5.37E5

Table 6.2 Material Properties of the Impactor (ARL)

	Impactor
	Density = 7.35E-06 lb-s^2/in
	Young's Modulus = 3.0E7 psi
	Poisson's Ratio = 0.3

6.1.4 Contact Definitions

In the dynamic experiment, there are two contacts involved. One contact will be between the lower surface of the board and the support, as the board rests on the support. Other contact will be between the upper surface of the board and the impactor, as the impactor imparts load to the board. These two contacts were incorporated in the FEA using contact definitions in LS-DYNA.

87

Rigid cylinders were defined using a "RIGIDWALL_GEOMETRIC_CYLINDER' card in LS-DYNA. This card requires a box id which consists of slave nodes. Two boxes were defined consisting of nodes on the circuit board where it comes in contact with the rigid cylinders (Figure 6.6). Contact between the rigid cylinders and bottom portion of the circuit board was incorporated using this card. Static coefficient of friction between the board and impactor was determined as 0.3 experimentally. This value was also incorporated in this card.

Figure 6.6 Boxes Defining the Slave Nodes

Contact between the upper surface of the circuit board and the lower portion of the impactor was incorporated using the "CONTACT_SURFACE_TO_SURFACE" card in LS-DYNA. Contact between these two components was established using part option. Coefficient of friction of 0.3 between the board and the impactor was also included in this contact card.

88

6.1.5 Boundary Conditions

Rigid cylinders shown in Figure 6.5 were constrained to move in all three translation and rotational degrees of freedom. Impactor was constrained to move only in the direction normal to the surface of the circuit board.

6.1.6 Loading

As discussed in chapter 5, dynamic testing was performed for three different heights. At each height three specimens were tested. In order to obtain the force curve for each drop height, all the three force curves obtained for three samples were averaged. Figure 6.7 through Figure 6.9 shows the force curves obtained for each drop height.
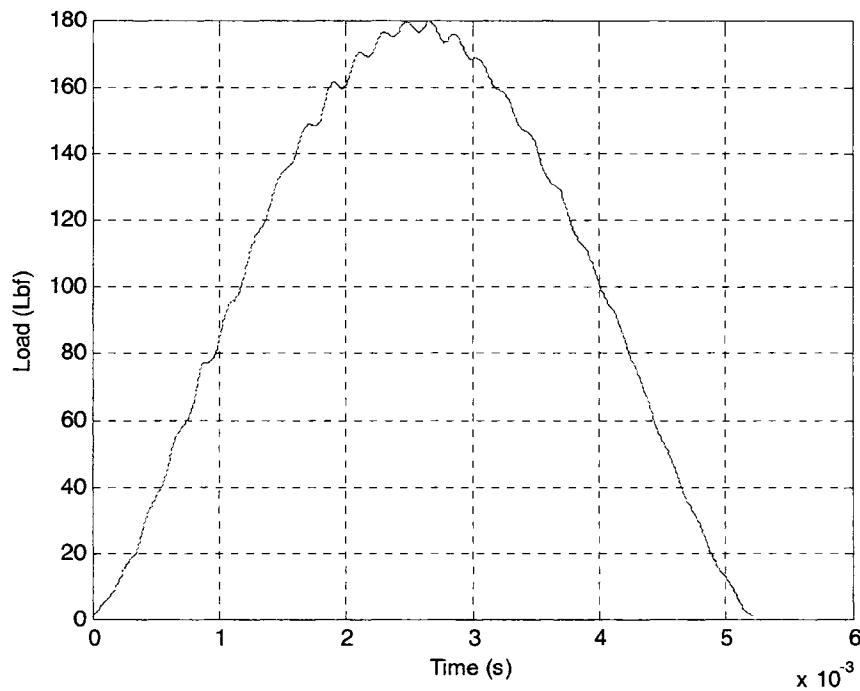
Figure 6.7 Force Curve for FEA for Drop Height of 0.5"

89
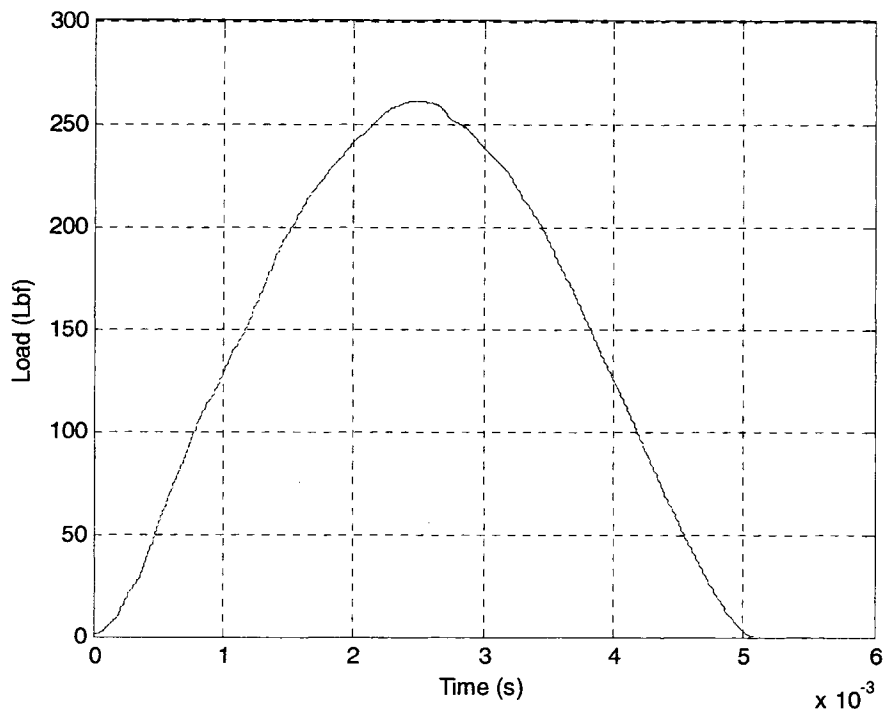
Figure 6.8 Force Curve for FEA for Drop Height of 1.06"
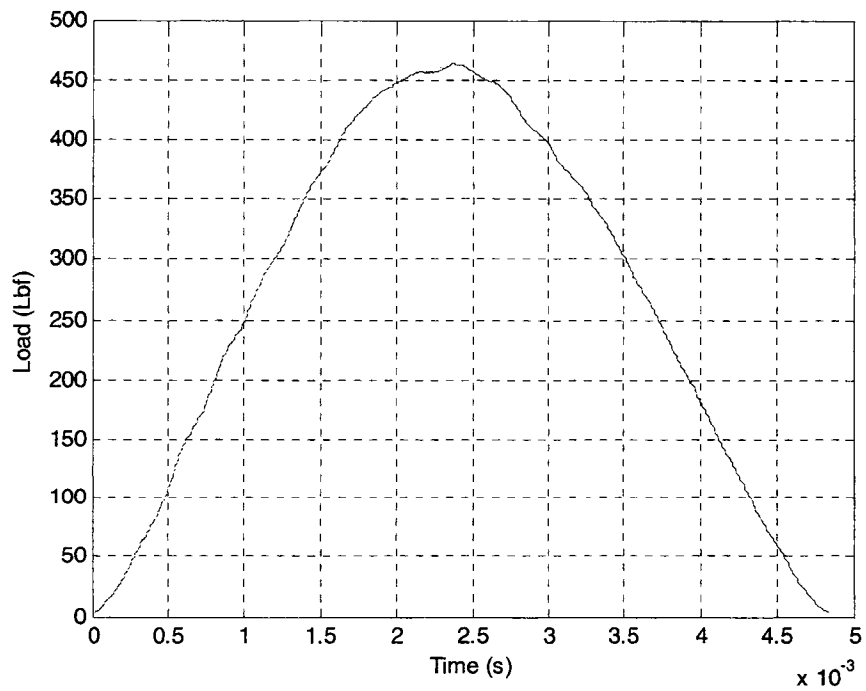
Figure 6.9 Force Curve for FEA for Drop Height of 3"

90

The force curves shown above were applied as pressure for FEA models at each height correspondingly. Figure 6.10 shows the application of pressure on the impactor surface. This pressure was applied using "LOAD_SEGMENT" card in LS-DYNA. As the surface area on the top of impactor is 1.167, a scale factor of reciprocal of area which is 0.857 was incorporated in this card.
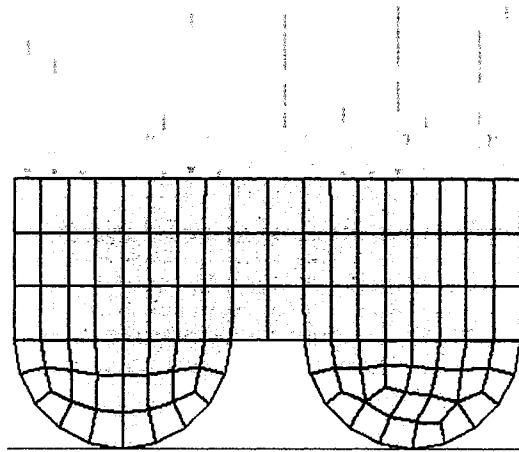
Figure 6.10 Application of Pressure on the Surface of the Impactor

6.1.7 Results

The FEA of impact problem was modeled by incorporating all necessary cards in LS-DYNA to model it close to the real experimentation. As the force increases the impactor was pushed towards the plate, the force was transmitted to the board through the contact between impactor and the board. Strain was extracted from the center of the board (corresponding to central location in experiment) using the "DATABASE_HISTORY_SHELL" card in LS-DYNA. The time interval for output request was maintained same as the corresponding time interval for the experiments. Comparison of experimental results with the corresponding FEA results was shown in Figures 6.11 through 6.13. At half inch drop height wavy behavior was observed in FEA

91

result. As the drop height increased the wavy behavior of the curve disappeared. Current models on an average take approximately 1663 seconds for the simulation. Optimization techniques were implemented on the current models to reduce this computational time which is discussed in detail in the next section.
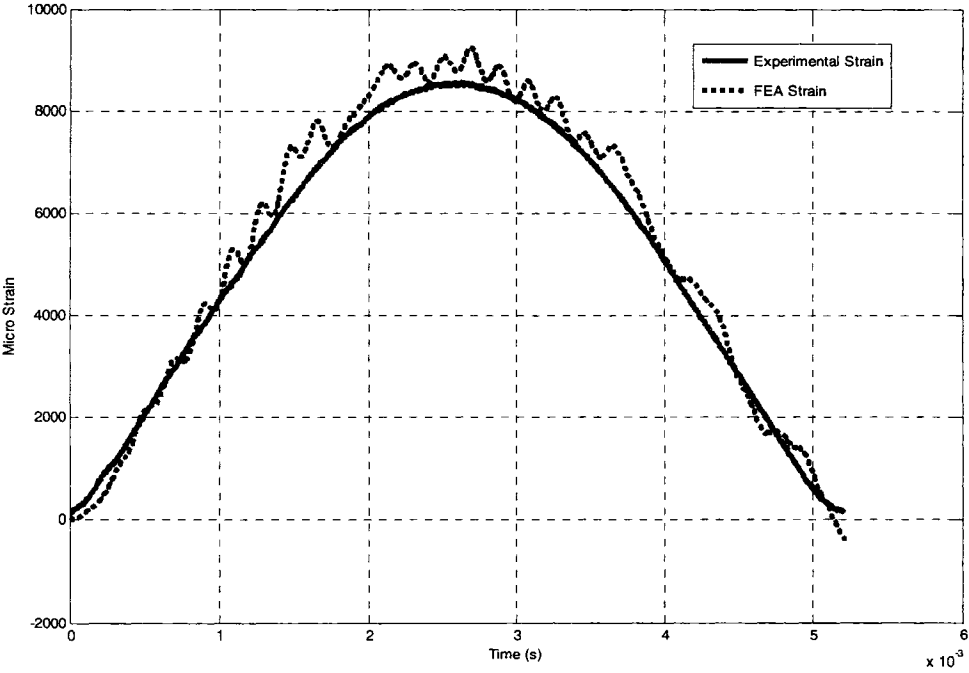
Figure 6.11 Comparison of FEA Strain with Experimental Strain at Drop Height 0.5"

92
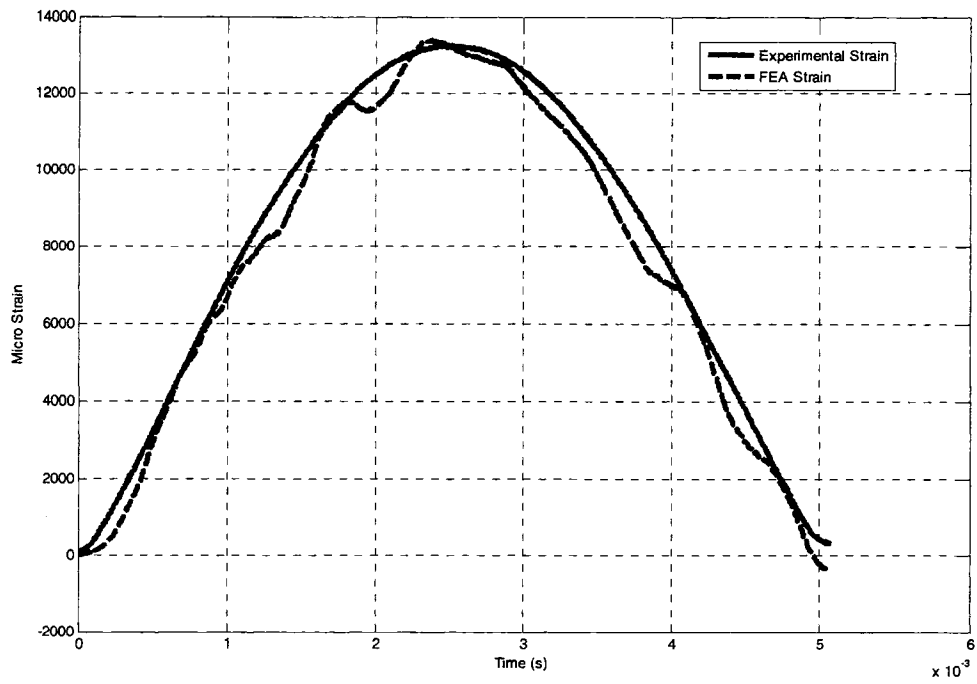
Figure 6.12 Comparison of FEA Strain with Experimental Strain at Drop Height 1.06"
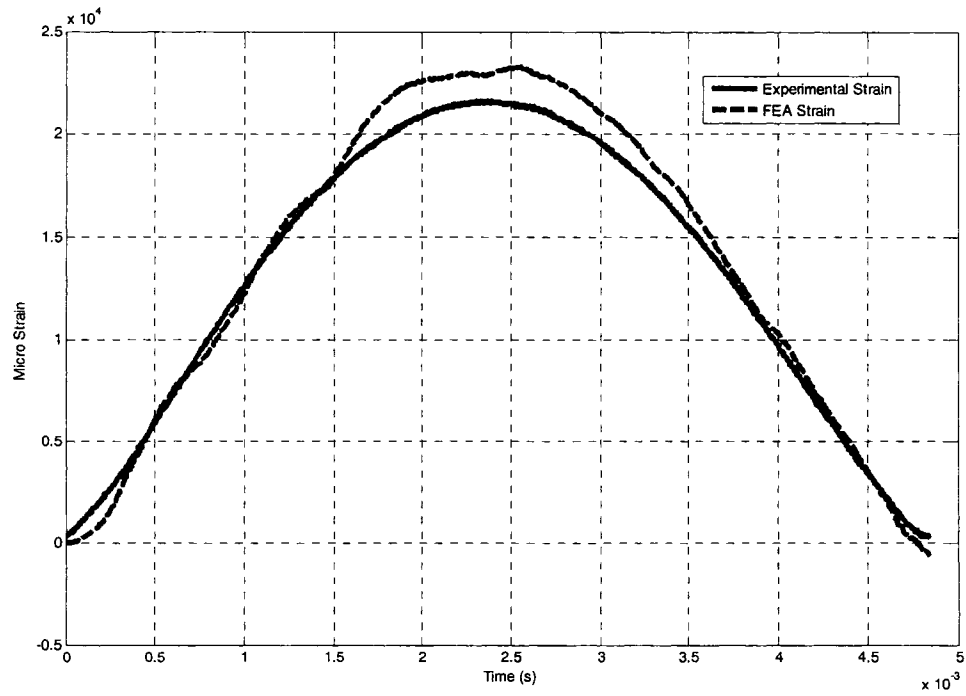
Figure 6.13 Comparison of FEA Strain with Experimental Strain at Drop Height 3"

93

6.2 Optimization of Computational Time

Optimization engine described in chapter 3 was utilized in reducing the computational time for the current model. The objective of the optimization problem is to minimize computational time by varying the mesh density on the circuit board. LS-DYNA input file for the current model was divided into two portions, fixed portion and variable portion.

- Fixed Code: This portion of the code consists of all control cards, database cards, nodal and element definitions of impactor, contact cards, boundary and load definitions.

- Variable Code: This portion of the code consists of nodal and element definitions of circuit board and output card.

The variables of optimization are number of elements along the length (N_1) and width (N_2) of the circuit board (Figure 6.14). Strain values measured at the central location of the circuit board were compared with the experimental strain values at each instant of time. The following formula was used for comparison of strain values:

$$As = \frac{\sum_{i=1}^{n}\left[S_{Exp} - S_{FEA}\right]^2}{\sum_{i=1}^{n}\left[S_{Exp}\right]^2} \qquad (6.1)$$

where,

As – Accuracy measure for strain

S_{Exp} – Strain data acquired experimentally

S_{FEA} – Strain data acquired through FEA at the corresponding location

i – From 1 to number of data points

94
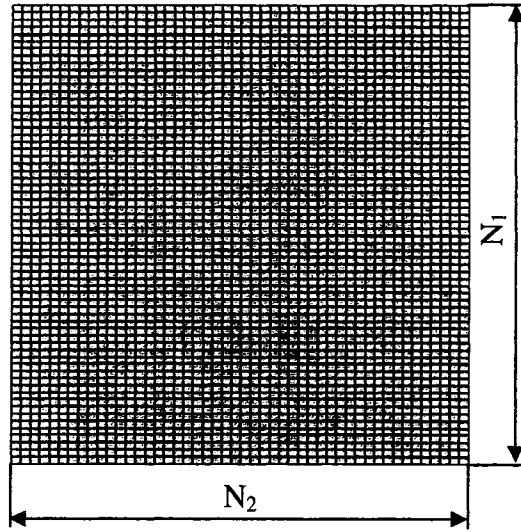
Figure 6.14 Variables of Optimization

The problem was subjected to the following constraints:

$$As \leq 0.05 \qquad (6.2)$$

$$20 \leq N_1, N_2 \leq 100 \qquad (6.3)$$

Initial values for N_1 and N_2 were chosen as 96 to start with an aspect ratio of one. Optimization study was first performed on a case with drop height of 1.06". A total of 44 function evaluations were carried out in the process of optimization. The progression of optimization search was shown in Figure 6.15. The search changed the number of elements from 96x96 to 24x22. Aspect ratio of the elements is changed from 1 to 1.09. The error between the experimental and FEA results was reduced from 0.3% to 0.26%. Computational time was reduced from 1587s to 60s. The FEA model before and after optimization was shown in Figure 6.16. Comparison of strain output before and after optimization with experimental strain was shown in Figure 6.17. It was observed that wavy behavior which was observed before optimization was not observed after optimization.

95
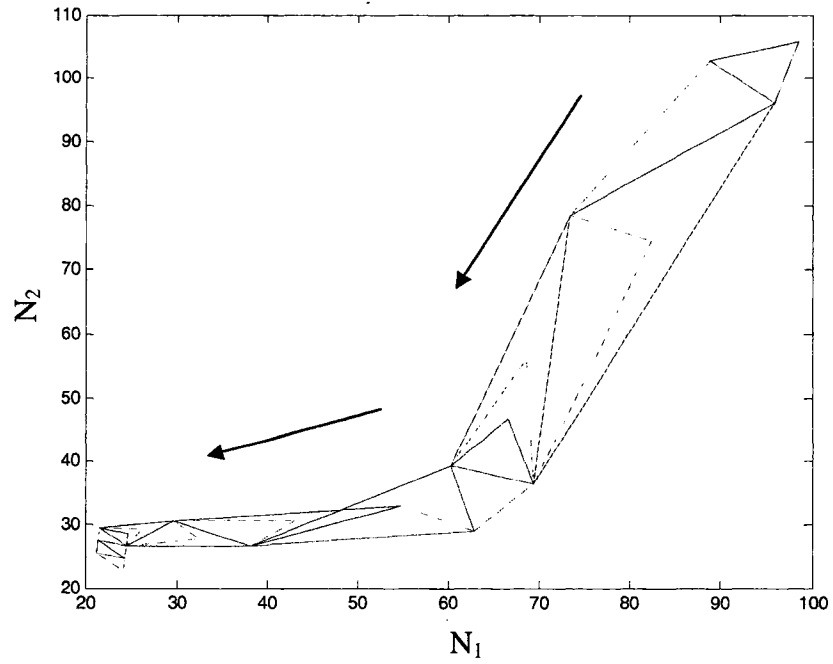
Figure 6.15 Progression of Optimization Search

Before Optimization   After Optimization
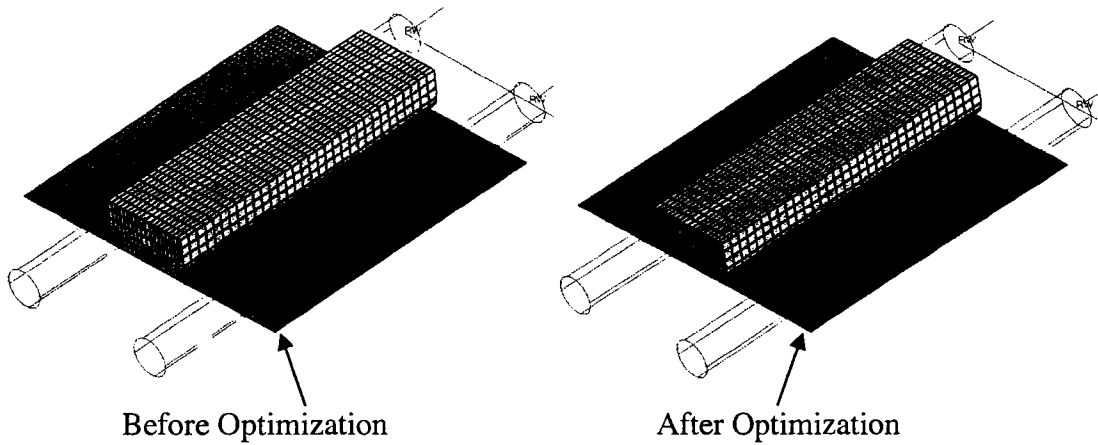
Figure 6.16 Comparison of FEA Model before and after Optimization

96
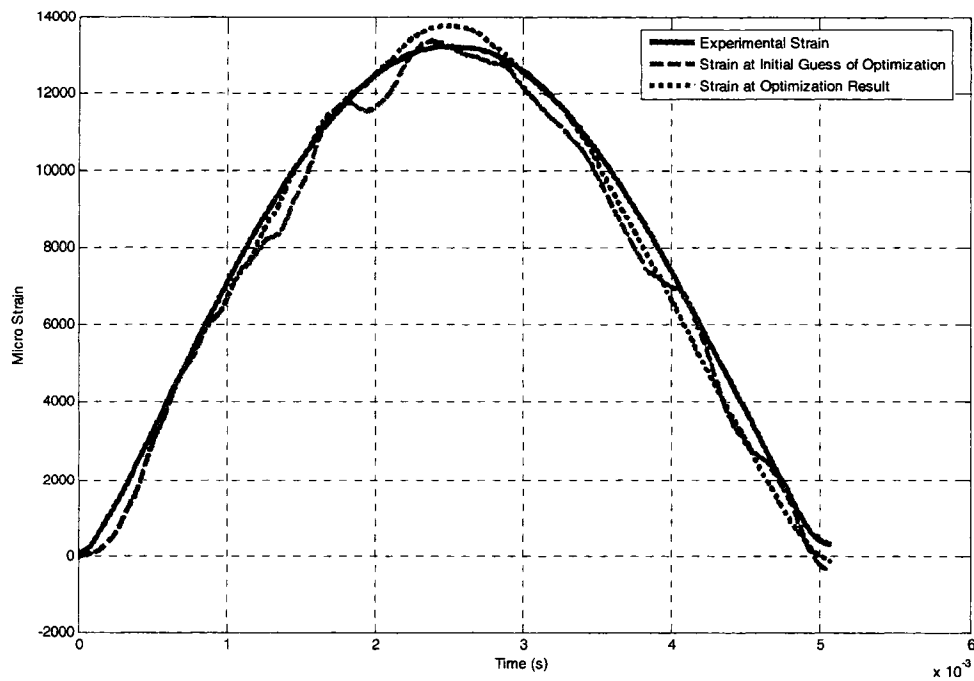
Figure 6.17 Comparison of Strain for FEA Model before and after Optimization (Drop Height 1.06")

Similar studies were performed on the cases for drop height of 0.5" and 3". Figure 6.18 and 6.19 show the comparison plots for strain before and after the optimization. One interesting observation was for all the cases the mesh density ended at the same number, even the objective function (computational time) was also ended with almost same number. Summary of results for all three cases were tabulated in Table 6.3. These results indicate that the optimization search is independent of the strain rate of the board.

97
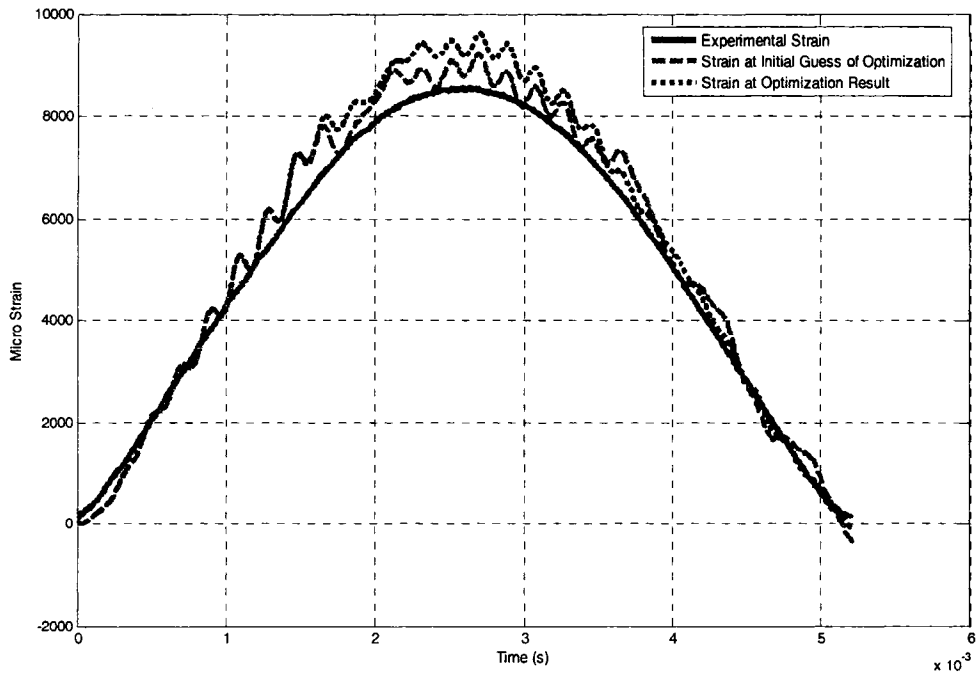
Figure 6.18 Comparison of Strain for FEA Model before and after Optimization (Drop Height 0.5")
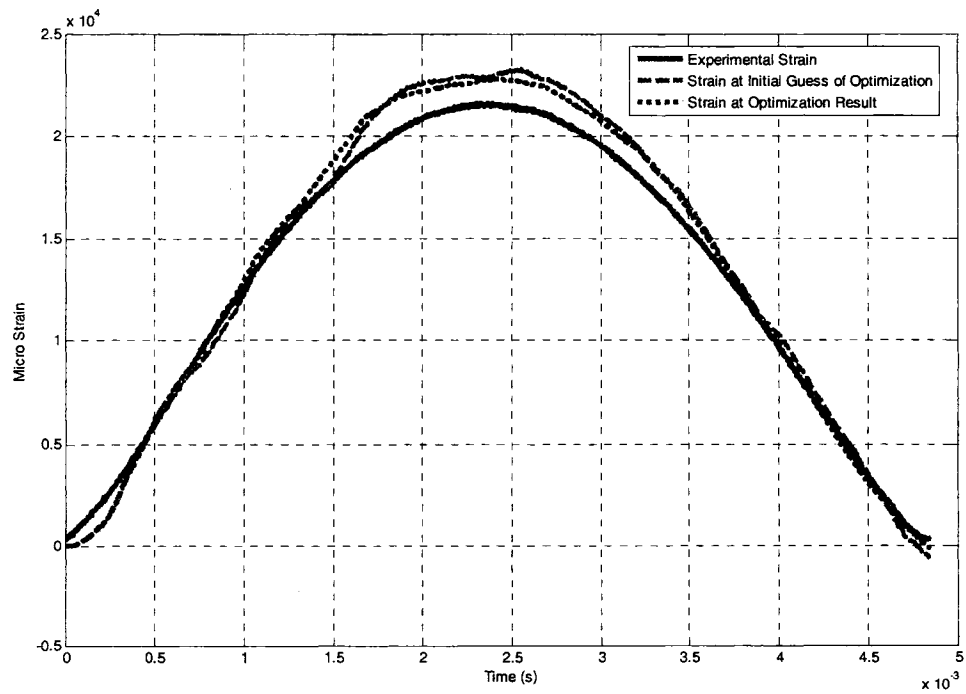
Figure 6.19 Comparison of Strain for FEA Model before and after Optimization (Drop Height 3")

98

Table 6.3 Optimization Results for Three Drop Height Cases

Drop Height (in)	Average Strain Rate (/s)	Blank Boards			
		N1xN2		Computational Time (s)	
		Before Optimization	After Optimization	Before Optimization	After Optimization
0.5	3.1	96x96	24x22	1680	60
1.06	4.7	96x96	24x22	1587	60
3	8.3	96x96	24x22	1722	63

The results indicate optimization engine works effectively with the FEA of impact/shock events.

99

CHAPTER 7

SUMMARY AND CONCLUSIONS

This chapter provides the summary of the research performed, followed by lessons learned during this research and thirdly, contribution of this research to the FEA of shock assessment of electronic components under dynamic loading. Finally, recommendations for future work that would build on this research were discussed.

7.1 Summary of Research Performed

The objective of this dissertation was to develop optimization algorithm that will be capable of optimizing the FEA models subjected to shock/impact environments. An algorithm was developed capable of achieving the desired goal of this research. Readily available commercial softwares were explored, which has some programming capability along with FEA capabilities. Due to the unsuccessful search, focus was directed towards programming languages which will be capable of interacting with the commercially available FEA softwares. Matlab and ANSYS-LSDYNA, seemed to be serving the purpose. Finally optimization engine was created in Matlab which can act as a link between the ANSYS-LSDYNA and optimization algorithm.

The developed optimization engine was applied successfully to the FEA of the projectile launch event. Optimization was done in two stages: 1) Conceptual stage, and 2) Optimization stage. In conceptual stage the projectile was replaced with the equivalent one sharing the same mass and inertial properties. The mesh densities on this equivalent

100

projectile were used as variables of optimization with computational time as objective function and acceleration result of high mesh density model as constraint. Significant reduction in the computational time of the FEA was achieved due to the reduction in the mesh densities. The aspect ratios obtained by the optimized result of equivalent model were applied to the original projectile model. This reduced the computational time of the actual projectile launch event by 95%.

To determine the survivability of the electronic components to the shock environment, experimental procedure was developed. Four point bending fixture based on ASTM standards was designed. Experiments were conducted in both static and dynamic range, to study the behavior of the board under different strain rates. United testing machine was used for the static range of experiments and Dynatup drop tower was used for the dynamic range of experiments. Strain gages were used to capture the response of the circuit boards using signal conditioner and oscilloscope. A total of six different strain rates were achieved successfully, out of which three were in the static range and three were in dynamic range.

FEA of the dynamic test cases were created. The FEA results showed similar behavior to that of the experimental results. Optimization engine was used to reduce the computational time on the FEA. Computation time was reduced by 96% compared to the initial model considered for FEA.

7.2 Lessons Learned

This section describes the lessons learned from the research performed in this dissertation. From the development of optimization engine, following lessons were learned:

- FEA program chosen for the analysis must have the capability to be written in the text format in order to apply optimization engine, and edited text file should reflect changes in the FEA model.

- Matlab serves as a very good interface between the optimization algorithm and the ANSYS-LSDYNA program.

- Constraints involving parameters which do not depend on the analysis result should be defined in the beginning of the optimization program, to avoid unnecessary computational time involving FEA models which violate the constraints.

- Reasonable values for initial guess and boundary limits should be assigned by considering all the geometrical limits of the model.

- In comparing the results at each instant of time with varying signs, squared error, which was described as accuracy measure in the current research will yield better comparison measure.

- Running the FEA models using double precision option will yield better accuracy in the results.

Lessons learned from the application of optimization engine to projectile launch event:

- The FEA text format file should be divided into fixed code and variable code.

- The features of the FEA which are going to be the variables of optimization should be created from Matlab for each FEA run.

- The created variable portion of the code should be combined with the fixed portion of the code in order to form a complete FEA file.

- The variables at each stage of optimization should be saved in order to continue the search in case of computer or power failure.

- Computer should be maintained at constant resource of memory during the optimization run, if any of the objective function or constraints involve the computational time.

- For moving components in an event like projectile launch, the aspect ratio for 3-D elements can be used as 2.44, and 0.52 for stationary components.

Lessons learned from circuit board testing and modeling include the following:

- The shock pulses created by the drop tower were repeatable.

- The overhang length of the circuit board beyond the support has significant effect on the vibration of the board.

- Second wave of shock was observed in case of specimens with overhang length of more than support span on each side.

- Small components like 1206 SMT resistors have very small influence on the overall behavior of the board. They increased the overall stiffness of the board, but not to a greater extent.

- Failure of the board was not observed in any of the dynamic test cases up to strain rate of 20.

- Lift off of the components was observed at a strain level of about 25,000$\mu\epsilon$, at strain rate of 20.

- Shell elements can be used in modeling the circuit board, which will help in reduction of computational time.

- Very low density should be used for the impactor, so that it won't absorb any energy during it's motion.

Lessons learned from applying optimization engine to the impact testing of circuit-boards:

- Optimization algorithm is independent of the strain rate.

- An aspect ratio of 1.09 can be used for rectangular shell elements.

- Optimization engine can be implemented in FEA problems involving shock/impact.

7.3 Original Contributions

This dissertation outlined the development and application of optimization engine to the FEA models of electronic components subjected to shock environments. This will allow the prediction of shocks transmitted to the components with very small amount of computational time based on user defined constraints. Before this method was developed, readily available software did not exist. This approach cuts the computational costs of FEA models to a greater extent.

The practical assessment approach to the electronic components on the circuit board was developed. This approach provides information necessary for circuit board redesign to improve failure risk of shock loading. By improving circuit board survivability to shock loading, electronic systems can perform their intended mission. For Army electronics, the increase survivability to shock loading could increase the survivability of operators during their mission.

In addition to the development of a practical assessment approach, other original contributions are related to the following: the development of a fixture for drop-impact

104

tester, data acquisition setup procedure for the test cases. This setup provided very repeatable pulses. With this setup, multiple, repeatable shock pulses can be produced on circuit boards with minimum cost.

7.4 Future Work

Current approach of optimization engine is limited to particular applications considered. This approach can be used to develop a more generalized package with more user friendly environment.

Testing was done for a small set of samples, with only one type of component mounted on the boards. The sampling size can be increased to have better confidence in the results. In the current fixture, there is very small room to test different types of components; another fixture with bigger support span can be modeled to have enough room to try bigger components. With bigger fixture different combinations of components can be mounted to study their effect. Each board was tested for one time shock load; it might be interesting to study the behavior under repeated shock loading. In some of the tests conducted, strain gage (3%) was out of range before the failure of board, in order to study the impact loads until the failure of boards strain gages with higher range should be used.

105

APPENDIX A

CALIBRATION PROCEDURE FOR 2310A SIGNAL CONDITIONING AMPLIFIER

The calibration procedure for 2310A signal conditioning amplifier should be done in two stages. Each stage was discussed in detail in this section. Figure A.1 shows the 2310A amplifier, it has four identical amplifiers. Figure A.2 shows the layout of strain gage connection terminals to the input slot of the equipment.
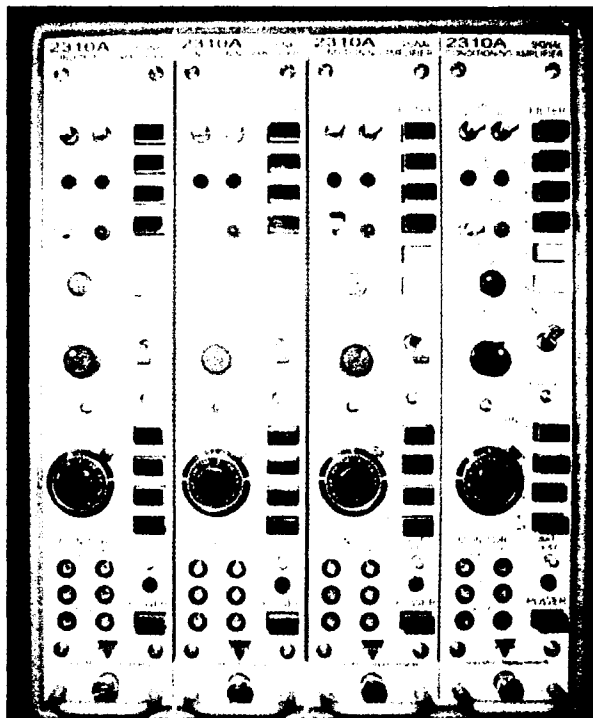
Figure A.1 2310 Signal Conditioning Amplifier

106
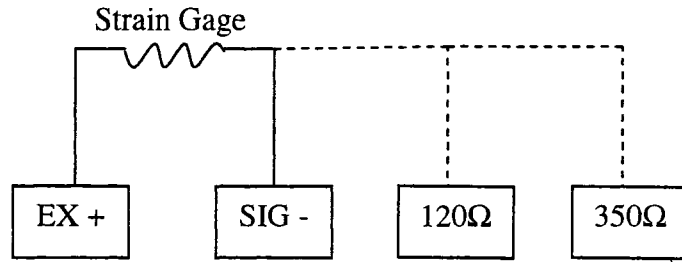
Figure A.2 Layout of Strain Gage Terminals to Input of 2310A Conditioner

Stage 1:

- For most of the dynamic/static testing, AC IN (white button) should not be depressed.

- For dynamic testing WB filter should be depressed that means, it is operating in wide band equivalent to no filter.

- With a strain gage connected to the input, excitation switch still at OFF position, depress X100 gain button, both output lamps at the top of the front panel should be completely dark. If not, turn the AMP BAL adjustment below the excitation toggle switch using small screwdriver to extinguish the lamps.

- With desired bridge excitation, turn the excitation toggle switch to ON; Just below output lamps, momentarily press the AUTO BAL toggle switch all the way down to the RESET position, and release. In 1 to 3 seconds the output lamps should extinguish, indicating balance, if not repeat from AUTO BAL.

- If the lamps are still bright, turn the TRIM knob to extinguish the lamps.

- Use the following equation to determine your gain

Excitation X Gain = 2000

And set the gain according to value obtained from above equation.

107

By now you should see zero reading on your output monitor wherever you are displaying

the signal.

Stage 2:

There are two calibration switches A and B. 'A' switch is for calibration in 200με

range, similarly 'B' switch is for calibration in 1000με range. The following two

equations relate the cal A or cal B values with the type of strain gage you are using:

$$Cal\ A = \left(\frac{2}{Gagefactor} \right) 200$$

$$Cal\ B = \left(\frac{2}{Gagefactor} \right) 1000$$

For example let's say you are using a strain gage with gage factor value equals to 2.

So when you turn Cal A switch upwards you should read a 200mv signal in the digital

display where ever you are outputting the signal. If it is not displaying 200mv adjust your

gain so that you will output 200mv. This calibrates the conditioner in such a way that it

gives a one-to-one relation between millivolts and micro strain.

$\longrightarrow$ 1 mv = 1 με

With the same gain settings you can try turning Cal A downwards which should give

-200mv, now you can turn cal A off and try Cal B upwards and downwards, it should

read +1000mv and -1000mv respectively. If you are successfully outputting the stated

voltages for corresponding switches, you can turn off both Cal A & B, and can start

testing. Momentarily check for the output lights, if they become bright at any time you

can use trim knob to dim them.

RELATION BETWEEN CROSSHEAD RATE AND STRAIN RATE ON THE BOARD

The relation between the crosshead rate and strain rate are derived from the simple

beam theory. Figure B.1 shows the four point setup with supporting fixture, crosshead

and the board.
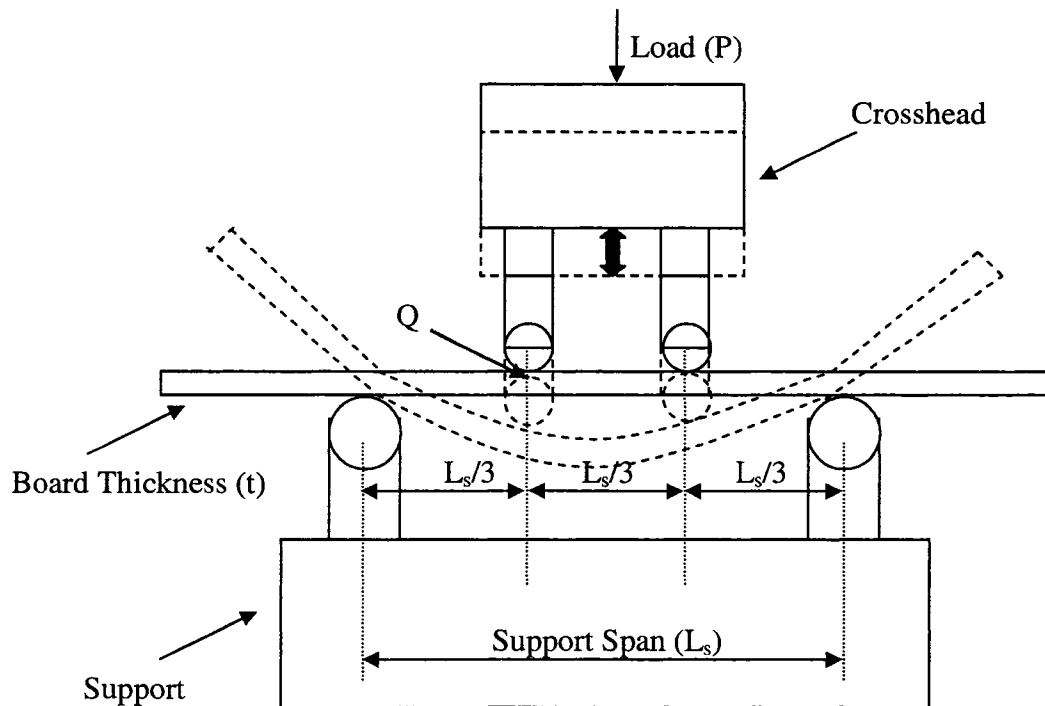
Figure B.1 United Test Fixture Outline Drawing

The support span of the beam can be considered as the following simply supported beam

as shown in Figure B.2.

109

P/2   P/2

a = L$_s$/3   L$_s$/3   L$_s$/3

X ⟶

Q
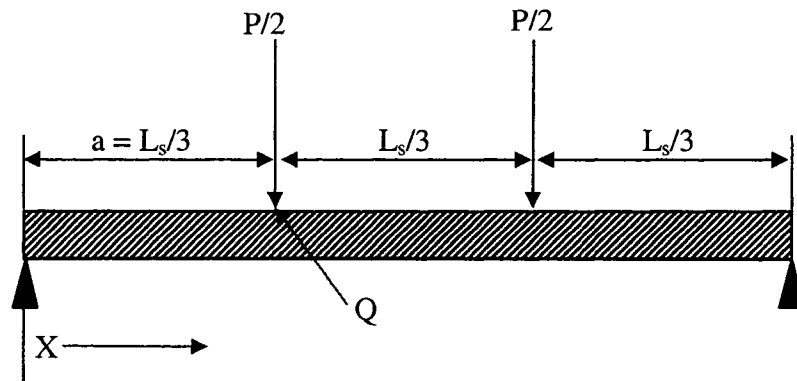
Figure B.2 Equivalent Simply Supported Beam

By considering the displacement of the point Q, the distance traveled by cross head at this location should be equal to the distance traveled by the board at this location (Ignoring the poisson's ratio effect of a board in bending). The deflection of a point Q for a simply supported beam with above loading conditions is given by

$$\delta = \frac{a(P/2)(a^2 + 3x^2 - 3Lx)}{6EI}$$ B.1

where
δ = Deflection of the beam at point 'Q'

a = Ls/3

x = Ls/3 for point Q

E = Young's Modulus

I = Moment of inertia for the cross sectional area

Equation B.1 can be reduced to the following by substituting values of 'a' and 'x'

$$\delta = \frac{5PL_s^3}{324EI}$$ B.2

Bending stress in the beam at point 'Q' is given by

110

$$\sigma = \frac{MC}{I}$$
B.3

where

$$M - \text{Moment at point } Q = \left(\frac{P}{2}\right)\left(\frac{L_s}{3}\right)$$

$$C - \text{Half of distance from neutral axis} = \frac{t}{2}$$

Equation B.3 reduces to the following by substituting the values of 'M' and 'C'

$$\sigma = \frac{PL_s t}{12I}$$
B.4

From Hook's law

$$\varepsilon = \frac{\sigma}{E}$$

$$= \frac{PL_s t}{12EI} \quad \text{substituting } \sigma \text{ from Equation B.4} \qquad \text{B.5}$$

substituting the above value into Equation B.2

$$\delta = \frac{5L_s^2}{27}\left(\frac{\varepsilon}{t}\right)$$
B.6

this can be rewritten as

$$\varepsilon = \frac{\delta t}{0.185 L_s^2}$$
B.7

Differentiating both sides gives the relation between straining of outer fibers to the rate of crosshead motion, which is given by

$$\dot{\varepsilon} = \frac{\dot{\delta} t}{0.185 L_s^2}$$
B.8

111

CONTROL CARDS

Control cards are optional cards in an LS-DYNA input file and can be used to change the defaults, activate solution options such as mass scaling, adaptive remeshing, and an implicit solution. A control card defines the properties such as termination time, time step controls, warpage angle for shell, hourglass effect, rigid wall effect etc. A sample control card is shown below:

```
*CONTROL_TERMINATION
$--------1---------2---------3---------4---------5---------6
$$   ENDTIM    ENDCYC     DTMIN    ENDENG    ENDMAS
      0.52       0.0       0.0       0.0       0.0
```

This card defines the termination of the simulation. This card provides different options to define the termination time. The parameters of the card are described below:

- ENDTIM. Specifies the Termination for the simulation. This is mandatory

- ENDCYC defines the termination cycle. The termination cycle is optional and will be used if the specified cycle is reached before the termination time. Default value 0.0 is used.

- DTMIN is the reduction factor for initial time step size to determine minimum time step. Default value 0.0 is used.

- ENDENG is the percent change in energy ratio for termination of calculation. If undefined, this option is inactive. Default value 0.0 is used.

- ENDMAS is the percent change in the total mass for termination of calculation. This option is relevant if and only if mass scaling is used to limit the minimum time step [13]. Default value 0.0 is used.

Card to specify the type of analysis:

I

```
*CONTROL_IMPLICIT_GENERAL
$--------1---------2---------3---------4---------5---------6
$$  IMFLAG       DT0    IMFLAG       NSBS       IGS     CNSTN
          1
```

- IMFLAG defines the type of analysis. It takes the values 0, 1, 2, 4, 5, 6 and –n where n is +ve any number other than the above numbers. IMFLAG 0 means explicit analysis and 1 means implicit analysis. n is the curve ID, which specifies the value of IMFLAG as a function of time. More details can be found from [13].

113

DATABASE CARDS

Database card defines the type of output format for results. The database card is shown

below:

```
*DATABASE_BINARY_D3PLOT
$------1--------2-------3-------4------5-------6------7-----8
$$ DT/CYCL    LCDT     BEAM   NPLTC PSETID  ISTATS TSTART    IAVG
1.0000E-03
```

The parameters of the card are described below:

- DT/CYCL defines the time interval between the outputs. DT/CYCL is 1.00E-03,

  implies 20 D3Plots are generated for total dynamic simulation time of 0.02 seconds.

- LCDT is the optional load curve ID specifying the time intervals between the

  dumps [13].

The Nodout card is used to define the number of data points intended when plotting a

graph. It is shown below:

```
*DATABASE_NODOUT
$-------1----- --2------3------4------5------6------7-----8
DT             BINARY
1.0000E-06        1
```

```
*DATABASE_HISTORY_NODE_SET
$----1------2------3-------4------5------6-------7-------8
ID1      ID2     ID3     ID4    ID5    ID6
28838    32128   32777
```

- DT Time interval between outputs. Default value 0.0 is used.

- BINARY is 1 indicates the ASCII file is written. Default is 1 or 2.

The DATABASE_HISTORY_NODE_SET card is used to define specific nodes for which the data are to be collected. The Nodout card can be used to produce less number of D3plots with large number of data points.

115

APPENDIX E

MATERIAL CARDS

Material cards are used to assign the respective material properties to the respective parts

in the model.

```
*MAT_ORTHOTROPIC_ELASTIC
$HMNAME MATS         1plate_mat
$-------1-------2-------3--------4-------5-------6------7------8
       MID        RO       EA       EB       EC    PRBA    PRCA    PRCB
        1 0.0001 3.8e+006  3.8e+006 3.8e+007   0.33   0.033   0.033


       GAB       GBC      GCA     AOPT
   1.4e+006  1.4e+007 1.4e+007      0.0




*MAT_PLASTIC_KINEMATIC
$--------1----------2----------3----------4----------5----------6---------7
       MID        RO        E       PR      SIGY     ETAN      BETA
        23.3900E-0410400000.0     0.33   68000.0  185185.0
```

- MID defines the material identification number. This number is used to assign

  this material to the parts in the model. Mandatory.

- RO defines the mass density. Mandatory.

- E defines the Young's modulus. Mandatory.

116

In the MAT_ORTHOTROPIC_ELASTIC card

- EA, EB and EC define the young's modulus in 3 orthogonal directions A, B and C respectively, which represent the material axes. Mandatory.

- PR defines the Poisson's ratio. Mandatory.

- PRBA, PRCA and PRCB represent the Poisson's ratios in the planes BA, CA and CB respectively. Mandatory.

- SIGY defines the Yield stress. Mandatory.

- GAB, GBC and GCA specify the shear modulus of the material in the planes AB, BC and CA. Mandatory.

- ETAN defines the Tangent modulus [13]. Default is 0.0.

117

APPENDIX F

SECTION AND PART CARDS

SECTION_SOLID card is used to indicate that solid elements are used in meshing a part. In this card we give SECID. This ID used in defining the part indicates that the specific part is made up of solid elements. PART card is used to define the characteristics of the part such as the material properties and element type of the part. A sample card is shown below:

```
*PART
$------1-------2-------3-------4-------5-------6-------7-------8
    PID    SECID     MID   EOSID    HGID    GRAV  ADPOPT    TMID
     1       2        4
```

- PID is the part identification number. This is a unique number and is used while defining the elements. Mandatory.

- SECID is the section ID which assigns element type used in meshing the part. Mandatory.

- MID is the material ID which assigns the material properties to the part. Mandatory.

All the other options are optional and a default value 0.0 is used. More details can be found from [13].

118

APPENDIX G

NODE AND ELEMENT CARDS

The purpose of NODE card is to define the node and its coordinates in the global system.

Also the boundary conditions in the global system can be specified. Generally nodes are

assigned to elements. ELEMENT_SOLID is used to define the solid elements. The eight

nodes, which form the element, the part to which the element belongs and the element ID

are defined in this card. The 2 cards are shown below:

```
*NODE
$------1------2-------3-------4-------5-------6-------7-------8------9
      NID           X             Y             Z            TC    RC
       1           2.0           8.5           1.75
```

```
*ELEMENT_SOLID
$-----1------2------3-----4-----5------6------7------8-------9------10
     EID    PID    N1    N2    N3    N4    N5    N6     N7    N8
      1      3    1001   1003  1006  1008  1011  1012   1015  1018
```

- NID and EID are the node and element identification numbers respectively.

- X, Y and Z are the coordinates of the node in the global system. Default is 0.0.

119

- TC and RC are translational constraints and rotational constraints. But the constraints are generally specified using boundary specific set option. Default is 0.0.

- In the ELEMENT_SOLID card PID represents the part to which that particular element belongs. Mandatory.

- N1 through N8 are the node Ids which form that particular element. Mandatory.

CONTACT CARDS

The contact cards are used to simulate the fastenings between various parts in an assembly. The Contact card is shown below:

```
*CONTACT_SURFACE_TO_SURFACE
$-------1--------2--------3--------4--------5--------6--------7--------8
        SSID     MSID     SSTYP    MSTYP    SBOXID   MBOXID   SPR      MPR
        1        2

        FS       FD       DC       VC       VDC      PENCHK   BT       DT
        0.1      0.1
```

- SSID indicates the slave segment ID representing the slave surface of the part in the contact.

- MSID indicates the master segment ID representing the master surface of the part in the contact.

There are different methods in which the slave and master surfaces can be defined. SET_SEGMENT is one such option in which the nodes and elements which form the contact surfaces are defined as set segments and the set segment is given a unique identification number. That number is used as SSID or MSID. The other methods by which slave and master surfaces can be defined are by defining the part which forms the contact surface or by defining a BOXID. Box is a 3 dimensional region defined by X, Y and Z coordinates. The defined box is given an ID and it is used in the contact card.

121

- FS and FD are coefficient of static and dynamic friction respectively [13]. Default is 0.0.

BOUNDARY CONDITION CARDS

BOUNDARY_SPC_NODE card is used to define the degrees of freedom for the nodes.

The card is shown below:

```
*BOUNDARY_SPC_NODE
$-------1--------2--------3--------4--------5--------6--------7--------8
 NID/NSID     CID     DOFX     DOFY     DOFZ    DOFRX    DOFRY    DOFRZ
    22200       0        1        1        1        1        1        1
```

- NID/NSID NID is node ID and NSID is node set ID. Hence a specific node or a set of nodes can be constrained using this card.

- DOFX is the degree of freedom in direction X .1 means it is constrained in that direction and 0 means its is not constrained.

- DOFRX is the Rotational degree of freedom in about X axis [13].

Except for NID all the other options have a default value 0.0.

123

APPENDIX J

LOAD CARD

LOAD_SEGMENT applies the distributed pressure load over one triangular or quadrilateral segment defined by the four nodes [13]. A sample LOAD_SEGMENT has been shown below:

```
*LOAD_SEGMENT
$--------1---------2---------3---------4---------5---------6---------7
     LCID        SF        AT        N1        N2        N3        N4
        1         1
```

Where,

- LCID in the card represents the load curve id. Mandatory.

- SF represents the scale factor for Load curve. Default is 1.0.

- AT represents the time for pressure or birth time of pressure. Default is 0.0.

- N1, N2, N3, N4 represents the node numbers.

One more card is used to define the body force loads prescribed base acceleration or prescribed angular velocity over a subset of complete problem. The card is shown below

124

```
*LOAD_BODY_GENERALIZED
$--------1---------2---------3---------4---------5---------6---------7
       N1        N2      LCID    DRLCID        XC        YC        ZC
        1     22000         1         0       0.0       0.0       0.0

       AX        AY        AZ       OMX       OMY       OMZ
      1.0       0.0       0.0       0.0       0.0       0.0
```

- N1 and N2 define the beginning and ending node ID's for body force load. Mandatory.

- LCID represents the curve ID, which is a force curve, applied to the above subset of nodes N1 through N2. Mandatory.

- AX, AY, AZ is the scale factor for the acceleration for their respective directions. Default is 0.0.

125

APPENDIX K

BOX CARD

This card is used to define a box-shaped volume. Two diagonally opposite corner points of a box are specified in global coordinates. The box volume is then used for various specifications, e.g., velocities, contact, etc.

```
*DEFINE_BOX
$--------1---------2---------3---------4---------5---------6---------7
      BOXID      XMN      XMX      YMN      YMX      ZMN      ZMX
          1        0      1.0      0.0      1.0      0.0      1.0
```

- BOXID defines the identity of the box.

- XMN, YMN, and ZMN define the minimum x, y, and z coordinates.

- XMX, YMX, and ZMX define the maximum x, y, and z coordinates.

126

APPENDIX L

OUTPUT CARD

This card is used to define a set of nodes or elements for which the output has to be

stored into the binary history file.


```
*DATABASE_HISTORY_SOLID/SHELL_SET
$--------1---------2---------3---------4---------5---------6---------7
        ID1       ID2       ID3       1D4       ID5       ID6       ID7
          1         2         3         4         5         6         7
```


- ID1 through ID7 represents the node number or element number for which the

  output database history is required.

127

APPENDIX M

QUICK STEPS TO APPLY OPTIMIZATION ENGINE

This appendix discusses the application of optimization engine to finite element model of an impact test done on a PCB board. Let's say we need to optimize the material characteristics for the board in the FEA to bring the FEA closer to the experimental results. So, in this case objective function will be the error between the experimental strain values and FEA strain values calculated on the board. The variables of optimization will be the parameters involved in the material card defined for the board in LS-DYNA. The FEA model should be created using the LS-DYNA with material characteristics for the board with initial guess values. LS-DYNA script file is written out and as shown below,

```
*KEYWORD
$$ HM_OUTPUT_DECK created 18:31:27 07-29-2006 by HyperMesh Version 7.0
$$ Ls-dyna Input Deck Generated by HyperMesh Version   : 7.0
$$ Generated using HyperMesh-Ls-dyna 970 Template Version : 7.0
*CONTROL_TERMINATION
$$  ENDTIM     ENDCYC      DTMIN     ENDENG     ENDMAS
    0.005074         0        0.0        0.0        0.0
*MAT_ORTHOTROPIC_ELASTIC
$HMNAME MATS        2MATL2_2
           11.9800E-04 3353000.0 3353000.0 1320000.0       0.14       0.18
0.18
   537000.0  421000.0  421000.0        2.0
                                       0.5        0.0        0.0
                                       0.5                   0.5                   0.0

..............................................

..............................................

*END
```

128

Now from the above input file remove the card related to material characteristics of the board and '*END' command. Now the input file should look like below,

```
*KEYWORD
$$ HM_OUTPUT_DECK created 18:31:27 07-29-2006 by HyperMesh Version 7.0
$$ Ls-dyna Input Deck Generated by HyperMesh Version  : 7.0
$$ Generated using HyperMesh-Ls-dyna 970 Template Version : 7.0
*CONTROL_TERMINATION
$$  ENDTIM    ENDCYC     DTMIN    ENDENG    ENDMAS
   0.005074        0       0.0       0.0       0.0
..............................................
..............................................
..............
```

Now name this file as fixed.k.

Now create a matlab code which can create a script file consisting of material card for the board and '*END' card. The matlab code is as shown below,

```
A(1)={'*MAT_ORTHOTROPIC_ELASTIC'};

matids=num2str(matidn);
densitys=num2str(densityn,4);
Exs=num2str(Exn,4);
Eys=num2str(Eyn,4);
Ezs=num2str(Ezn,4);
vxys=num2str(vxyn,4);
vyzs=num2str(vyzn,4);
vzxs=num2str(vzxn,4);
Gxys=num2str(Gxyn,4);
Gyzs=num2str(Gyzn,4);
Gzxs=num2str(Gzxn,4);
cids=num2str(cidn);
A{2}=[matids,',',densitys,',',Exs,',',Eys,',',Ezs,',',vxys,',',vyzs,'.'
,vzxs];
A{3}=[Gxys,',',Gyzs,',',Gzxs,',',cids];
A(4)={'0,0,0,0.5,0,0'};
A(5)={'0,0,0,0.5,0.5,0,0'};
A(6)={'*END'};
```

According to this code, each line of the LS-DYNA script file for material card of the board and '*END' command were stored in a variable A in the form of rows from 1

129

through 6. Now the lines in each row of this variable have to pasted below the fixed code

created earlier to complete the LS-DYNA input file using the following matlab code,

```
copyfile('fixed.k','combined.k','f')

%Writing the dot k file with new values obtained from optimisation
program.
fid = fopen('combined.k','a+')
fprintf(fid,'%s \n',A{:})
fclose(fid);

%run modified file
dos('"C:\Program Files\Ansys Inc\v90\ANSYS\bin\intel\ls970.exe" PR=DYNA
i="combinedmesh1.k"')
```

In the above code a file with name combined.k was created and fixed.k was copied into

combined.k and then combined.k was opened and the rows of the variable A were printed

and then the file was closed and LS-DYNA was initiated using the DOS command. After

running the file the objective function is calculated using the following matlab code.

```
%Reading experimental time and strain values
 [P]=xlsread('Exptime.xls');
 [Q]=xlsread('Expstrain.xls');

%Calculating Accuracy Constraint
Yexp=Q;
Yfea=ystrain;
acc=0;
sumYexp=0;
for i=1:2530
acc=acc+(Yexp(i)-Yfea(i))^2;
sumYexp=sumYexp+Yexp(i)^2;
end
acc=acc/(sumYexp);
Y=acc; %Finding the objective function.
```

Constraints on the parameters involved in the material card can be defined using the

following matlab code,

```
%Constraints
g(1)=Ezn-66E+4; %Lower limit for Ezn is 66E+4
g(2)=198E+4-Ezn;%Upper limit for Ezn is 198E+4
```

130

```
g(3)=vxyn-0.07;  %Lower limit for vxyn is 0.07

g(4)=0.21-vxyn;  %Upper limit for vxyn is 0.21
g(5)=vyzn-0.09;  %Lower limit for vyzn is 0.09
g(6)=0.27-vyzn;  %Upper limit for vyzn is 0.27
g(7)=Gxyn-286E+3;  %Lower limit for Gxyn is 286E+3
g(8)=805E+3-Gxyn;  %Upper limit for Gxyn is 805E+3
g(9)=Gyzn-210E+3;  %Lower limit for Gyzn is 210E+3
g(10)=631E+3-Gyzn;  %Upper limit for Gyzn is 631E+3

for i=1:10
    if g(i)<=0
        g(i)=10^10*g(i)^2;
    else
        g(i)=0;
    end;
end;
y=acc+sum(g);  %Penalties for the constraints were added to objective
               function
```

All this matlab code is written as a function format with input as initial values for the parameters for material card and output as the strain measurement comparison to experimental values. Let's say the name of this function as f23mesh.m.

The optimization algorithm program has to be run with the initial guess values, the matlab code for the optimization algorithm is as shown below. It uses three fuzzy logic controllers expand_a.fis, contract.fis, and reflect.fis.

```
clc;
clear all;
format short e;
global funev
global myvar

theta_2=readfis('expand_a.fis');
theta_half=readfis('contract.fis');
theta_center=readfis('reflect.fis');


n=5;
x=[132e4,0.14,0.18,537e3,421e3];
x=[1,1,1,1,1]
alpha=0.5;
error=1;
count=0;               %iteration counter
funev=1;               %function evluation counter

first_iter=1;    %first iteration counter
```

```
yhighmax=1.0;
ynewmin=0;
ynewmax=1;
Dynewmin=-0.01;
Dynewmax=0.01;


%figure;


%Generate the inital polygon
delta1=((n+1)^(0.5)+n-1)*alpha/(n*2^(0.5));
delta2=((n+1)^(0.5)-1)*alpha/(n*2^(0.5));
for i=2:n+1,
    for j=1:n,
        if(i==j+1)
            x(i,j)=x(1,j)+delta1;
        else
            x(i,j)=x(1,j)+delta2;
        end;
    end;
end;


% Evaluate the function values of the initial polygon
for i=1:n+1,
    for j=1:n,
        y(j)=x(i,j);
    end;

    if i==1
        funev=1;
    else
        funev=funev+1;
    end
    z(i)=f23mesh(y);
end;
% funev=n+1;
funev=funev+1;


theta=0;
disp([count,z,theta])
disp(x)
xx=[x;x(1,:)];
plot(floor(xx(:,1)),floor(xx(:,2)),'m')
titlestr=['objective function value',num2str(min(z))];title(titlestr);
%hold on;

% Find the mean value of the polygon
mean=0;
for i=1:n+1,
    mean=mean+z(i);
end;
mean=mean/(n+1);
t=0;
for j=1:n+1,
```

132

```
        t=t+(z(j)-mean)^2;
end;
t=sqrt(t/(n+1));

% Search for the minimum using while loop
while  (t>=error)

    % find the point with the highest function value
    zh=z(1);
     h=1;
     for j=2:n+1,
         if (z(j)>zh) zh=z(j);
             h=j;
         end;
     end;

    % find the point with the lowest function value
    zl=z(1);
     l=1;
     for i=2:n+1,
       if (z(i)<zl)
           zl=z(i);
             l=i;
         end;
     end;

    % find the point with the second highest function value
    if(h==1)         %not 'el' it is one

       m=2;
         zm=z(2);               % zm second highest function value
         for k=3:n+1,
          if(z(k)>zm)
             zm=z(k);
                 m=k;
             end;
         end;
     else
         m=1;
         zm=z(1);
         for k=2:n+1
          if( (z(k)>zm)&(k~=h))
             zm=z(k);
                 m=k;
             end;
         end;
     end;

    % Generate the new reflection point
     for i=1:n
         xs(i)=0.0;
         for j=1:n+1
             xs(i)=xs(i)+x(j,i);
         end;
     end;
```

133

```
    xc=(xs-x(h,:))/n;
    yhigh=abs((zh-zl)/zh);          %move the center toward the lowest
point
    if yhigh>yhighmax
        yhigh=yhighmax;
    end;

    thetac=evalfis([yhigh],theta_center);
     xc=(1-thetac)*xc+thetac*x(1,:);
     xnew=2*xc-x(h,:);
    fnew=f23mesh(xnew);
    funev=funev+1;

    if first_iter==1
        first_iter=0;
        Dynew=0;
        fnew_old=fnew;
    else
        Dynew=(fnew-fnew_old)/fnew_old;
        fnewlast=fnew_old;
        fnew_old=fnew;
     end;

    ynew=abs((zh-fnew)/zh);

    %(fnew-zl)/abs(zl);
     %yg=(fnew-zm)/abs(zm);
    %yhalf=abs((zh-zl)/zh);

    if(fnew<zl)                      %case #1: New point is lower than
zl (theta=2)

        if ynew > ynewmax           %accomodate the range of the variables
            ynew=ynewmax;
        end;
        if Dynew < Dynewmin
            Dynew=Dynewmin;
        end;
        if Dynew > Dynewmax
            Dynew=Dynewmax;
        end;
        if Dynew < Dynewmin
            Dynew=Dynewmin;
        end;
        theta=evalfis([ynew,Dynew],theta_2)
        %[fnew,fnew_old,ynew,Dynew,theta]
        %[fnewlast,fnew,ynew,Dynew,theta]
        theta=(theta-2)*1.0+2;
        %xc1=0.875*xc+0.125*x(1,:);          % New point is moved toward the
lowest point


        xnew1=xc+(theta+1)*(xc-x(h,:));
        fnew1=f23mesh(xnew1);
```

134

```
        funev=funev+1;

        if (fnew1<zl)
            x(h,:)=xnew1;
            z(h)=fnew1;
            %fnew_old=fnew1;
          else
            x(h,:)=xnew;
            z(h)=fnew;
            theta=1;
        end;


    elseif ((fnew<zm)&(fnew>zl))       %case #2: New point is between the
second highest point and zl (theta=1)


        theta=1;
        x(h,:)=xnew;
        z(h)=fnew;
    elseif ((fnew<zh)&(fnew>zm))       %case #3: New point is between the
highest and the second highest points (theta=1)


        theta=1;
        x(h,:)=xnew;
        z(h)=fnew;


    elseif (fnew>=zh)                           %case #4 New point is higher
than the highest point (theta=-0.5)


         if yhigh>yhighmax
             yhigh=yhighmax;
         end;
         theta=evalfis([yhigh],theta_half);
        %[yhigh,theta]
        theta=(theta+.5)*1.0-0.5;
        %xc2=0.97*xc+0.03*x(1,:);       % New point is moved toward the
lowest point
        xnew2=xc+theta*(xc-x(h,:));
        fnew2=f23mesh(xnew2);
        funev=funev+1;
          if(fnew2<zh)
            x(h,:)=xnew2;
            z(h)=fnew2;
            %fnew_old=fnew2;
          else                                      % Generate new polygon
around the lowest point in case of failure
        theta=0;
         for i=1:n+1,
                x(i,:)=(x(i,:)+x(1,:))/2.0;
         end;
        for i=1:n+1,
                for j=1:n,
                    y(j)=x(i,j);
                end;
            funev=funev+(n+1);
            z(i)=f23mesh(y);
            end;
```

135

```
        end;
      end;


    % evaluate termination criterion

    mean=0;
     for i=1:n+1,
         mean=mean+z(i);
     end;
     mean=mean/(n+1);
     t=0;
     for j=1:n+1,
         t=t+(z(j)-mean)^2;
     end;
     t=sqrt(t/(n+1));
    count=count+1;

    %disp([count,z,theta,thetac])
    %disp(x)
    %xx=[x;x(1,:)];                          %generate polygon
    %if (count/2)==round(count/2)
    figure(2)
    xx=[x;x(1,:)];
    if(rem(count,2)==0)
        plot(xx(:,1),xx(:,2),'m:');
    else
        plot(xx(:,1),xx(:,2),'b-');
    end;
    hold on;
    titlestr=['objective function value',num2str(z1)];title(titlestr);
    %else
    %    plot(xx(:,1),xx(:,2),'g');
     %end;
    %axis equal;
    %grid on;
    %hold on;

end;                                         %end of while


for i=1:n+1,
    for j=1:n,
        y(j)=x(i,j);
    end;
    z(i)=f23mesh(y);
end;
z1=z(1);
l=1;
for i=2:n+1,
    if (z(i)<z1)
       z1=z(i);
         l=i;
    end;
end;
```

136

```
%disp('The minimum point is:');
for i=1:n,
    xl(i)=x(1,i);
%    disp(x(1,i));
end;
```

This program has to be run to start the process of optimization. In order to run this program the following files should be in the same working directory,

- F23mesh.m

- expand_a.fis

- contract.fis

- reflect.fis

- Exptime.xls

- Expstrain.xls

After finishing the optimization process, the parameter values at each stage of optimization will be stored in a variable called "myvar".

137

REFERENCES

1. Rudolph, J. Scavuzzo, and Henry, C. Pusey, *"Naval Shock Analysis and Design,"* Booz-Allen and Hamilton, Inc, 2000.

2. Lim, C. T., and Low Y. J., *"Investigating the drop impact of Portable Electronic products,"* Electronic Components Conference, pp. 1270-1274, 2002.

3. Turkiyyah, G. M., and Fenves, S. J., *"Knowledge-Based Assistance for Finite-Element Modeling,"* IEEE, 1996.

4. Fonseca, I. M., Bainum, P. M., and Santos, M. C., *"CPU time consideration for LSS structural/control optimization models with different degrees of freedom,"* Nacta Astronautica, Vol 54, Issue 4, pages 259-266, Feb 2004,.

5. Holzhauer, D., and Grosse, I., *"Finite Element Analysis using Component Decomposition and Knowledge-Based Control,"* Engineering with Computers, Vol. 15, pp. 315-325, 1999.

6. Pinfold, M., and Chapman, C., *"The Application of Knowledge Based Engineering Techniques to the Finite Element Mesh Generation of an Automotive Body-in-white Structure,"* Journal of Engineering Design, Vol. 10, No. 4, 1999.

7. Pinfold, M., and Chapman, C., *"Using Knowledge based Engineering to Automate the Post-Processing of FEA Results,"* International Journal of Computer Applications in Technology, Vol. 21, No. 3, pp. 99-106, 2004.

8. Lee, D., and Kim, S. Y., *"A Knowledge-Based Expert System as a Pre-Post Processor in Engineering Optimization,"* Expert Systems with Applications, Vol. 11, No. 1, pp. 79-87, 1996.

9. Spendley, W., Hext, G., and Himsworth, F., *"Sequential Application of Simplex Designs in Optimization and evolutionary Operation,"* Technometrics, Vol. 4, pp. 441, 1962.

10. Nelder, J., and Mead, R., *"A Simplex Method for Function Minimization,"* Computer Journal, Vol. 7, pages. 308-313, 1965.

11. Trabia, M., and Lu, X., *"A Fuzzy Adaptive Simplex Search Optimization Algorithm,"* ASME Journal of Mechanical Design, Vol. 123, pp. 216-225, 2001.

12. JEDEC Standard JESD22-B 104-B, Mechanical Shock, 2001.

13. Goyal, S., Buratynski, E., *"Methods for Realistic Drop Testing: International Journal of Microcircuits and Electronic Packaging,"* Vol. 23, Nov 1, 2000.

14. Lim, C. T., and Low, Y. J., *"Investigating the drop impact of Portable Electronic products,"* Electronic Components Conference, pp. 1270-1274, 2002.

15. Lim, C. T., Ang, C. W., Tan, L. B., Seah, S. K. W., Wong, E. H., *"Drop Impact survey of Portable Electronic Products,"* Electronic Components and Technology Conference, 2003.

16. Seah, S. K. W., Lim, C. T., Wong, E. H., Tan, V. B. C., Shim, V. P. W., *"Mechanical Response of PCBs in Portable Electronic Products During Drop Impact,"* Electronic Packaging and Technology Conference, 2002.

17. Yu, Q., Kikuchi, H., Ikeda, S., Shiratori, M., Kakino, M., Fujiwara, N., *"Dynamic Behavior of Electronic Package and Impact Reliability of BGA Solder Joints,"* Proceedings of the Intersociety Conference on Thermal Phenomena, 2002.

18. Juso, H., Yamaji, Y., Kimura, T., Fujita, K., Kada, M., *"Board Level Reliability of CSP,"* Electronic Components and Technology Conference, 1998.

19. Varghese, J., Dasgupta, A., *"Test Tailoring Methodology for Impact Testing of Portable Electronic Products,"* Proceedings of IMAC-XXI Conference on Structural Dynamics, 2003.

20. Varghese, J., Dasgupta, A., *"Failure Site Transition During Drop Testing of Printed Wiring Assemblies,"* Proceedings of ASME InterPACK Conference, 2005.

21. Heaslip, G., Punch, J., Rodgers, B., Ryan, C., Reid, M., *"A Simulated and Experimental Comparison of Lead-Free and Tin-Lead Solder Interconnect Failure Under Impact Stimuli,"* Proceedings of ASME InterPACK Conference, 2005.

22. Juso, H., Yamaji, Y., Kimura, T., Fuijita, K., Kada, M., *"Board Level Reliability of CSP,"* ECTC, pages 525-31, 1998.

23. Hong, B. Z., Su, L., *"On Thermal Stresses and Reliability of PBGA Chip Scale Package,"* ECTC, pages 503-10, 1998.

24. Amagai, M., *"Chip Scale Package (CSP) Solder Joint Reliability and Modeling,"* IEEE 36th Annual International Reliability Physics Symposium, pages 260-8, 1998.

25. Vogel, D., Auersperg, J., Micheal, B., Mahindhara, R., *"CSP Reliability Studies Peroformed with Combined FEA and MicroDAC Measurements,"* Chip Scale Rev, pages 76-82, 1998.

26. Ghaffarina, R., *"Key Factors in Chip-Scale Package Assembly Reliability,"* Chip Scale Rev, pages 2(5):29-34, 1998.

27. Ejim, T., *"High Reliability Telecommunications Equipment: A Tall Order of Chip-Scale Packages,"* Chip Scale Rev, pages 2(5):44-8, 1998.

28. Ho, S. H., Zheng, P. J., Wu, J. D., and Hung, S. C., *"On the Reliability and Failure of PBGA Interconnects under Bending Cyclic Test,"* IMAPS, Boston, MA, pages 247-52, 2000.

29. Wu, J. D., Ho, S. H., Huang, C. Y., Liao, C. C., Zheng, P. J., Hung, S. C., *"Board Level Reliability of a Stacked CSP subjected to Cyclic Bending,"* Microelectronics Reliability Journal, pages 407-416, 2002.

30. Hung, S. C., Zheng, P. J., Ho, S. H., Lee, S. C., Chen, H.N., Wu, J.D., *"Board Level Reliability of PBGA using Flex Substrate,"* Microelectronics Reliability Journal, pages 677-687, 2000.

31. Goyal, S., Papadopoulos, J. M., Sullivan, P. A., *"The Dynamics of Clattering II: Equation of Motion and Examples,"* Journal of Dynamic Systems, Measurement and Control, pages 94-102, 1998.

32. Varghese, J., Dasgupta, A., *"Test Methodology for Impact Testing of Portable Electronic Products,"* ASME International Mechanical Engineering Congress & Exposition, pages 16-21, Nov 2003.

33. Frank Stepniak., *"Failure Criteria of Flip Chip Joints During Accelerated Testing,"* Micro Electronics Reliability Journal, pages 1921-1930, 2002.

34. Shetty, S., Lehtinen, V., Dasgupta, A., Halkola, V., Reinikainen, T., *"Fatigue of Chip Scale Package Interconnects Due to Cyclic Bending,"* Journal of Electronic Packaging, March 25, 2000.

35. Michael Pecht, Patrick McCluskey, Jillian Evans, *"Product Integrity and Reliability in Design,"* Chapter 8, 2001.

36. Michael Pecht, Patrick McCluskey, Jillian Evans, *"Product Integrity and Reliability in Design,"* Chapter 13, 2001.

37. Blattau, N., Hillman, C., *"Failure Mechanisms in Electronic Products at High Altitudes,"* CALCE Electronic Products and Systems Center.

38. Wong, E. H., et al., *"Drop Impact Test – Mechanics and Physics of Failure,"* Proceedings of 4th EPTC, pages 327-333, 2002.

39. Wong, E. H., et al., *"Tackling Board Level Drop Impact Reliability of Electronic Interconnections,"* Interpack, 2003.

40. Wong, E. H., and Seah, S. K. W., *"Fundamental of Drop Impact,"* presented in JEDEC Working Group Meeting, 2003.

41. Mackintosh, M., *"The Reliability of Integrated Circuits,"* Micro Electronics and Reliability Journal, Vol. 5, pages 27-37, 1966.

42. Yibin Zhang, Dganta Das, Asaf Katz, and Michael Pecht, *"Trends in Component Reliability and Testing,"* Semiconductor International, pages 101-106, Sept. 1999.

43. Michael Pecht, Anand A. Shukla, Nikhil Kelkar, and Judy Pecht, *"Criteria for the Assessment of Reliability Models,"* IEEE Transactions on Components, Packaging, and Manufacturing Technology – Part B, Vol 20, Pages 229-234, August, 1997.

44. Margaret Jackson, Parthasarathy Srinivasan, Patrick McCluskey, Abhijit Dasgupta, Peter Sandborn, and Michael Pecht, *"Application-specific Reliability Assessment of Electronic Parts,"* CALCE Electronic Products and Systems Consortium.

45. Michael Pecht, *"Reliability Engineering in the 21st Century,"* CALCE Electronic Products and Systems Center.

46. Alander, T., Nurmi, S., Heino, P., and Ristolainen, E., *"Impact of Component Placement in Solder Joint Reliability,"* Microelectronics Reliability Journal, Pages 399-406, 2001.
47. MIL Standard MIL-STD-883E, Method 2002.3, *"Mechanical Shock."*

48. IEC Standard IEC 60068-2-27, *"Environmental Testing-Part 2: Tests, Test Ea and Guidance: Shock."*

49. JEDEC Standard JESD22-B110, *"Subassembly Mechanical Shock."*

50. Wong, E. H., *"Dynamics of Board-Level Drop Impact,"* Journal of Electronic Packaging, 2004.

51. Tong Yan Tee, Hun Shen Ng, Chwee Teck Lim, Eric Pek, Zhaowei Zhong, *"Impact life Prediction Modeling of TFBGA Packages Under Board Level Drop Test,"* Microelectronics Reliability Journal, pages 1131-1142, 2004.

52. Haiyu Qi, Sanka Ganesan, Michael Osterman, Michael Pecht, *"International Conference on the Business of Electronic Product Reliability and Liability,"* 2004.

53. Greg M. Heaslip, and Jeff M. Punch, *"Analysis of Experimental Shock and Impact Response Data of a Printed Wire Board,"* ASME International Mechanical Engineering Congress, pages 125-133, 2003.

54. Thomas A. Deiters, Mary Baker, Kyle C. Indermuehle, and Charles W. Engelhardt, *"Using Analysis to Design for Drop or Other Shock Environments,"* Sound and Vibration Journal, Vol 34, Issue 10, pages 26-30, OCT 2000.

55. II-Ho Jung, Tae-Won Park, Jong-Hwi Seo, Sang-Won Han, and Sung-Hun Kim, *"Structural Vibration Analysis of Electronic Equipment for Satellite under Launch Environment,"* Advances in Nondestructive Evaluation; 11th Asian Pacific Conference on Nondestructive Testing, pages 1440-1445, 2003.

56. Hsing-Ling Wang, Shia-Chung Chen, Lei-Ti Huang, and Ying Chieh Wang, *"Simulation and Verification of the Drop Test of 3C Products,"* 8th International LS-DYNA Users Conference, 2004.

57. Jason Wu, *"Global and Local Coupling Analysis for Small Components in Drop Simulation,"* Mechanical Technology Center, PCS, Motorola.

58. Carroll, D., Zampino, M., and Jones, K., *"Bending Simulation of BGA SMT Assemblies and Application to System Level Drop Simulation,"* Proceedings of ASME IPACK, 2005.

59. Urmila Diwekar, *"Introduction to Applied Optimization,"* University of Illinois at Chicago, 2003.

60. LS-Dyna *"Theory Manual,"* Livermore Software Tehnology Corporation.

61. Ls-Dyna *"970 Keyword Users Manual,"* Livermore Software Technology Corporation.

62. "MATLAB: The Language of Technical Computing," 2006, The Mathworks Inc.

63. Berman, M., Hopkins, D., Powers, B., and Minnicino, M., *"Numerical and Experimental Modeling of the Transition from Transient to Quasi-static Loading of Printed Wiring Assemblies,"* SEM Annual Conference and Exposition on Experimental and Applied Mechanics, 2003.

64. Cordes, J., Carlucci, D., and Jafar, R., *"Dynamics of a Simplified Launched Projectile,"* 21st International Symposium on Ballistics, 2004.

65. Hollis, M., *"Use of Finite-Element Stress Analysis in the Design of a Tank-Cannon-Launched Training Projectile,"* Computers in Engineering: Proceedings of the ASME International Computers in Engineering Conference and Exposition, 1994.

66. Trabia, M., Bendan, O., Samaan, L., Chakka, K. V., Kuncham, J. V. K., Nallani, G., Sridharala S., Chowdhury, M., *"Finite Element Modeling of Projectile Launch Dynamics,"* 76th Shock & Vibration Symposium, 2005.

67. Kuncham, J. V. K., *"Shock Effects on Electronic Components within a Projectile,"* M.S. Thesis, University of Nevada, Las Vegas, Las Vegas, Nevada, 2006.

68. ASTM Designation D6272, *"Standard Test Method for Fexural Properties of Unreinforced and Reinforced Plastics and Electrical Insulating Materials by Four-Point Bending,"* 2000.

VITA

Graduate College
University of Nevada, Las Vegas

Srujanbabu Sridharala

Local Address:
        969 East Flamingo Road,
        Apt#121
        Las Vegas NV 89119

Permanent Address:
        D.No. 25-9-3,
        Rajavari Street
        Visakhapatnam
        Andhra Pradesh, INDIA 530001

Degrees:
        Master of Science in Mechanical Engineering, 2002
        Tennessee Technological University, Cookeville, TN

        Bachelor of Technology, Mechanical Engineering, 1999
        Nagarjuna University, Andhra Pradesh, INDIA

Honors and Awards
   - GREAT (Graduate Research Training) scholarship for summer 2006.
   - 3rd place winner for a paper presentation in AIAA region VI student conference 2006.
   - 2nd place winner for a paper presentation in AIAA region VI student conference 2005.
   - Member of Tau Beta Pi (Engineering honor society).
   - Listed "Who's Who among Students in American Universities and Colleges", 7th Edition.
   - First place winner of HPV 2005 as a part of ASME program.
   - President of AIAA student chapter at UNLV.
   - Secretary for SAMPE student chapter at UNLV.

144

Publications:

1. "Design, analysis and Fabrication of a Composite Roller Skate Chassis", SAMPE Fall Technical conference, Nov 2006.

2. "Shock Reduction for Electronic Components within a Projectile", ASME International Mechanical Engineering Congress & Exposition, Nov 2006.

3. "Optimization of Finite Element Modeling Methodology for Projectile Models", ASME International Mechanical Engineering Congress & Exposition, Nov 2006.

4. "Optimization of a light-weight composite explosion-proof vessel for use in air transport", AIAA (American Institute of Aeronautics and Astronautics) Region VI Student Conference,2006.

5. "Optimization of joint design for side panel of a military vehicle for shock reduction", SAVIAC (Shock and Vibration Information Analysis Center) 76th Shock and Vibration Symposium, 2005.

6. "Finite element modeling of electronic components inside projectile", SAVIAC (Shock and Vibration Information Analysis Center) 76th Shock and Vibration Symposium, 2005.

7. "Mesh density optimization to reduce computational time for a circuit-board in a missile", AIAA (American Institute of Aeronautics and Astronautics) Region VI Student Conference,2005.

Dissertation Title: Methodology for Finite Element Modeling of Electronic Components under Dynamic Loading

Thesis Examination Committee:
    Chairperson, Dr.Mohamed B Trabia, Ph.D.
    Chairperson, Dr.Brendan J. O'Toole, Ph.D.
    Committee Member, Dr. Ajit K. Roy, Ph.D.
    Committee Member, Dr. Woosoon Yim, Ph.D.
    Committee Member, Dr. Mostafiz Chowdhury, Ph.D.
    Graduate College Faculty Representative, Dr. Samaan Ladkany, Ph.D.